TCC Training Seminar on Climate Analysis Information

26 – 30 November 2012

Tokyo, Japan

Tokyo Climate Center
Japan Meteorological Agency

TCC Training Seminar on
Climate Analysis Information

26 – 30 November 2012
Tokyo, Japan

Contents

Schedule

TCC Training Seminar on Climate Analysis Information

Tokyo, Japan, 26 – 30 November 2012

Draft Schedule

Day 1 - Mon., 26 Nov.		
10:00 – 10:30	1. Opening session - Welcome address - Self-introduction by participants - Group photo - Courtesy call on JMA's Director-General	
10:30 – 11:00	Coffee Break	
11:00 – 12:30	2. Lecture: Introduction of products on the TCC website	A. Shimpo (TCC)
12:30 – 14:00	Lunch	
14:00 – 15:50	3. Lecture: Introduction to Climatology	T. Ose (MRI/JMA)
15:50 – 16:10	Coffee Break	
16:10 – 18:00	3. Lecture: Introduction to Climatology (cont.)	T. Ose (MRI/JMA)
18:30 – 20:00	Reception	Invitation by JMA
Day 2 - Tue., 27 Nov.		
9:30 – 11:00	4. Lecture: Use of ClimatView and Statistical analysis	K. Yoshimatsu (Monitoring Unit)
11:00 – 11:20	Coffee Break	
11:20 – 12:45	5. Lecture: Monitoring and prediction of El Niño and La Niña	A. Narui (El Niño Unit)
12:45 – 14:00	Lunch	
14:00 – 15:50	6. Lecture: Climate System Monitoring - Introduction of TCC products on the TCC website focusing on Asian monsoon	S. Tanaka (Analysis Unit)
15:50 – 16:10	Coffee Break	
16:10 – 18:00	7. Exercise - Part I - Introduction of ITACS - Basic operation of ITACS	Y. Maruyama (Analysis Unit)
Day 3 - Wed., 28 Nov.		
9:30 – 11:20	7. Exercise - Part I (cont.) - Production of charts and statistical analysis	Y. Maruyama (Analysis Unit)
11:20 – 11:40	Coffee Break	
11:40 – 12:30	8. Lecture: Climate System Monitoring - Example analysis of past phenomena	S. Tanaka (Analysis Unit)
12:30 – 14:00	Lunch	
14:00 – 18:00	9. Exercise - Part II - Production of climate analysis information	Guided by Analysis Unit
Around 16:00	Coffee Break	
Day 4 - Thu., 29 Nov.		
9:30 – 12:30	9. Exercise - Part II (cont.) - Production of climate analysis information - Preparation for presentation	Guided by Analysis Unit
Around 11:00	Coffee Break	
12:30 – 14:00	Lunch	
14:00 – 15:30	9. Exercise - Part II (cont.) - Production of climate analysis information - Preparation for presentation	Guided by Analysis Unit
15:30 – 15:50	Coffee Break	
15:50 – 18:20	10. Presentation by participants	Presentation (20 min.) followed by Q&A (5 min.)
Day 5 - Fri., 30 Nov.		
9:30 – 12:30	10. Presentation by particpants (cont.)	Presentation (20 min.) followed by Q&A (5 min.)
12:30 – 12:45	11. Wrap up and Closing	
12:45 – 14:00	Lunch	
14:00 – 18:00	Technical Tour	

List of Participants

Provisional List of Participants

Bangladesh
Mr Md. Rashaduzzaman
Meteorologist
Storm Warning Centre
Bangladesh Meteorological Department
Agargaon, Dhaka - 1207
Bangladesh
Tel.: +880 2 9135742
Fax: +880 2 8118230
E-mail: info@bmd.gov.bd,
rashad.zaman@yahoo.com

Hong Kong, China
Mr Tong Hang-wai
Scientific Officer
Hong Kong Observatory
134A Nathan Road, Kowloon, Hong Kong
Hong Kong, China
Tel.: +852 2926 3112
Fax: +852 2311 9448
E-mail: hwtong@hko.gov.hk

Indonesia
Dr Ardhasena Sopaheluwakan
Head, Climate Analysis and Information Subdivision
Indonesian Agency for Meteorology, Climatology and Geophysics (BMKG)
Jl. Angkasa 1 No.2 Kemayoran
P.O. Box 3540 JKT, Jakarta 10720
Republic of Indonesia
Tel.: +62 811 218563
Fax: +62 21 65866236
E-mail: ardhasena@bmkg.go.id,
ardhasena@gmail.com

Mr Amsari Mudzakir Setiawan
Staff, Climate Early Warning Subdivision
Center for Climate, Agroclimate and Marine Climate, BMKG
Jl. Angkasa 1 No.2 Kemayoran
P.O. Box 3540 JKT, Jakarta 10720
Republic of Indonesia
Tel.: +62-21-4246321, +62-856-1163755
Fax: +62-21-4244710, 6540214
E-mail: amsari.setiawan@bmkg.go.id,
amsari_ms@yahoo.com

Lao People's Democratic Republic
Mr Phousavanh Siyavong
Technical Staff
Climate Monitoring and Statistical Analysis
Department of Meteorology and Hydrology
P.O. Box 811 Vientiane
Lao People's Democratic Republic
Tel.: + 856 21 215010
Fax: +856 21 223446
E-mail: Tophousavanh@gmail.com

Malaysia
Ms Nurizana Amir Aziz
Assistant Director
Climatological and Hydrological Section
Malaysian Meteorological Department
Jalan Sultan, 46667 Petaling Jaya, Selangor
Malaysia
Tel.: +603 7967 8227
Fax: +603 7956 3621
E-mail: nurizana@met.gov.my

Mongolia
Ms Bayaraa Jargalan
Long Range Weather Forecaster
Weather Forecasting Section
National Agency for Meteorology and Environment Monitoring (NAMEM)
Juulchny Gudamj-5, Ulaanbaatar-46
Mongolia
Tel.: +976 99193600, +976 11326606
Fax: +976 11326612
E-mail: Meteo_jj@yahoo.com

Myanmar
Dr Lai Lai Aung (Ms)
Staff Officer
Department of Meteorology and Hydrology
Office No. 5, Ministry of Transport,
Nay Pyi Taw
Myanmar
Tel.: +95 67 411446
Fax: +95 67 411449
E-mail: dg.dmh@mptmail.net.mm

Nepal
Ms Indra Kumari Manandhar
Senior Divisional Chemist
Department of Hydrology and Meteorology
Babar Mahal, Kathmandu
Nepal
Tel.: +977 1 4280752
Fax: +977 1 4262348
E-mail: ikmanandhar@yahoo.com, indra@dhm.gov.np

Philippines
Ms Jorybell A. Masallo
Weather Specialist II
Philippine Atmospheric, Geophysical and Astronomical Services Administration (PAGASA)
Science Garden Complex, Agham Road, Diliman
Quezon City 1101
Philippines
Tel.: +632 4340955
Fax: +632 4340955
E-mail: jorybell.masallo@yahoo.com

Sri Lanka
Mr Athula Kumara Karunanayake
Deputy Director
Department of Meteorology
383 Bauddhaloka Mawatha, Colombo 7
Sri Lanka
Tel.: +94 11 2682041
Fax: +94 11 2698311
E-mail: athu1970@yahoo.com

Thailand
Mr Mongkol Prongsungoen
Meteorologist
Climatological Center
Meteorological Development Bureau
Thai Meteorological Department
4353 Sukhumvit Road, Bang-Na, Bangkok 10260
Thailand
Tel.: +66 2 3989929
Fax: +66 2 3838827
E-mail: mongpr@yahoo.com

Viet Nam
Mr Nguyen Duc Hoa
Meteorological Forecaster
National Hydro-Meteorological Service
Ministry of Natural Resources and Environment
83 Nguyem Chi Thanh Street, Hanoi
Viet Nam
Tel.: +84 43 8244917
Fax: +84 43 9330731
E-mail: duchoakttv@gmail.com

Japan Meteorological Agency
1-3-4 Otemachi, Chiyoda-ku
Tokyo 100-8122 Japan
E-mail: tcc@met.kishou.go.jp

Lecturers
Mr Akihiko Shimpo
Dr Tomoaki Ose
Mr Kazuyoshi Yoshimatsu
Dr Akio Narui
Mr Shotaro Tanaka
Mr Yuya Maruyama

Mr Shuhei Maeda
Mr Norihisa Fujikawa
Mr Takafumi Umeda
Ms Yayoi Harada
Ms Hitomi Saito
Mr Kengo Miyaoka
Mr Akira Ito
Mr Ryoji Nagasawa

Tokyo Climate Center, JMA
Ms Teruko Manabe
Mr Ryuji Yamada
Mr Kenji Yoshida

Introduction to Climatology

Introduction to Climatology

Tomoaki OSE (tomoaose@mri-jma.go.jp)
Climate Research Department, Meteorological Research Institute (MRI/JMA)
1-1 Nagamine, Tsukuba, 305-0052, JAPAN

1. Climate and Climate system

According to WMO website, “At the simplest level the weather is what is happening to the atmosphere at any given time. Climate in a narrow sense is usually defined as the "average weather," or more rigorously, as the statistical description in terms of the mean and variability of relevant quantities over a period of time.”

Although climate is the synthesis of the weather, climate is not maintained only by atmosphere itself but is formed in the interactions among many components of the Earth. This system is named as climate system. The global climate system consists of atmosphere including its composition and circulation, the ocean, hydrosphere, land surface, biosphere, snow and ice, solar and volcanic activities (Fig.1). These components interact on various spatial and temporal scales through the exchanges of heat, momentum, radiation, water and other materials.

The purpose of the lecture is to know how climate and its variability is formed and changed in the global climate system and what kind of role each component of the climate system plays.

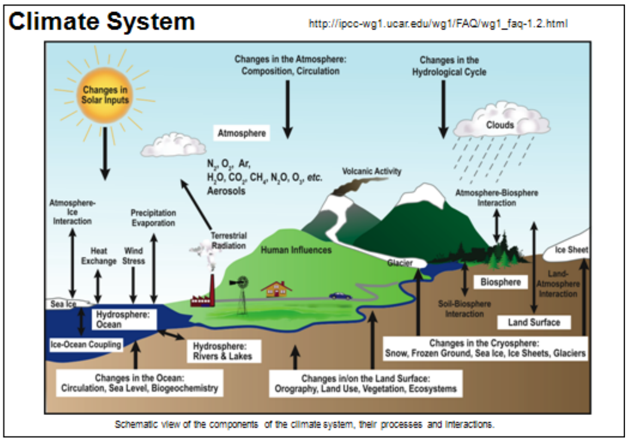

Figure 1 Climate system.
(From ipcc-wg1.ucar.edu)

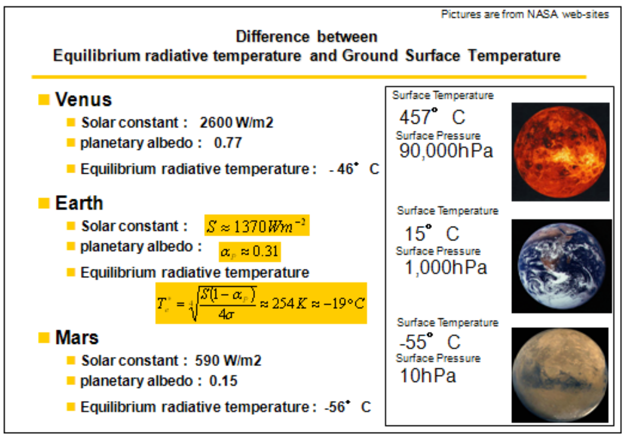

Figure 2 Raditive balance of planets.
(Pictures are from NASA website)

2. Global mean temperature and Radiative balance

Global mean temperature of planets, which is the temperature “observed from space”, is estimated by global radiation balance between absorbed solar radiation and terrestrial emission from the planet. Incoming solar radiation is reflected back to space by a fraction of the planetary albedo. For the Earth, the observed mean ground temperature (15℃) is warmer by 34℃ than the estimated temperature (-19℃). The reason is suggested by comparing other planet cases (Fig.2). The mean ground temperature for Mars with thin atmosphere is warmer only by 1℃ than the estimated temperature. For Venus with thick atmosphere, the difference is 503℃. Radiative absorption by greenhouse gas in atmosphere is an important factor to determine mean ground temperature as well as planetary albedo.

The Earth's atmosphere has different characteristics for shortwave and longwave radiations (Fig.3). It is transparent (58%) for shortwave radiative flux from the sun as an approximation except for the reflection due to clouds (23%). On the other hand, the longwave radiation flux emitted from the Earth's ground is absorbed (90%) once in the atmosphere approximately and then mostly emitted back to the ground (greenhouse effect). Upper cold atmosphere and clouds emit less longwave flux to space than the ground emits. As a net, surface ground is heated by shortwave radiation from the sun, and atmosphere is cooled by longwave emission to space. The vertical contrast of the heating between ground and atmosphere creates thermal instability, which is compensated by vertical transport processes of sensible and latent heat energy due to turbulences, convections and waves.

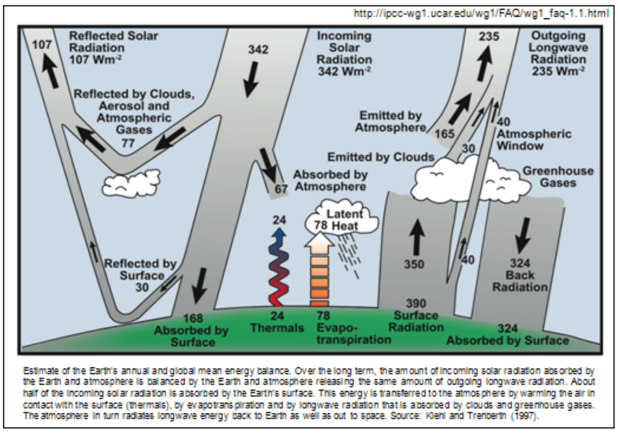

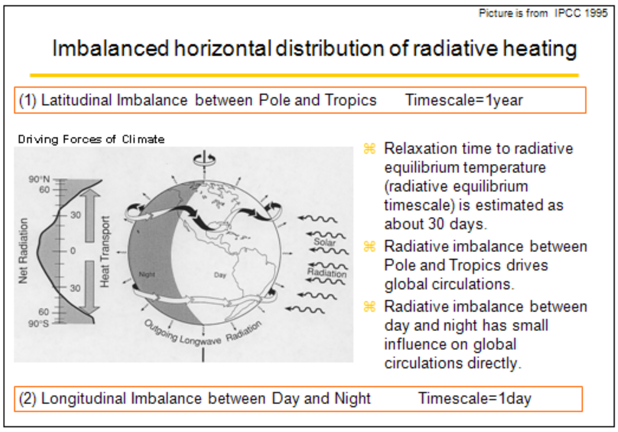

Figure 3 Vertical energy balance.
(From ipcc-wg1.ucar.edu)

Figure 4 Horizontal radiative imbalance.
(Picture is from IPCC 1995)

3. Annual mean circulation and Horizontal heating contrast

Longitudinal contrast of radiative heating is created between day and night (Fig.4). But, generally, as compared with the annual cycle, the diurnal heating contrast does not produce significant temperature differences between day and night and related global circulations because a relaxation time to a radiative equilibrium is estimated as 30 days for the Earth (James, 1995), which is much longer than a day scale. However, diurnal cycles play a dominant role in local precipitation occurrences particularly in the tropical to subtropical lands and surrounding seas.

Latitudinal heating contrast on the Earth is created on seasonal time-scale by the different incoming shortwave radiation between near the poles and the tropics (Fig.4). Local surface temperature determining outgoing longwave radiation is not adjusted instantly enough to compensate for the showtwave radiation contrast. A part of absorbed radiative energy in low latitudes is transported poleward by meridional circulations and waves in atmosphere and ocean, and these heat transports keep high-latitudes warmer than the radiative equilibrium. Poleward/equatorward air motions form westerly/easterly wind in the upper/lower subtropics (Fig.5) through Coriolis force due to the rotation of the Earth (or the angular momentum conservation about the Earth's rotation axis). Extra-tropical waves are also responsible for creating mid- to high latitude's westerly jets.

4. Seasonal change and Heat capacity

Seasonal change is definitely produced by the seasonally changing solar incidence with its maxima at the South Pole in December and at the North Pole in June. However, zonally averaged features of wind and temperature are not drastically changed in the troposphere (lower than about 100hPa) through the whole year; westerly jets in both hemispheres, hot tropics and cold poles (Fig.5). This fact is attributed to basically unchanged distribution of sea surface temperature (SST) due to large heat capacity of the oceans. SSTs roughly determine the location of deep cumulus occurrences, which leads to vertical energy mixing in the troposphere and drives global circulations (Webster, 1994).

Stratospheric climate above 100hPa varies following the seasonal march of the sun (Fig.5) because of the seasonal change of ozone-related shortwave heating and small heat capacity of thin stratospheric atmosphere; cold around a winter pole, warm around a summer pole, westerly jet in a winter hemisphere and easterly in a summer hemisphere. Atmospheric circulations also contribute to the stratospheric climate; a cold tropopause in the tropics is steadily created by upward motion.

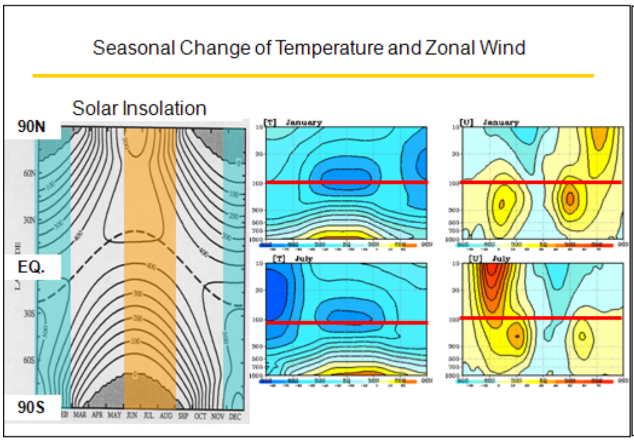

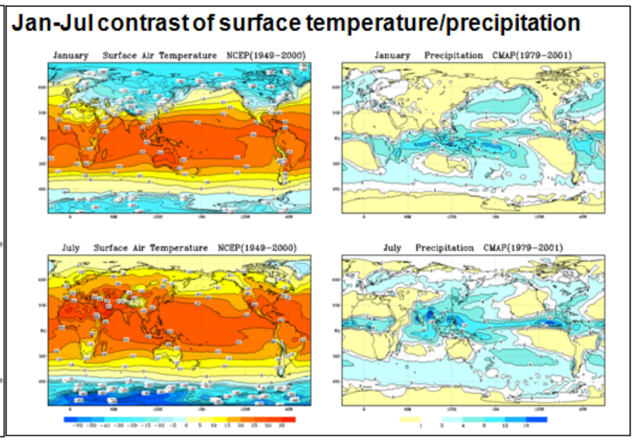

Figure 5 (Left) seasonal change of solar insolation and (right) zonally averaged temperature and winds in January (uppers) and July (lower). (the figure for solar insolation is from IPCC 1995)).

Figure 6 (Left) surface air temperature and (right) precipitation in (upper) January and (lower) July.

Heat capacity of land surface is small as compared with that of the oceans. Surface air temperature over the northern continents is much higher than SSTs at the same latitudes in the northern summer (especially in daytime) and much colder in the northern winter (Fig.6). The large contrasts of surface air temperature between continents and the oceans add a significant feature to regional seasonal changes of rainfall and wind around the continents in low and mid-latitudes, which is named as monsoon. A concentrated subtropical rainfall forms a typical summer monsoon system consisting of an upper-level anti-cyclonic circulation, a monsoon trough, a low-level jet, a subtropical rainfall band expanding north(south)eastward and extensive downward motions causing dry region in the north(south)westward area of the northern (southern) hemisphere (Rodwell and Hoskins, 1996), as shown in the Asian region of Fig. 7.

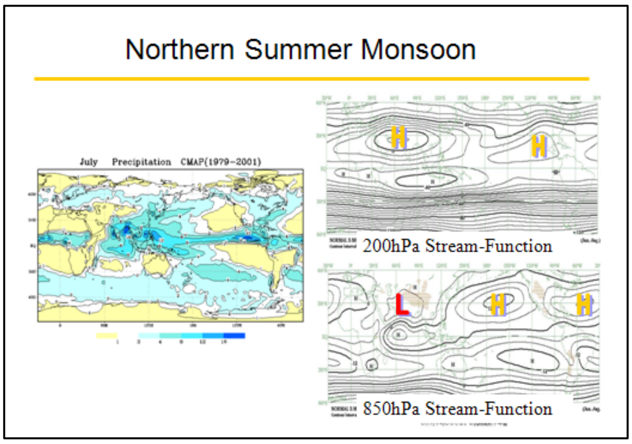

Figure 7 (Left) precipitation, (upper-right) 200hPa streamfunction and (lower-right) 850hPa streamfunction in July.

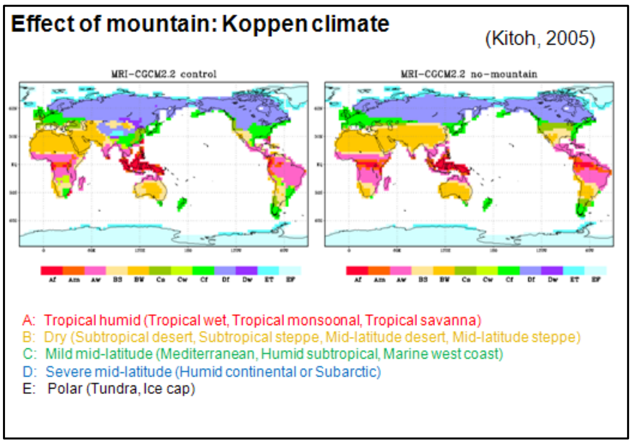

Figure 8 Koppen climate maps simulated by a climate model (left) with mountains and (right) without mountains.
(From Kitoh 2005 in Japanese)

5. Climate model and Experiments

A good way to understand climate system is to modify or remove some elements of the climate system (Fig. 1). It is not easy to modify a real climate system of the Earth by changing the Earth orbit or removing mountains. Instead, we can easily modify virtual climate systems simulated numerically in climate models based on physics and other fundamental sciences. From the comparison between with/without mountain model experiments (Fig. 8), we can see that mountains would be responsible for the real world climate of humid summer and somewhat cold winter in the eastern parts of the continents. Paleo climate is another climate system we can confirm based on observational evidences. It gives us a chance to test the ability of climate models to simulate another different climate.

6. Intra-seasonal to Interannual variability

Climate varies naturally with time. Atmosphere itself includes internal instability mechanisms, typically the baroclinic instability around the extratropical westerly jets, so that it may be considered as chaotic or unpredictable beyond a few weeks. However, some atmospheric low-frequency (>10 days) teleconnections are analyzed such as wave patterns along the westerly jet waveguides and other ones from the northern mid-latitudes across the equatorial westerlies (Fig. 9), which are consistent with the Rossby-wave propagation theory. Numerical ensemble predictions from many disturbed atmospheric initials are a reasonable tool to capture mean weathers in next few weeks.

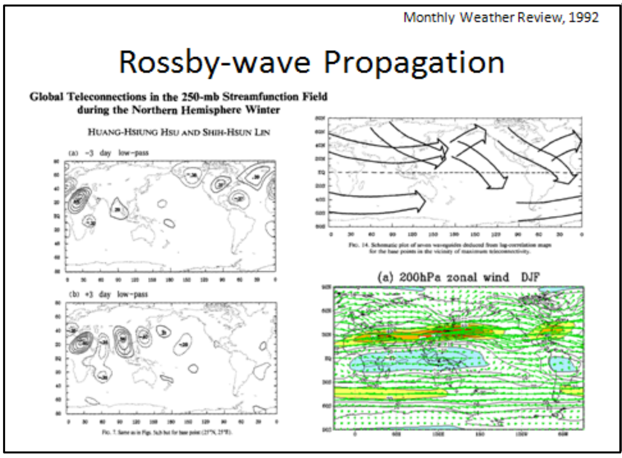

Figure 9 (Left) a teleconection pattern of 250hPa streamfunction, (upper-right) various propagations and (lower-right) 200hPa climatological zonal wind in DJF. (From Hsu and Lin 1992)

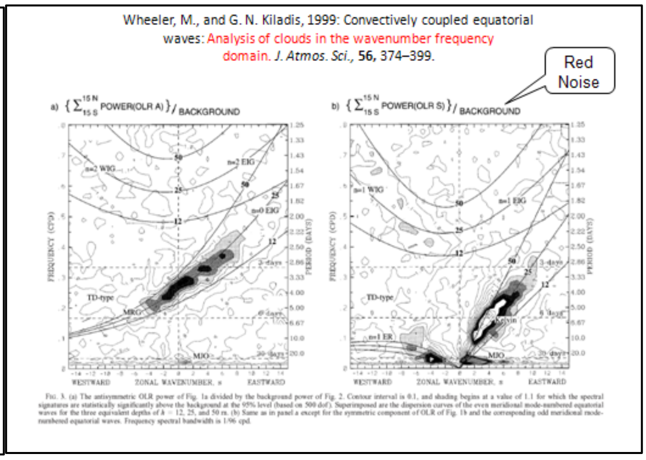

Figure 10 Spatial and temporal power-spectrums in the tropics of (left) asymmetric and (right) symmetric OLR variability about the equator. (From Wheeler and Kiladis 1999).

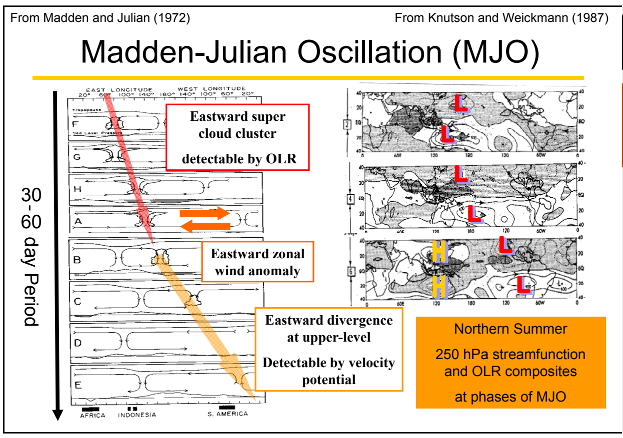

Figure 11 (Left) schematic time-sequence of Madden-Julian Oscillation (MJO) along the equator (from Madden and Julian, 1972). (Right) composite maps of OLR and 250hPa streamfunction anomaly at MJO phases (from Knutson and Weickmann 1987).

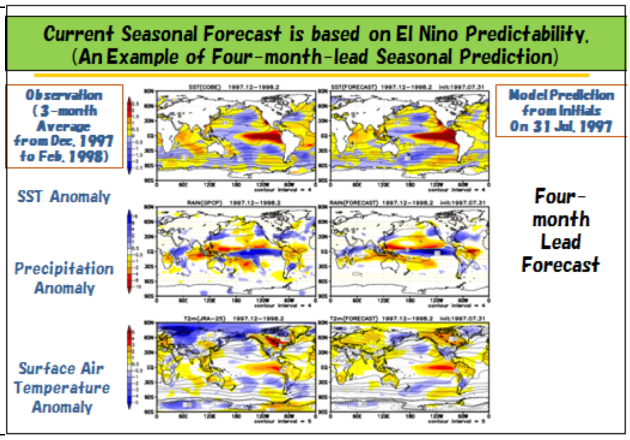

Figure 12 (Left) observed SST, precipitation and surface air temperature anomalies for DJF 1997-98. (Right) the same except for four-month lead prediction.

Some time-space power-spectrum peaks, indicating organized atmospheric variability coupled with convective activity, are imbedded in red noise backgrounds in the tropics. Variability of outgoing longwave radiation (OLR) associated with equatorial waves, such as Kelvin waves, equatorial Rossby waves (ER) and mixed Rossby-Gravity waves (MRG), can be detected, as well as tropical depressions and easterly waves (TD-type) in Fig. 10. Madden-Julian Oscillation (MJO) is an eastward-moving oscillation of surface pressure, precipitation and winds along the equator with the period of 30-60 days and planetary scale wavenumbers (Fig. 11). Monitoring MJO or watching OLR and velocity potential anomalies may be very helpful for intra-seasonal prediction in the tropics to the subtropics and even in the mid-latitudes (Fig. 11).

Atmosphere-ocean interactions are able to produce longer time-scale natural variability in atmosphere with periods beyond months up to several and decadal years. A typical example is ENSO (El Niño / Southern Oscillation) with the period of 2-7 years, which is influential to worldwide climate even out of the tropical Pacific. El Niño events, related surface air temperature and precipitation anomalies are predicted successfully on seasonal to inter-annual scales (Fig.12). The El Niño SST anomaly tends to keep seasonally steady precipitation (heating) anomalies over the equatorial central Pacific. Upper and lower-level tropical atmospheric response to a steady heating anomaly can be explained based on forced equatorial waves or the Gill-pattern (or Matsuno-Gill pattern) (Fig. 13). Recently, terms of El Niño Modoki or Central Pacific (CP)-El Niño are used for the equatorial Pacific phenomena with warm SST anomaly and enhanced precipitation in the central Pacific but cold SST anomaly and suppressed precipitation in the eastern Pacific, distinctive from normal El Niño events or Eastern Pacific (EP)-El Niño (Fig. 14).

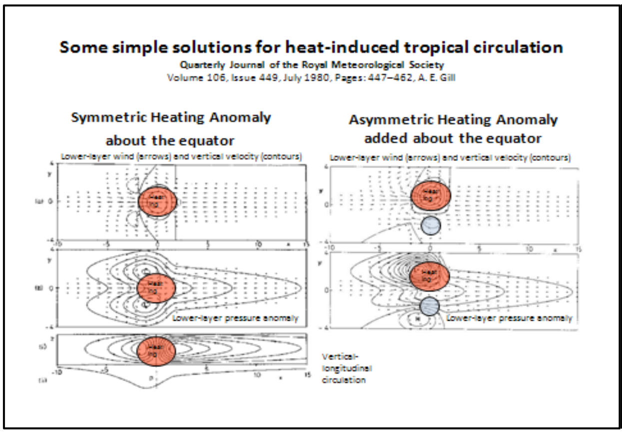

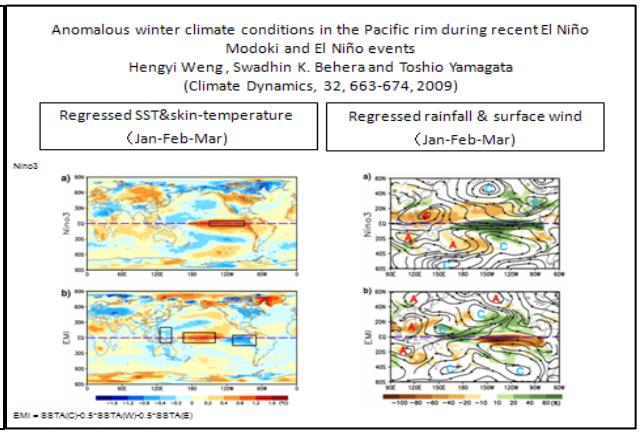

Figure 13 Tropical atmospheric responses to equatorially (left) symmetric and (right) plus asymmetric heating anomalies (from Gill 1980).

Figure 14 Comparison between (lower) El Niño Modoki or CP-El Niño and (upper) normal El Niño or EP-El Niño events. (Left) related surface air temperature anomalies, (right) precipitation anomalies. (From Weng et al. 2009)

The remote effect of El Niño during the mature stage is stored in the Indian Ocean capacity and still influential to the Indo-western Pacific climate even during summer following the ENSO (Fig.

15). A dipole mode with an east-west SST anomaly contrast sometimes occurs around Sep-Oct in the tropical Indian Ocean, which is at least partially independent from ENSO events (Fig. 16). Occurrence of this mode affects climate over various regions including tropical eastern Africa and the maritime continent.

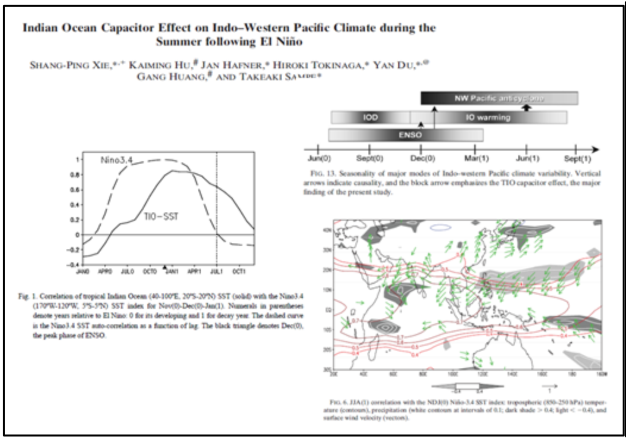

Figure 15 Indian Ocean capacitor effect. (Left) lagged correlation of tropical Indian Ocean SST with Nino 3.4 SST for NDJ. (Upper-right) seasonality of major modes. (Lower-right) correlation of the NDJ Nino3.4 SST with the following JJA climate. (From Xie et al. 2009)

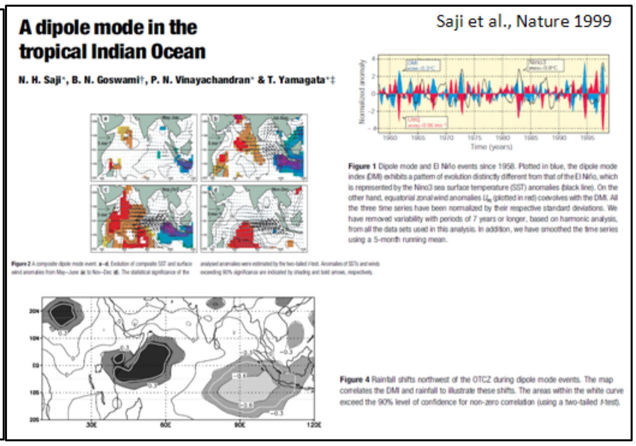

Figure 16 A dipole mode in the tropical Indian Ocean. (Upper-left) time-evolution of the dipole mode SST anomaly, (lower-left) rainfall shift during the dipole mode, (right) historical records for dipole mode and El Niño events. (From Saji et al. 1999).

7. Decadal variability and Climate change

Decadal variability and climate change involve feedbacks from other elements of the climate system. Changes of vegetation and soil moisture amplify the dramatic drying trend in 1980’s in Sahel region, which is basically forced by a southward precipitation shift of the Inter-tropical Convergence Zone due to cooler/warmer SST anomaly in the northern/southern Atlantic Ocean (Fig. 17). Decadal variabilities are also found in SST anomaly from the North Pacific to the tropics. A possible mechanism is the subduction hypothesis; high latitudes’ cold surface water is subducted in the North Pacific and flows into the subtropical deeper ocean along the surfaces of constant density, then back up to the equatorial Pacific surface again by upwelling. This is consistent with the analysis showing that the decadal SST variability in the central North Pacific spreads into the deep ocean (Fig. 18).

Natural change in external conditions of climate system (e.g., the increase of aerosol by volcano eruption) forces climate to change. Paleo climates may be related to different external conditions of the Earth orbit, greenhouse gas concentrations, land-sea distribution, topography, solar and volcano activities. Various feedbacks may be caused through relevant responses of ice coverage, clouds, dust and deep ocean circulations.

Human activity also changes external conditions of the climate system, typically the increase of greenhouse gases (CO_2, CH_4, N_2O, etc.) which are leading to warmer climate during relatively short periods. The climate models driven with natural forcing only cannot explain the observed increase of the global mean temperature in the 20th century while the models with anthropogenic forcing included capture the real global warming (Fig. 19). The influences of global warming appear not only in global mean temperature but also in future regional precipitation (Fig. 20), where wet/dry region generally tends to become further wetter/drier due to enhanced horizontal moisture transports.

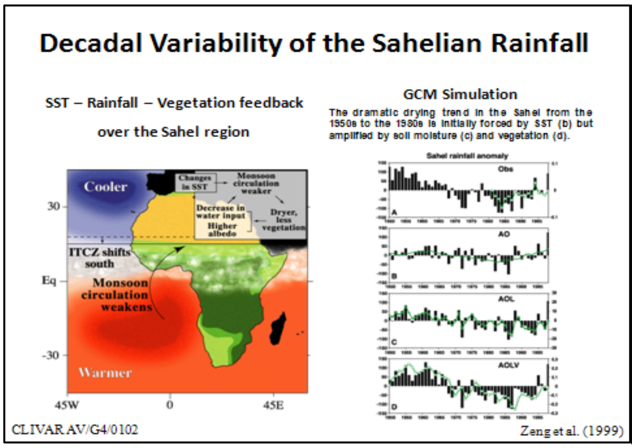

Figure 17 Decadal variability of the Sahel Rainfall. (Left) a possible mechanism, (Right) observed historical Sahel rainfall anomaly and GCM simulations (from Zeng et al. 1999).

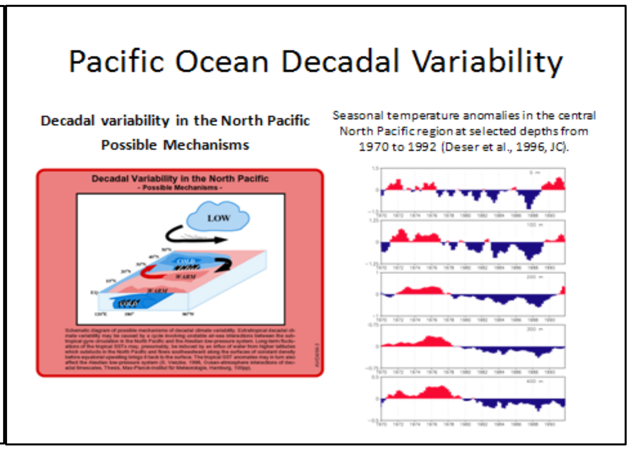

Figure 18 Decadal variability of the North Pacific Ocean. (Left) a possible mecanism, (right) time-sequence of ocean temperature at various depths (from Deser et al. 1996).

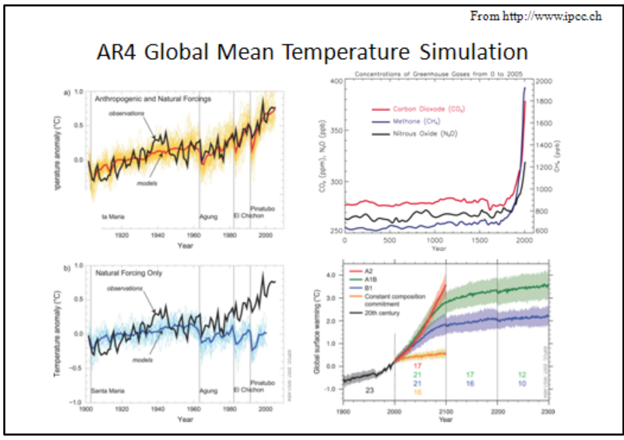

Figure 19 Observation and simulations for global mean temperature change in 20th century (upper-left) with and (lower-left) without anthropogenic forcing. (Right) Future projections of global mean temperature under various scenarios. (From http://www.ipcc.ch).

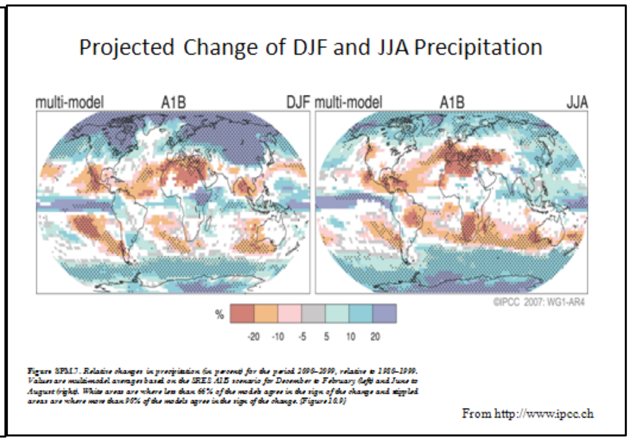

Figure 20 Future projection of relative precipitation changes (%) between 2090-2099 and 1980-1999. (Left) Dec-Jan-Feb and (right) Jun-Jul-Aug. (From http://www.ipcc.ch).

The global warming tends to change not only average climate but also the strength and frequency of extreme weather events because of moisture increase. Precipitation intensity increases over most regions of the world, especially over the northern extratropics and the equatorial lands (Fig. 21). This is the case even for drier future mean climate regions. On the other hand, the annual maximum number of consecutive dry days also tends to increase in most of the tropics, the subtropics and the mid-latitudes (Fig. 21), where drier future mean climate is projected seasonally. Tropical cyclone frequency tends to decrease over active tropical cyclone regions at present and increase over the other regions (Fig. 22). This fact may be explained from the projection that mean vertical circulations triggering tropical cyclone occurrences tend to be suppressed on average because of upper troposphere further warmer than near-surface in the future mean climate. At the same time, the frequency of strong tropical cyclones is projected to increase due to moisture increase (Fig. 22).

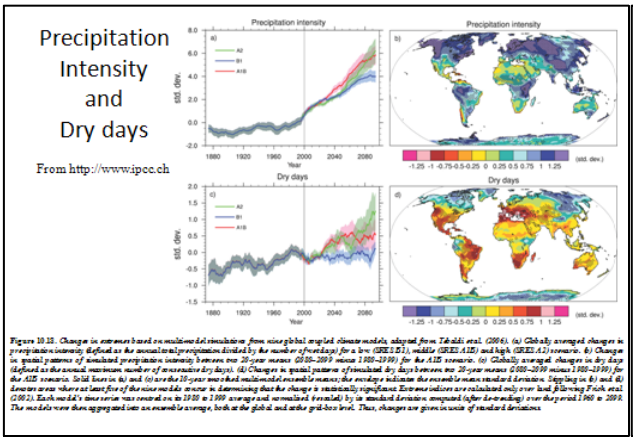

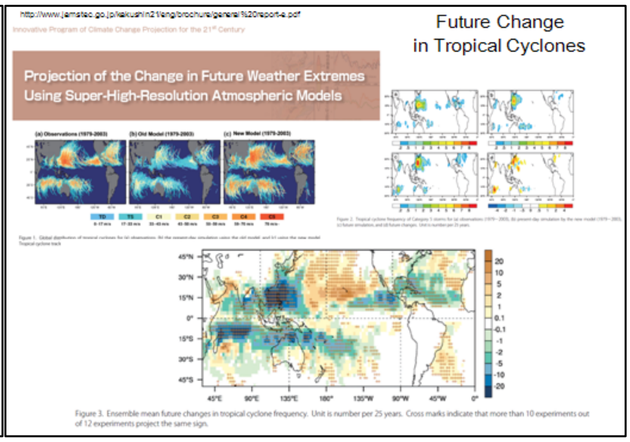

Figure 21 Future projections for changes of (uppers) precipitation intensity and (lowers) dry days. Those are normalized with their standard deviations. (From http://www.ipcc.ch).

Figure 22 Future projection of changes of (lower) tropical cyclone frequency and (upper-right) strong tropical cyclone frequencies. (From http://www.jamstec.go.jp/kakushin21/eng/brochure/general%20report-e.pdf)

8. Summary

Unusual weather and climate are attributed to unusual atmospheric flows, storms and convective disturbance. Diagnostic analysis shows that those disturbances are often related to atmospheric intrinsic waves and phenomena. However, atmospheric environment is maintained and influenced by other elements sustaining the climate system. Sometimes, unusual and steady convective activity is connected to long-term SST anomalies related to ocean variability. Numerical ensemble simulations starting from many disturbed atmospheric and oceanic initials are a reasonable tool to capture mean weathers and climate in weeks to seasons.

Radiative processes including longwave absorption by greenhouse gases and shortwave reflection by snow, ice, clouds and aerosols determine the local Earth's ground temperature. The distribution of ground temperature is influential to vertical and horizontal atmospheric and oceanic stabilities, the amount of water vapor and the speed of water cycle. Then, those can affect atmospheric and oceanic flows, the features of storms and convections and eventually our daily lives. Therefore, we need to continue careful watches and diagnostics for global and local climate systems (Fig.1), as well as its future projection.

References

Deser, C., M. A. Alexander and M. S. Timlin, 1996: Upper-ocean thermal variations in the North Pacific during 1970-1991. *J. Climate*, **9**, 1840-1855.

Gill, A. E., 1980: Some simple solutions for heat-induced tropical circulation. *Quart. J. Meteor. Soc.*, **106**, 447-462.

Hsu, H.-H., and S.-H. Lin, 1992: Global teleconnections in the 250-mb streamfunction field during the Northern Hemisphere winter. *Mon. Wea. Rev.*, **120**, 1169-1190.

IPCC Fourth Assessment Report (AR4) Climate Change 2007: The Physical Science Basis.

Kitoh, A., 2005: Climate model simulation on the role of mountain uplift on Asian monsoon. *The Geological Society of Japan*, **111**, XIX.

Knutson, T. R. and K. M. Weickmann, 1987: 30-60 day atmospheric oscillations: composite life cycles of convection and circulation anomalies. *Monthly Wea. Rev.* **115**, 1407-1436.

Madden, R. A. and P. R. Julian, 1994: Observations of the 40–50-day tropical oscillation—A review, *Monthly Wea. Rev.,* **122**, 814–37.

Saji, N. H., B. N. Goswami, P. N. Vinayachandran and T. Yamagata, 2009: A dipole mode in the tropical Indian Ocean. *Nature*, **401**, 360-363.

Rodwell, M.J. and B. I Hoskins, 1996: Monsoons and the dynamics of deserts. *Q. J. R. Meteor. Soc.*, **122**, 1385-1404.

Webster, P. J., 1994: The role of hydrological processes in ocean-atmosphere interactions, *Review of Geophysics*, **32**,427-476.

Weng, H., K. Ashok, S. Behera, S. A. Rao and T. Yamagata, 2007: Impacts of recent El Nino Modoki on dry/wet conditions in the Pacific rim during boreal summer. *Clim Dyn.*, **29**, 113-129.

Wheeler, M., and G. N. Kiladis, 1999: Convectively coupled equatorial waves: Analysis of clouds in the wavenumber frequency domain. *J. Atmos. Sci.,* **56,** 374–399.

Xie, S.-P., K. Hu, J. Hafner, H. Tokinaga, Y. Du, G. Huang and T. Sampe, 2009: Indian Ocean capacitor effect on Indo-western Pacific climate during the summer following El Niño. *J. Climate*, **22**, 730-747.

Zeng, N., J. D. Neelin, K.-M. Lau and C. J. Tucker, 1999: Enhancement of interdecadal climate variability in the Sahel by vegetation interaction. *Science*, **286**, 1537-1540.

Text books

James, I. N., 1995: Introduction to Circulating Atmospheres. Cambridge University Press, 422pp.

Trenberth, K.E.(ed.), 1992: Climate System Modeling. Cambridge University Press, 788pp.

Wallace, J.M. and P. V. Hobbs, 2006: Atmospheric Science. Academic Press, 483pp.

Use of ClimatView and Statistical Analysis

Use of ClimatView and Statistical analysis

1. Monitoring of the GCOS networks

1. 1 Background

Current and historical data related to extreme weather and climate events are necessary for seasonal and interannual climate prediction as well as for climate research, monitoring of climate variability and detection of climate change. The importance of these activities has been recognized on numerous occasions by governments at various meetings, in particular by the Intergovernmental Panel on Climate Change (IPCC) and by the Conference of the Parties to the United Nations Framework Convention on Climate Change (UNFCCC). In response to these requirements from the climatological community, the Global Climate Observing System (GCOS) program was established in 1992 to meet the needs for:

- Climate system monitoring, climate change detection and monitoring the impacts of and the response to climate change;
- Data for application to national economic development;
- Research towards improved understanding, modeling and prediction of the climate system.

Meanwhile, GCOS established the networks of surface and upper air observation stations run by WMO member National Meteorological and Hydrological Services (NMHSs). These "baseline" networks constitute a minimum number of appropriately-distributed sites to provide globally-representative, high-quality data records of key climate variables for monitoring global trends. The GCOS Surface Network (GSN) consists of over 1000 land surface stations selected from the WMO stations (Fig.1).

Since the need for monitoring the performance of these networks was recognized, DWD (German Meteorological Service) and JMA have implemented the monitoring activities as the GSN Monitoring Centre since 1999.

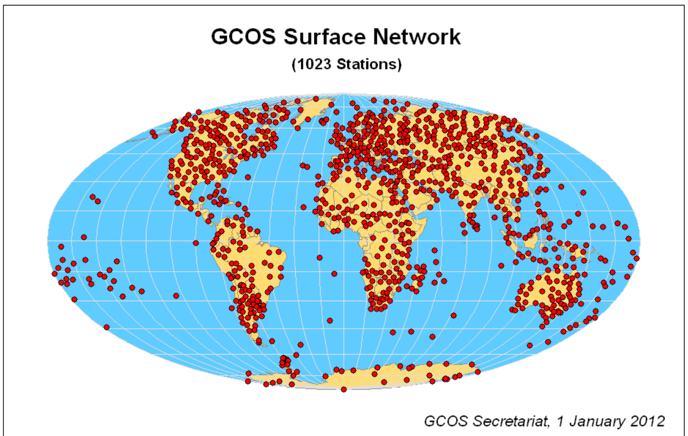

Fig.1 Distribution of GCOS Surface Network(January 2012)

Refer to: http://www.wmo.int/pages/prog/gcos/documents/GSN_map_2012.png

1.2 Monitoring of GSNMC

The monitoring results by GSNMCs are available on the web site (http://www.gsnmc.dwd.de/) and CLIMAT data are sent to the GSN Analysis Centre in Asheville, NCDC/NOAA. The monitoring report integrated the monthly basis products are also published once a year and sent to the GCOS Secretariat.

The reception rate of CLIMAT report from the GSN stations shows a slight increase from 2010 to

2012 to somewhat more than 80% (Fig. 2). Since the GSN is the minimum configuration for global climate monitoring, the reception rate is needed to be improved more.

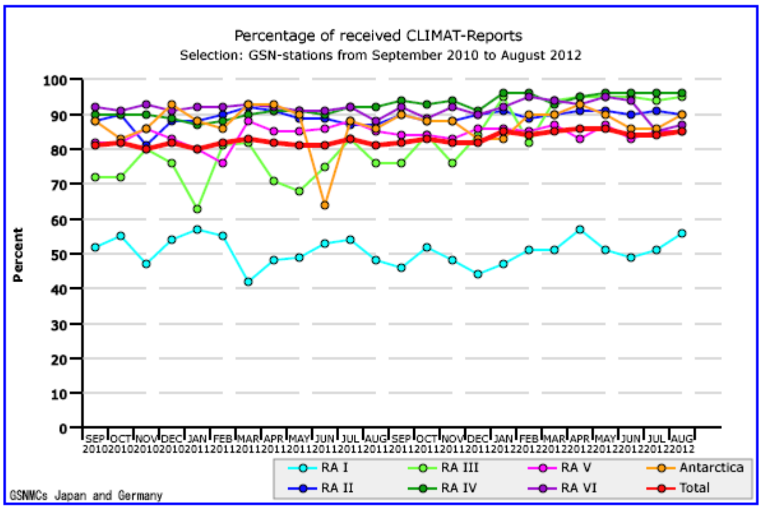

Fig.2 Percentage of received CLIMAT messages from GSN stations (Sep 2010 – Aug 2012)

1.3 CBS Lead Centre for GCOS Data

Based on the monitoring result of GSNMCs, the CBS Lead Centre in each region contacts with the National Focal Point (http://www.wmo.int/pages/prog/www/ois/rbsn-rbcn/FocalPointsGCOS.doc) to identify problems related to CLIMAT report. Each CBS Lead Centre also may give technical advice for preparing a CLIMAT message in the correct format (Fig. 3).

JMA took the responsibility of CBS Lead Centre for GCOS data in East / Southeast Asia and started the activity in 2005 year as the trial one. In 2007, nine CBSLCs are established in each area in the world (http://www.wmo.int/pages/prog/gcos/index.php?name=CBSLeadCentres).

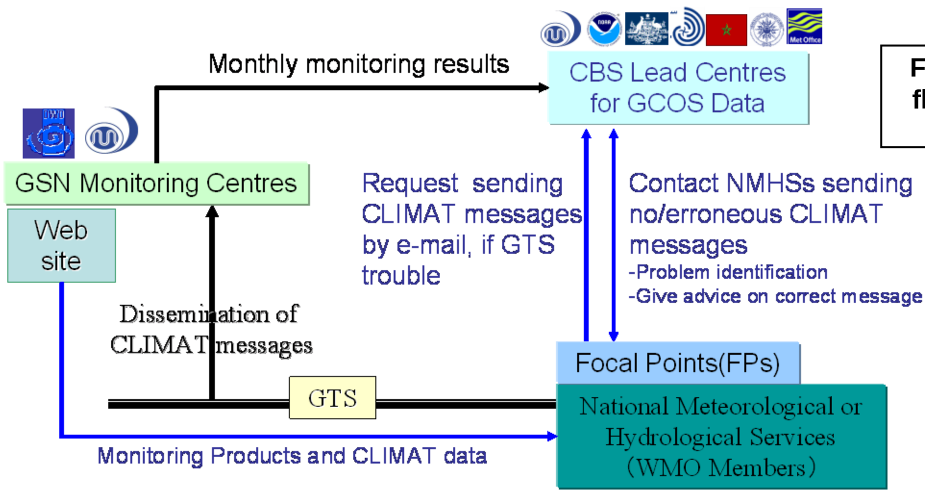

Fig.3 Information flow related CBS Lead Centre

2. Usage of ClimatView

ClimatView is an interactive database launched by JMA on the TCC website in August 2007. Monthly temperature and precipitation data from CLIMAT reports since 1982 are available. NMHSs can monitor the availability of CLIMAT report over the GTS. It is expected to facilitate exchange of climate data.

Data on ClimatView are derived from CLIMAT reports received at DWD (Germany NMHS) and JMA. Data are updated on around 9th day, 14th day (JMA), and the end of the month (DWD+JMA).

Please refer to http://ds.data.jma.go.jp/tcc/tcc/index.html in order to use ClimatView.

Before using ClimatView, please read the explanations, which include precautions and usage.

1. Click on the area of interest

   On the top page of ClimatView, a global map is shown. Clicking on an area of interest shows another map of the area with the distribution of monthly mean temperatures. The month and year are selected on the top page (the default value is the most recent month).

2. Distribution map

   The user can choose the indicated area, month/year and element (monthly mean temperature, monthly total precipitation, monthly mean of daily maximum/minimum temperature, monthly mean temperature anomaly, monthly total precipitation ratio, normal of monthly mean temperature and normal of monthly total precipitation).

   Hovering over a station on the distribution map page shows the data of the chosen element and the name of the station in a pop-up balloon.

   Data at all stations in the selected area can be shown as a table by clicking the "Data list" button.

3. Historical graph and data

   A time-sequential graph for two years can be displayed by clicking on the station. The period of the graph can be changed (1 year, 2 years, 5 years and all years are available). The list of data used for the graph is indicated below it, and can be download as a text file by clicking the "Download" button.

3. Statistical research on El Nino impact by using Excel

El Nino/Southern Oscillation (ENSO) events influence global atmospheric circulations and convective activities. The influence to surface climate also appears globally. JMA implemented a statistical research about the relationships between ENSO and surface climate. The results are indicated in schematic figures on the TCC web site (fig.1, http://ds.data.jma.go.jp/tcc/tcc/products/climate/ENSO/index.htm). The impact on ENSO was tested by t-test (fig 2).

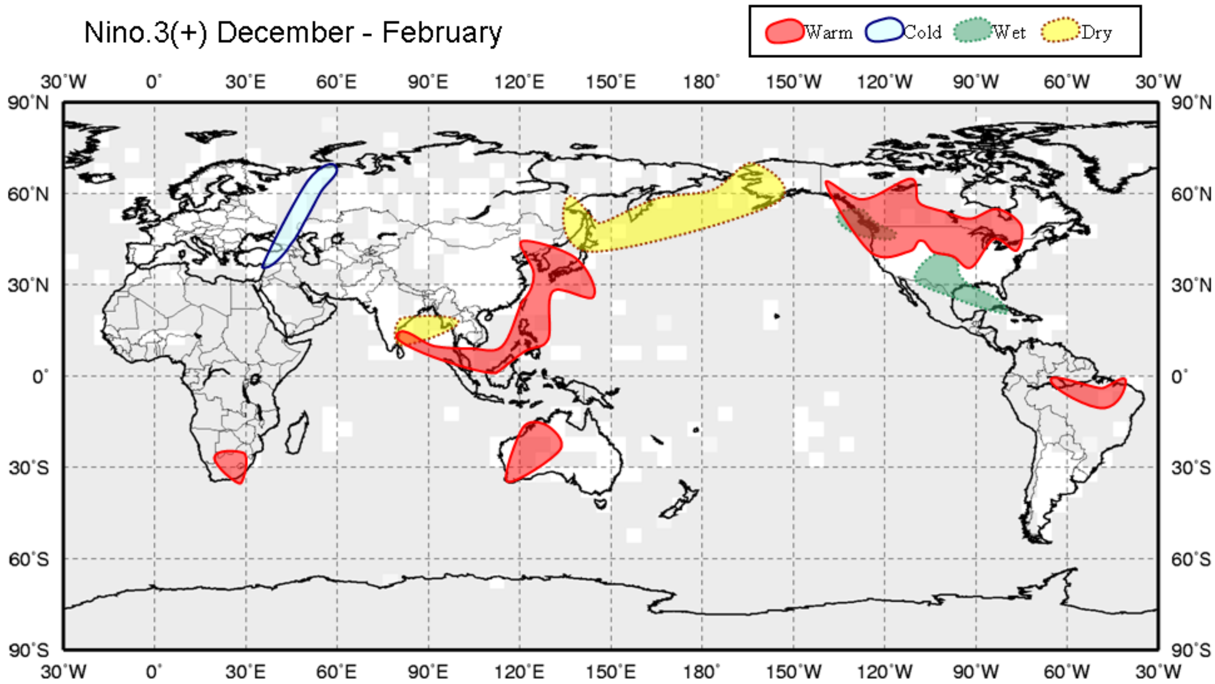

Fig. 1 Climate tendencies in El Nino Phase

Shadings indicate neither temperature nor precipitation data were enough to produce composite data.
Light shadings indicate either temperature or precipitation data were enough to produce composite data.

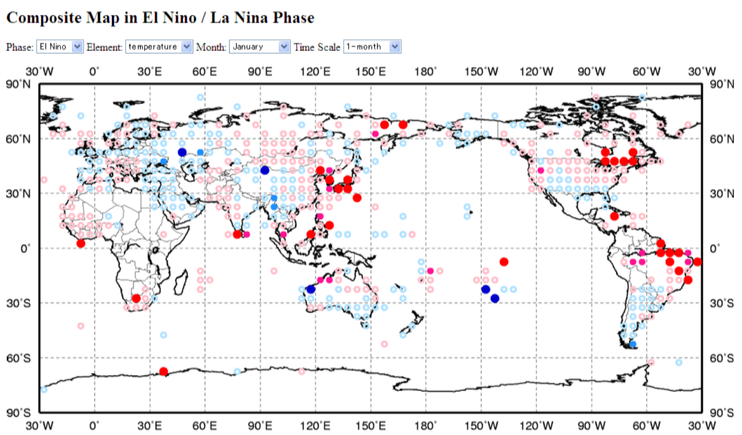

Fig. 2 Composite Map in El Nino

RED (**BLUE**):
Normalized temperature anomaly compared with neutral phase >= 0 (< 0)
GREEN (**Brown**):
Precipitation ratio compared with neutral phase >= 100% (< 100%)
Larger filled-marks:
Significant at 95% or more of confidence level
Smaller filled-marks:
Significant at 90% or more and less than 95% of confidence level

<Exercise>

In this work, we examine the statistical relationship between ENSO and surface climate by using the data in December 1979 – December 2011. The method is very simple as follows;

1) Select the historical surface climate data (temperature and precipitation)
2) Sort the data at a station (three running-mean) by the phase of El Nino, La Nina and neutral
3) Average the data in each phase compare the averaged data
4) Test the statistical significance

Here, this statistical research is similar to the method of JMA, but not exactly the same. In JMA research, detrended area-averaged climate data are used. The results from this research and JMA's research do not necessarily correspond to each other.

Open the Excel file "ENSO-Impact.xls". It has "Answer" sheet, "Work" sheet, "Data" sheet, and "Nino3 5-month mean" sheet. Details of the process are described below. "Data" sheet include temperature and precipitation data, which are used in this exercise. "Nino3 5-month mean" sheet has 5-month running mean SST anomaly in Nino.3 region.

1. First, make a copy of "Work" sheet as "Work (x)" (X=2, 3 …).

2. Second, copy the data in the "Data" sheet, then paste the data in green cell in the sheet of "Work (X)".

47807		Fukuoka	
year	month	temperature	precipitation
1979	12	9.3	82
1980	1	6.2	57
1980	2	5.1	32
….			
2011	10	19.7	127
2011	11	16.3	166.5
2011	12	8.5	38

Copy

The "Data" sheet

		Fukuoka	
year	month	temperature	precipitation
1979	12	9.3	82
1980	1	6.2	57
1980	2	5.1	32
….			
2011	10	19.7	127
2011	11	16.3	166.5
2011	12	8.5	38

→ Paste

The sheet of "Work (X)"

3. Confirm three month average temperature and three month cumulative precipitation. They are automatically calculated in the blue-colored cells, when data exist for consecutive three months (the preceding, the concerned and the following ones). Since we consider the El Nino as seasonal phenomenon, we make these calculations.

				Fukuoka						Fukuoka	
5 month mean SST deviation (NINO.3)	ENSO event	year	mid-month	3 month mean temperature	3 month total precipitation		ENSO event	year	mid-month	3 month mean temperature	3 month total precipitation
0.6	EL	1979	12								
0.5	EL	1980	1	6.866667	171						
0.4	NE	1980	2	6.966667	221						
0.3	NE	1980	3	9.566667	267						

Blue-colored cells in these two columns are filled automatically, when all three months have monthly data. Here, three months are the preceding, the concerned and the following ones.

The sheet of “Work (X)”

4. Copy and paste the calculated data (value) to the next blue cells. -- Copy the cells from column “ENSO event” to column “3 month total precipitation”. Then select the cell “L3”. On the <Edit> menu, click <Paste Special>, and then select <value>. If you did not do this work, the 3 month data are unreasonable after next process.

				Fukuoka						Fukuoka	
5 month mean SST deviation (NINO.3)	ENSO event	year	mid-month	3 month mean temperature	3 month total precipitation		ENSO event	year	mid-month	3 month mean temperature	3 month total precipitation
0.6	EL	1979	12								
0.5	EL	1980	1	6.866667	171						
0.4	NE	1980	2	6.966667	221						
0.3	NE	1980	3	9.566667	267						

Copy

Select these columns. Then on the <Edit> menu, click <Paste Special>, and select <value>

The sheet of “Work (X)”

5. Next, sort the data. -- Click a cell in the pasted column from “ENSO event” to “3 month total precipitation”. On the <Data> menu, click <Sort>. In the <Sort by> box, click the column of “mid-month” with <Ascending> sort option, and <Then by> box, click the column of “ENSO event” with <Ascending> sort option, and then click <OK>.
6. Statistical results are shown from column “R” to column “Y” except the result for Dec-Feb (mid-month = 1).
   Please calculate average temperature in each El Nino and La Nina phase using “average” function.
7. After that, calculate the statistical significance on the difference of average using “ttest” function.
   Example: “=TTEST (O3:O12, O23:O34, 2, 2)” for t-test,
   “=TTEST (O3:O12, O23:O34, 2, 3)” for Welch-test
8. Make a graph of the average of 3 month mean temperature for each phase. You may change the graph option.

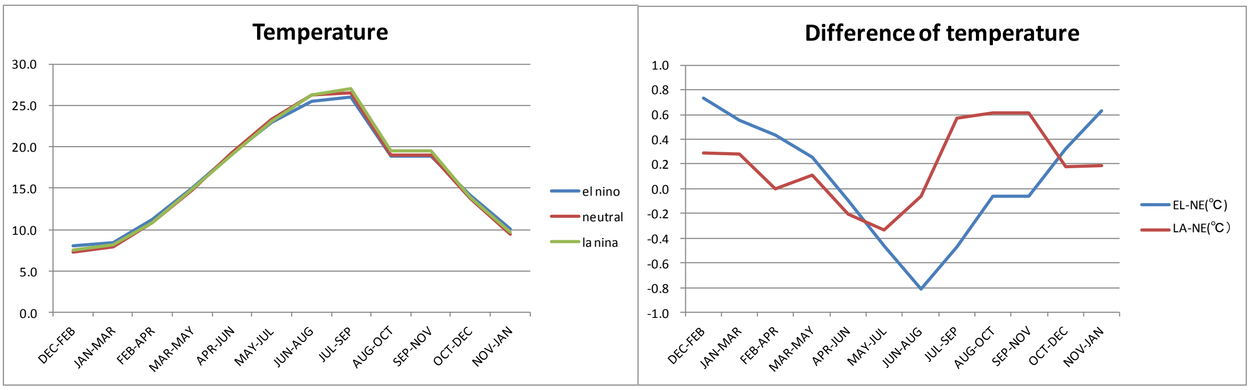

9. Make a graph of average of 3 month total precipitation for each phase. -- Similar to above, using the precipitation table.

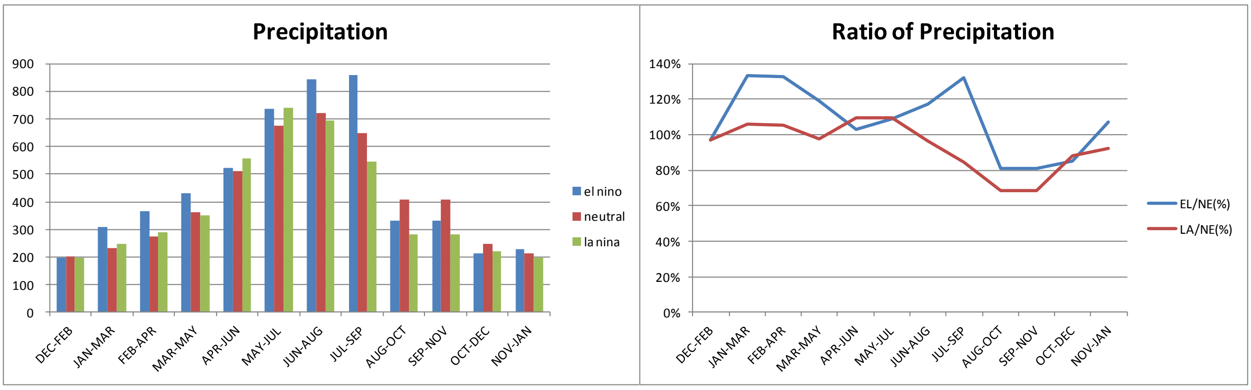

10. Grasp the character of data including statistical tests.

Appendix

"**Manual on Codes**" WMO-No.306

FM 71-XII CLIMAT **Report of monthly values from a land station**

CODE FORM:

SECTION 0	CLIMAT	MMJJJ	IIiii		
SECTION 1	111	$1\overline{P_0P_0P_0P_0}$	$2\overline{PPPP}$	$3s_n\overline{TTT}s_ts_ts_t$	$4s_n\overline{T_xT_xT_x}s_n\overline{T_nT_nT_n}$
		$5\overline{eee}$	$6R_1R_1R_1R_1n_rn_r$	$7S_1S_1S_1p_Sp_Sp_S$	$8m_Pm_Pm_Tm_Tm_{Tx}m_{Tn}$
		$9m_em_em_Rm_Rm_Sm_S$			
SECTION 2	(222	$0Y_bY_bY_cY_c$	$1\overline{P_0P_0P_0P_0}$	$2\overline{PPPP}$	$3s_n\overline{TTT}s_ts_ts_t$
		$4s_n\overline{T_xT_xT_x}s_n\overline{T_nT_nT_n}$	$5\overline{eee}$	$6R_1R_1R_1R_1n_rn_r$	$7S_1S_1S_1$
		$8y_Py_Py_Ty_Ty_{Tx}y_{Tx}$	$9y_ey_ey_Ry_Ry_Sy_S$)		
SECTION 3	(333	$0T_{25}T_{25}T_{30}T_{30}$	$1T_{35}T_{35}T_{40}T_{40}$	$2T_{n0}T_{n0}T_{x0}T_{x0}$	$3R_{01}R_{01}R_{05}R_{05}$
		$4R_{10}R_{10}R_{50}R_{50}$	$5R_{100}R_{100}R_{150}R_{150}$	$6s_{00}s_{00}s_{01}s_{01}$	$7s_{10}s_{10}s_{50}s_{50}$
		$8f_{10}f_{10}f_{20}f_{20}f_{30}f_{30}$	$9V_1V_1V_2V_2V_3V_3$)		
SECTION 4	(444	$0s_nT_{xd}T_{xd}T_{xd}y_xy_x$	$1s_nT_{nd}T_{nd}T_{nd}y_ny_n$	$2s_nT_{ax}T_{ax}T_{ax}y_{ax}y_{ax}$	
		$3s_nT_{an}T_{an}T_{an}y_{an}y_{an}$	$4R_xR_xR_xR_xy_ry_r$	$5i_wf_xf_xf_xy_{fx}y_{fx}$	
		$6D_{ts}D_{ts}D_{gr}D_{gr}$	$7i_yG_xG_xG_nG_n$)		

Notes:

(1) CLIMAT is the name of the code for reporting monthly values from a land station.

(2) The CLIMAT code form consists of five sections:

Section number	*Symbolic figure group*	*Contents*
0	—	Code name and groups MMJJJ IIiii
1	111	Monthly data of the month referred to in MMJJJ including number of days missing from the records. This section is mandatory
2	222	Monthly normals corresponding to the month referred to in MMJJJ including number of years missing from the calculation
3	333	Number of days in the month with parameters beyond certain thresholds during the month referred to in MMJJJ
4	444	Extreme values during the month referred to in MMJJJ and occurrence of thunderstorms and hail

Symbolic letters and remarks as to the methods of coding (Section1)

$\overline{P_0P_0P_0P_0}$	Monthly mean pressure at station level, in tenths of a hectopascal, omitting the thousands digit. (FM 71)
$\overline{PPPP}$	Monthly mean pressure, in tenths of a hectopascal, omitting the thousands digit or monthly mean geopotential, in standard geopotential metres, for surface stations. (FM 71, FM 72)
s_n	Sign of the data, and relative humidity indicator. (Code table 3845) (FM 12, FM 13, FM 14, FM 18, FM 22, FM 36, FM 62, FM 63, FM 64, FM 67, FM 71, FM 72, FM 86)
$\overline{TTT}$	Monthly mean air temperature, in tenths of a degree Celsius, its sign being given by s_n. (FM 71, FM 72)
$s_ts_ts_t$	Standard deviation of daily mean values relative to the monthly mean air temperature, in tenths of a degree Celsius. (FM 71)
$\overline{T_xT_xT_x}$	Mean daily maximum air temperature of the month, in tenths of a degree Celsius, its sign being given by s_n. (FM 71)
$\overline{T_nT_nT_n}$	Mean daily minimum air temperature of the month, in tenths of a degree Celsius, its sign being given by s_n. (FM 71)
$\overline{eee}$	Mean vapour pressure for the month, in tenths of a hectopascal. (FM 71, FM 72)
$R_1R_1R_1R_1$	Total precipitation for the month. (Code table 3596) (FM 71, FM 72)
n_rn_r	Number of days in the month with precipitation equal to or greater than 1 millimetre. (FM 71, FM 72)
$S_1S_1S_1$	Total sunshine for the month to the nearest hour. (FM 71)
$p_Sp_Sp_S$	Percentage of total sunshine duration relative to the normal. (FM 71)
m_Pm_P	Number of days missing from the records for pressure. (FM 71)
m_Tm_T	Number of days missing from the records for air temperature. (FM 71)
m_{Tx}	Number of days missing from the record for daily maximum air temperature. (FM 71)
m_{Tn}	Number of days missing from the record for daily minimum air temperature. (FM 71)
m_em_e	Number of days missing from the records for vapour pressure. (FM 71)
m_Rm_R	Number of days missing from the records for precipitation. (FM 71)
m_Sm_S	Number of days missing from the records for sunshine duration. (FM 71)

Annual cycle of atmospheric circulation and sea surface temperatures in the tropics

Annual cycle of atmospheric circulation and sea surface temperatures in the tropics

This report summarizes characteristics seen in the annual cycle of atmospheric circulation and sea surface temperatures (SSTs) in the tropics with particular focus on areas around the equator using climatological normal data (i.e., the 1981 – 2010 average). JRA/JCDAS (Onogi et al. 2007) atmospheric circulation data and COBE-SST (JMA 2006) sea surface temperature (SST) data were used for this explanatory text. The outgoing longwave radiation (OLR) data referenced to infer tropical convective activity were originally provided by NOAA.

1. SSTs in the tropics

In the western tropical Pacific, which has some of the highest SSTs in the world, values exceeding 29˚C are seen throughout the year (Figures 1 and 2 (b)). SSTs in the western equatorial Pacific show their first annual peak in May and the first half of June, and areas of high SSTs then move northward. SSTs east of the Philippines (15˚N – 20˚N) reach their annual maximum from the second half of June to early August, and values exceeding 29.5˚C extend to around 150˚E. SSTs exceeding 28˚C extend further northward, passing 30˚N from late July to the first half of September. Areas of high SSTs gradually migrate southward in boreal autumn (September – November), and SSTs in the western equatorial Pacific show their second annual peak in November. Areas of high SSTs in the western Pacific move into the Southern Hemisphere with a core reaching around 10˚S – 15˚S.

In the eastern Pacific, SST values along the equator remain below those observed north and south of it throughout the year (Figures 1 and 2 (c)). Zonally elongated high SSTs exceeding 27˚C are seen north of the equator (5˚N – 15˚N) throughout the year, with their northernmost position observed in September. In boreal spring (March – May), double high-SST areas are seen north and south of the equator (5˚S – 15˚S) with comparable magnitudes. SSTs north of the equator are higher than those south of it throughout the year except in boreal spring.

In the equatorial Indian Ocean, SSTs reach their annual maximum in April and May (Figures 1 and 2 (a)). Areas of high SSTs gradually extend northward in the North Indian Ocean, and SSTs in the 5˚N – 15˚N area show their annual maximum and first peak in late April and May with some values exceeding 30˚C. SSTs in the North Indian Ocean temporarily decrease in the summer monsoon season and bottom out in August before increasing and reaching a second peak in October when the summer monsoon withdraws. Areas of high SSTs move into the Southern Hemisphere in boreal winter (December – February) and early spring.

In the Atlantic, equatorial SSTs reach their annual maximum in boreal spring (Figures 1 and 2 (d)). The core of high SSTs is seen in the Gulf of Mexico and the Caribbean Sea in boreal summer (June – August), and areas of high SSTs extend eastward from summer to autumn before moving into the Gulf of Guinea in boreal winter.

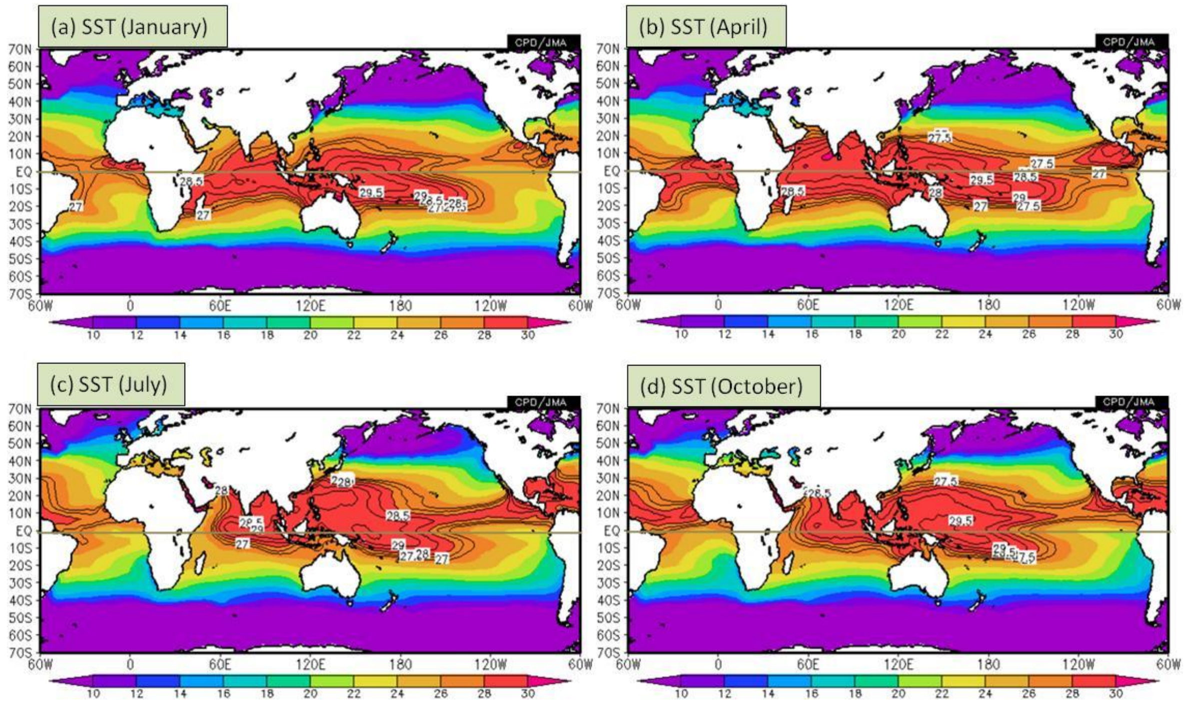

Figure 1 Monthly mean normal SSTs

The base period for the normal is 1981 – 2010. (a), (b), (c) and (d) indicate January, April, July and October, respectively. The contours show SSTs at intervals of 0.5˚C for values of 27˚C and above. The gray lines indicate the equator.

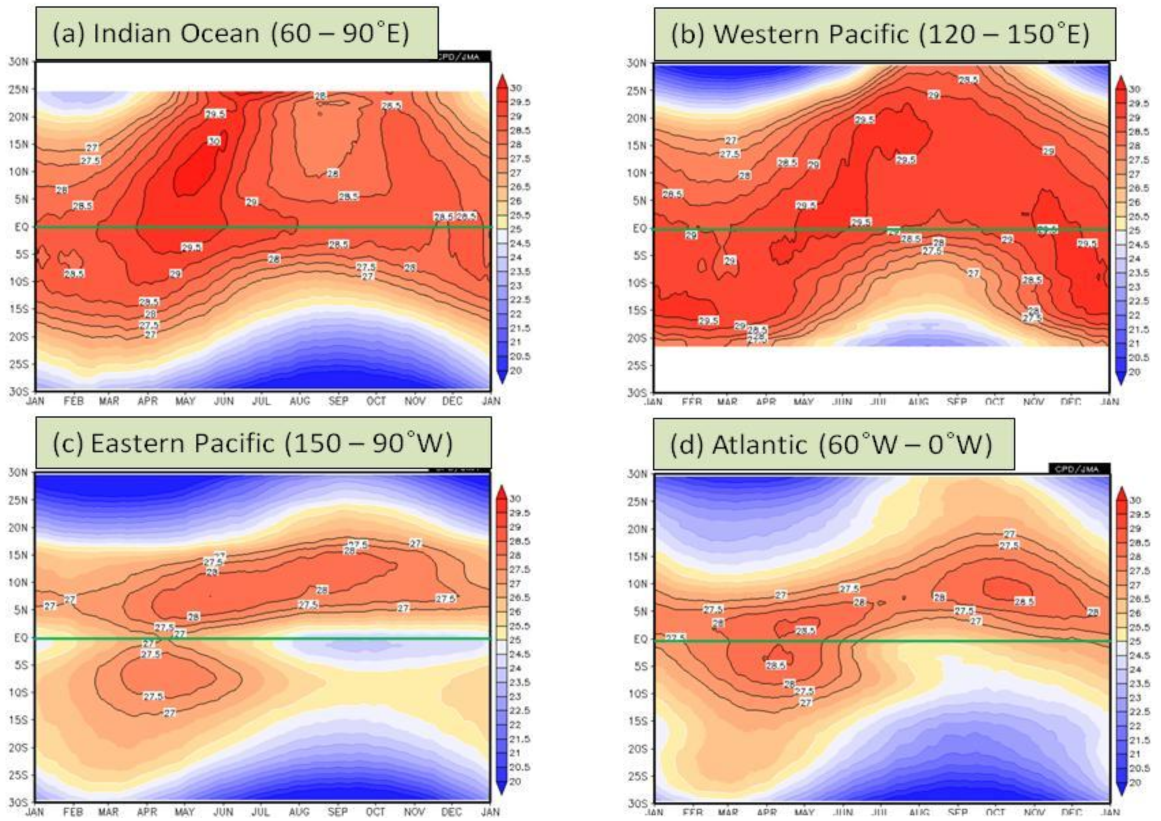

Figure 2 Annual cycle of zonal-mean daily-average normal sea surface temperatures (SSTs)

The base period for the normal is 1981 – 2010. (a), (b), (c) and (d) show the Indian Ocean (60˚E – 90˚E), the western Pacific (120˚E – 150˚E), the eastern Pacific (150˚W – 90˚W) and the Atlantic (60˚W – 0˚W), respectively. The contours show SSTs at intervals of 0.5˚C for values of 27˚C and above. The green lines indicate the equator.

2. Tropical convective activity

Large-scale active convection areas in the tropics are seen from South America to Central America, over Africa and from the eastern Indian Ocean to the western Pacific, where convective activity is the most enhanced and the most significant among the three regions (Figure 3). These areas migrate northward or northwestward from boreal winter to summer and southward or southeastward from boreal summer to winter.

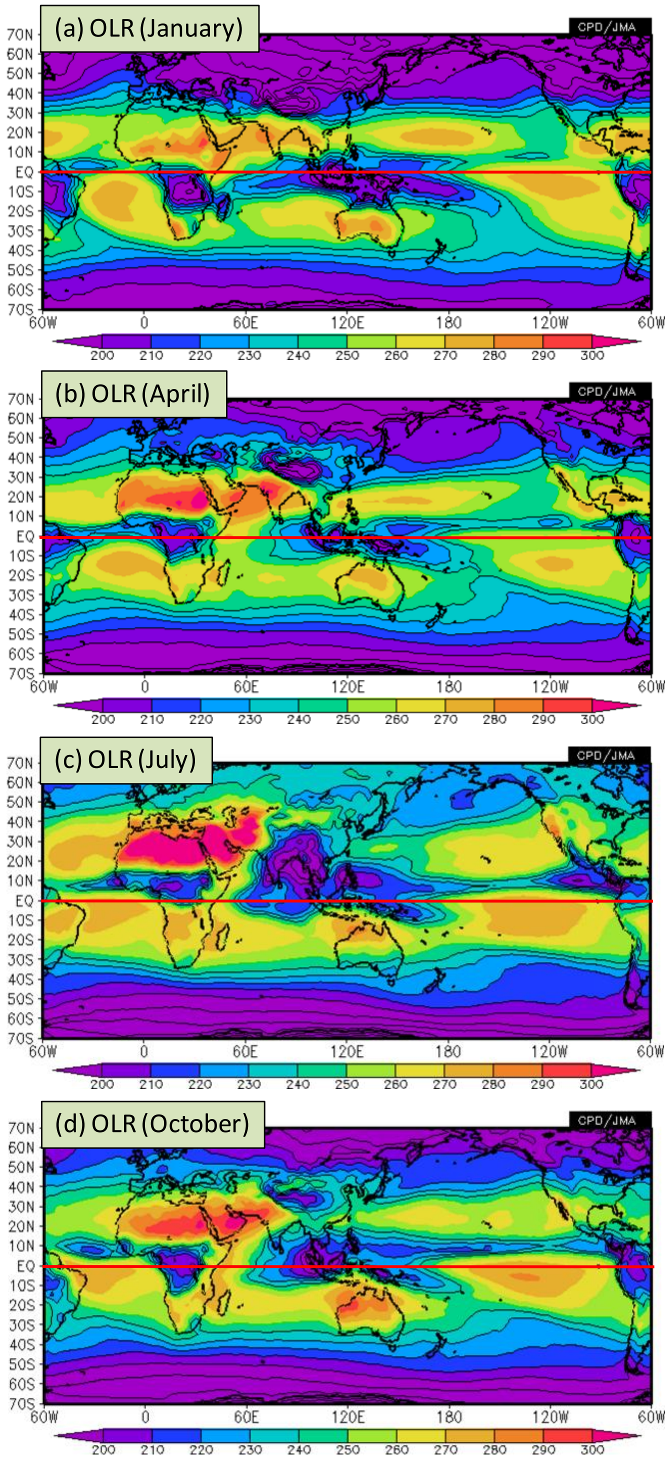

Figure 3 Monthly mean normal outgoing longwave radiation (OLR)
The base period for the normal is 1981 – 2010. (a), (b), (c) and (d) indicate January, April, July and October, respectively. The contours show OLR at intervals of 10 W/m^2 for values of 240 W/m^2 and below. The red lines indicate the equator.

In the western Pacific, convective activity around the equator is enhanced throughout the year (Figures 3 and 4 (b)). Enhanced convective activity east of the Philippines (10˚N – 20˚N) persists from June to October, reaching its annual maximum and its northernmost extent in the first half of August. The core of active convection is seen north of Australia in boreal winter.

In the eastern Pacific, active convection areas are confined to approximately between 5˚N and 15˚N, corresponding to the intertropical convergence zone (ITCZ) (Figures 3 and 4 (c)). Convective activity south of the equator (around 5˚S) is moderately enhanced in March and April, showing the double ITCZ.

In the Indian Ocean, convective activity over central and eastern equatorial areas is generally enhanced throughout the year (Figures 3 and 4 (a)). Active convection areas in the North Indian Ocean move northward from May to July, exhibiting their annual maximum intensity and their northernmost extent in the second half of July and the first half of August. This northward migration of active convection areas lags that of high SSTs (Figure 2 (a)) by approximately one or two months. In boreal winter and early spring, convective activity is enhanced mainly south of the equator centered near 5˚S.

In the Atlantic, convective activity north of the equator (0˚ – 10˚N) generally remains enhanced throughout the year (Figures 3 and 4 (d)). In the 60˚W – 0˚W zonal average field, the annual cycle of active convection areas is approximately parallel to that of areas of high SSTs (Figure 2 (d)).

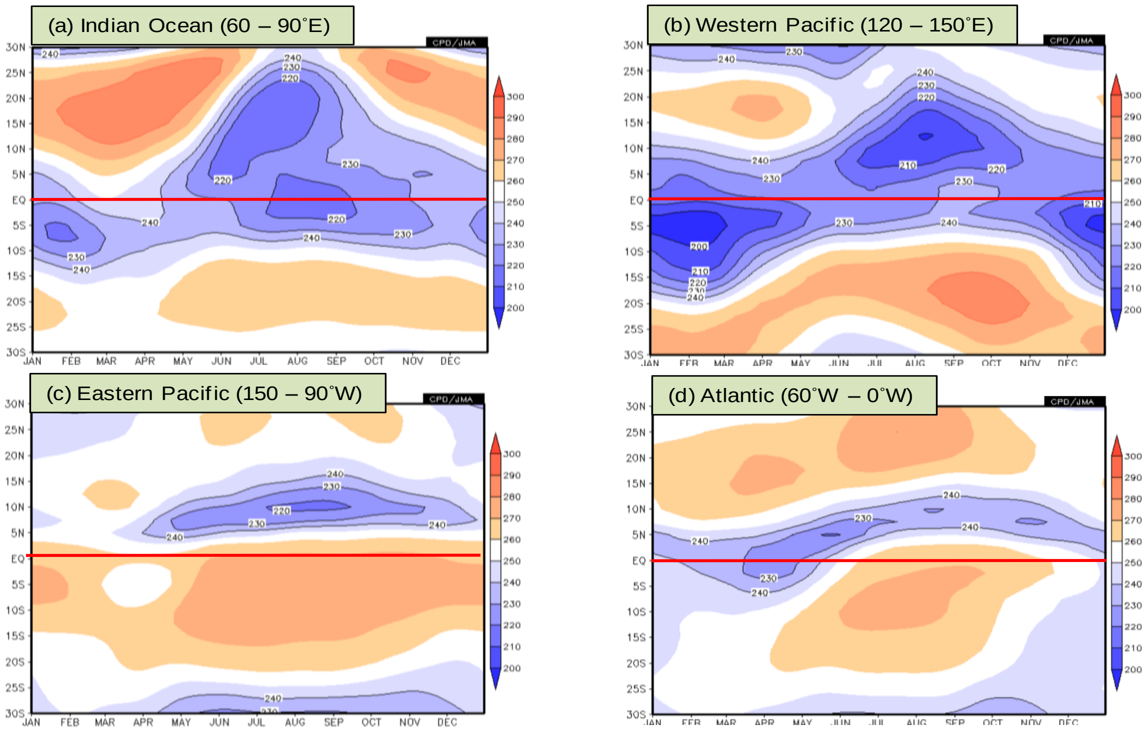

Figure 4 Annual change in zonal-mean daily-average normal OLR

The base period for the normal is 1981 – 2010. (a), (b), (c) and (d) show the Indian Ocean (60˚E – 90˚E), the western Pacific (120˚E – 150˚E), the eastern Pacific (150˚W – 90˚W) and the Atlantic (60˚W – 0˚W), respectively. The contours show OLR at intervals of 10 W/m^2 for values of 240 W/m^2 and below. The red lines indicate the equator.

3. Atmospheric circulation in the tropics

3.1 Lower-tropospheric circulation (Figure 5)

Zonally elongated high-pressure systems (subtropical highs) are seen over subtropical areas of the North and South Pacific, the North and South Atlantic, and the South Indian Ocean throughout most of the year centered near 30˚N or 30˚S. The subtropical highs are strongest in summer and weakest in winter. The centers of subtropical highs over the Pacific and the Atlantic are observed in eastern parts of these oceans. Easterly winds (i.e., northeasterly and southeasterly trade winds in the Northern and Southern Hemisphere, respectively) prevail throughout the year in the tropical area between the subtropical highs of the Northern Hemisphere and the Southern Hemisphere.

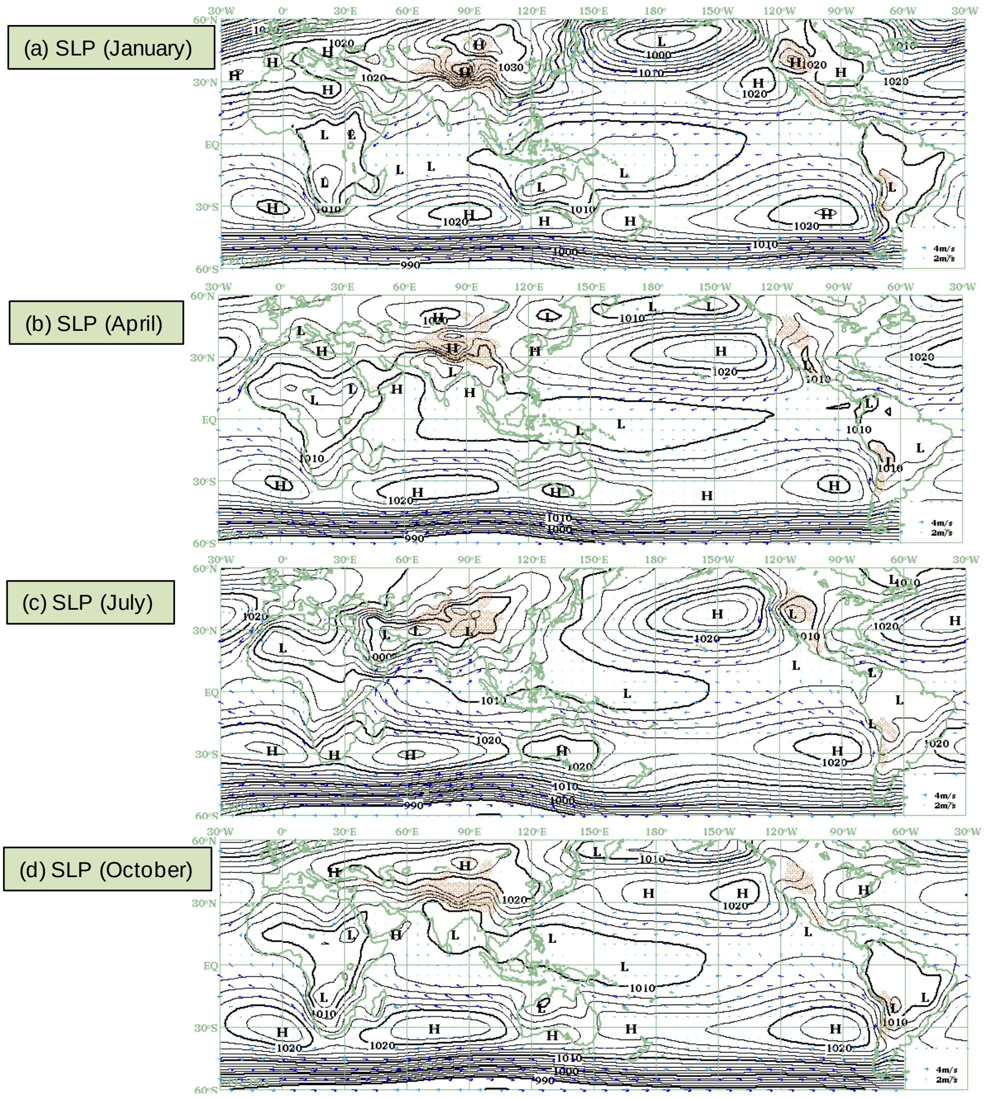

Figure 5 Monthly mean normal sea level pressure (SLP) and surface wind vectors
The base period for the normal is 1981 – 2010. (a), (b), (c) and (d) indicate January, April, July and October, respectively. The contours show SLP at intervals of 10 hPa for values below 990 hPa and 2 hPa for values above 990 hPa. The arrows denote wind vectors 10 m above the surface.

3.2 Upper-tropospheric circulation (Figure 6)

Anticyclones are seen over subtropical continents in the summer hemisphere. For example, the Tibetan High is developed over southern Eurasia in boreal summer. Distinct troughs are seen over central parts of the North Pacific and the North Atlantic in boreal summer; that over the Pacific is referred to as the mid-Pacific trough. In boreal winter, a pair of troughs straddling the equator is seen over the eastern Pacific and the central Atlantic, and related westerly winds prevail around equatorial areas. A pair of anticyclones straddling the equator is seen over the western Pacific in boreal winter.

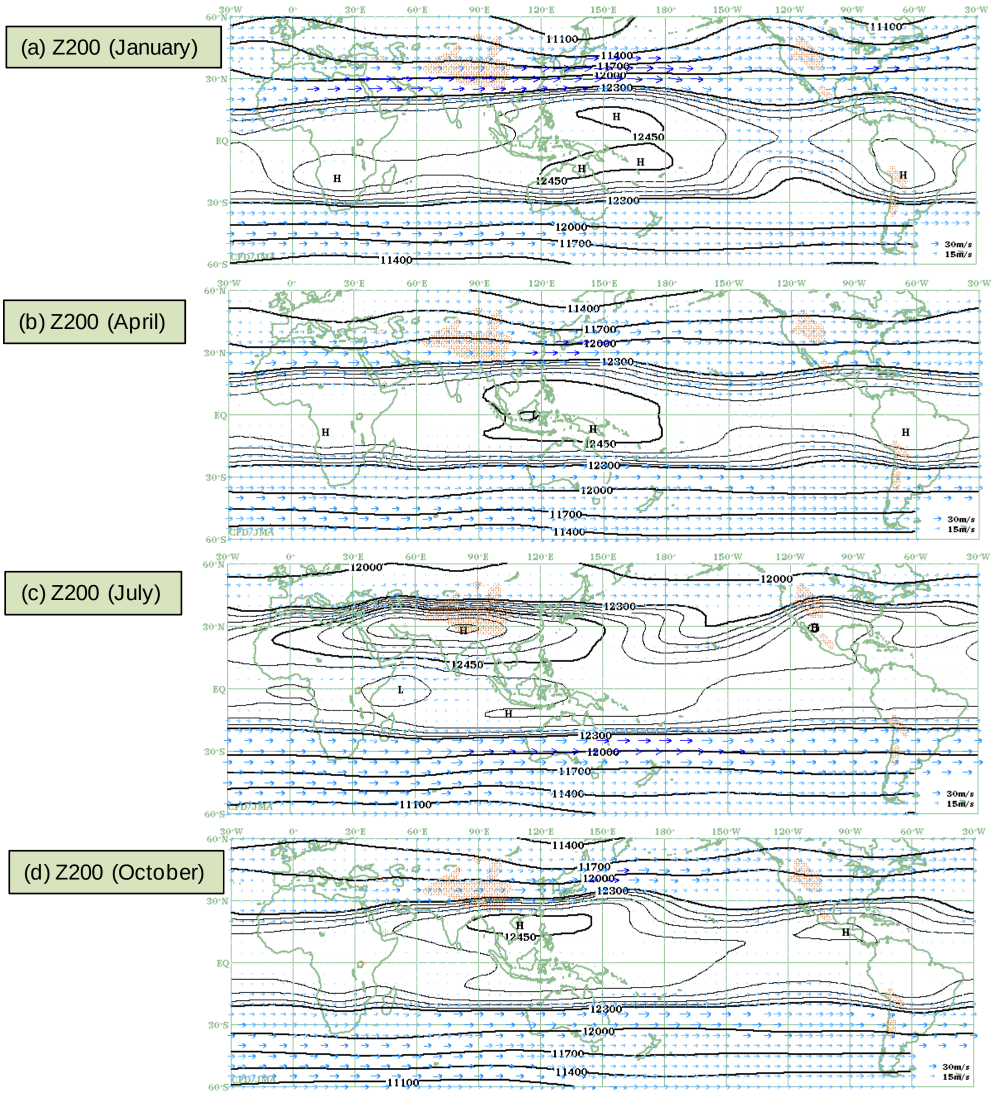

Figure 6 Monthly mean normal 200-hPa geopotential height and wind vectors
The base period for the normal is 1981 – 2010. (a), (b), (c) and (d) indicate January, April, July and October, respectively. The contours show 200-hPa geopotential height at intervals of 300 m for values below 12,300 m and 30 m for values above 12,300 m. The vectors denote 200-hPa wind vectors.

3.3 Zonal-vertical circulation along the equator (Figure 7)

Upward flow is seen over the western Pacific in line with large-scale active convection. In the upper troposphere, the upward flow is split into westward and eastward flow descending over the western Indian Ocean and the eastern Pacific, respectively. In the lower troposphere, the downward flow changes direction in the western Pacific. These zonal-vertical movements are collectively called the Walker circulation. Those over the Pacific and the Indian Ocean are distinct in boreal winter and summer, respectively.

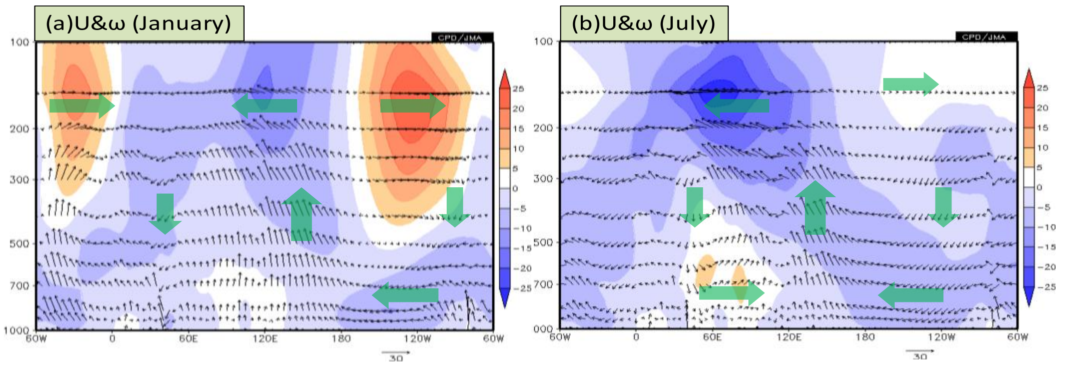

Figure 7 Zonal-vertical sections of monthly mean normal circulation along the equator (5˚S – 5˚N average)
The base period for the normal is 1981 – 2010. (a) and (b) indicate January and July, respectively. The vectors indicate zonal-vertical circulation, and their vertical components (unit: Pa/s) are multiplied by -300. The shading denotes zonal wind speeds (unit: m/s) at intervals of 5 m/s, and positive (warm color) and negative (cold color) values show westerly and easterly winds, respectively.

3.4 Meridional-vertical circulation zonally averaged in the hemisphere (Figure 8)

Upward and downward flow is seen over the tropics of the summer and winter hemispheres where air temperatures in the lower troposphere are relatively high and low, respectively. In the upper troposphere, most of the upward flow moves southward across the equator and descends over 10 – 30 degrees latitude in the winter hemisphere. In the lower troposphere, the downward flow changes direction toward the summer hemisphere. This meridional-vertical movement is collectively called the Hadley circulation. The annual cycle of ascending-flow areas is in line with that of active convection areas, which is approximately parallel to that of solar elevation.

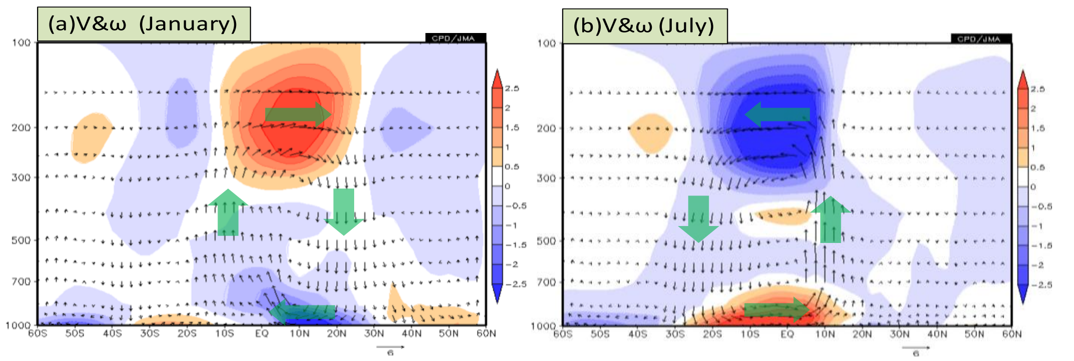

Figure 8 Meridional-vertical sections of monthly mean normal circulation zonally averaged in the hemisphere
The base period for the normal is 1981 – 2010. (a) and (b) indicate January and July, respectively. The vectors indicate meridional-vertical circulation, and their vertical components (unit: Pa/s) are multiplied by -100. The shading denotes meridional wind speeds (unit: m/s) at intervals of 0.5 m/s, and positive (warm color) and negative (cold color) values show southerly and northerly winds, respectively.

3.5 Zonal and meridional winds along the equator

In the lower troposphere, the zonal components of equatorial winds (Figure 9 (a)) along the central and eastern Pacific are easterly throughout the year, showing their annual maximum in boreal winter. Zonal winds along the western equatorial Pacific and Indonesia show westerly and easterly winds in boreal winter and summer, respectively. Westerly and easterly winds over the eastern equatorial Gulf of Guinea and other parts of the equatorial Atlantic, respectively, are seen throughout the year.

In the lower troposphere, the meridional components of equatorial winds (Figure 9 (b)) along the eastern Pacific are southerly throughout the year, exhibiting their annual maximum in September and their minimum in March. Equatorial meridional winds from the Indian Ocean to the dateline region are northerly and southerly from December to March and from May to October, respectively, reversing in direction in April and November. In boreal summer, predominant southerly winds are seen over the western equatorial Indian Ocean, corresponding to the movement of the Somali jet. Southerly winds are generally seen throughout the year over the equatorial Atlantic, especially in the Gulf of Guinea.

In the upper troposphere, the zonal components of equatorial winds (Figure 10 (a)) over the Indian Ocean and the western Pacific are easterly throughout the year, showing their annual maximum in boreal summer. Easterly and westerly winds are seen along the central and eastern equatorial Pacific in boreal summer and winter, respectively.

In the upper troposphere, the meridional components of equatorial winds (Figure 10 (b)) over parts of the Atlantic (30˚W – 0˚) and parts of the eastern Pacific (around 120˚W) are northerly, and those in other areas (i.e., most equatorial areas of the globe) are northerly and southerly in boreal summer and winter, respectively.

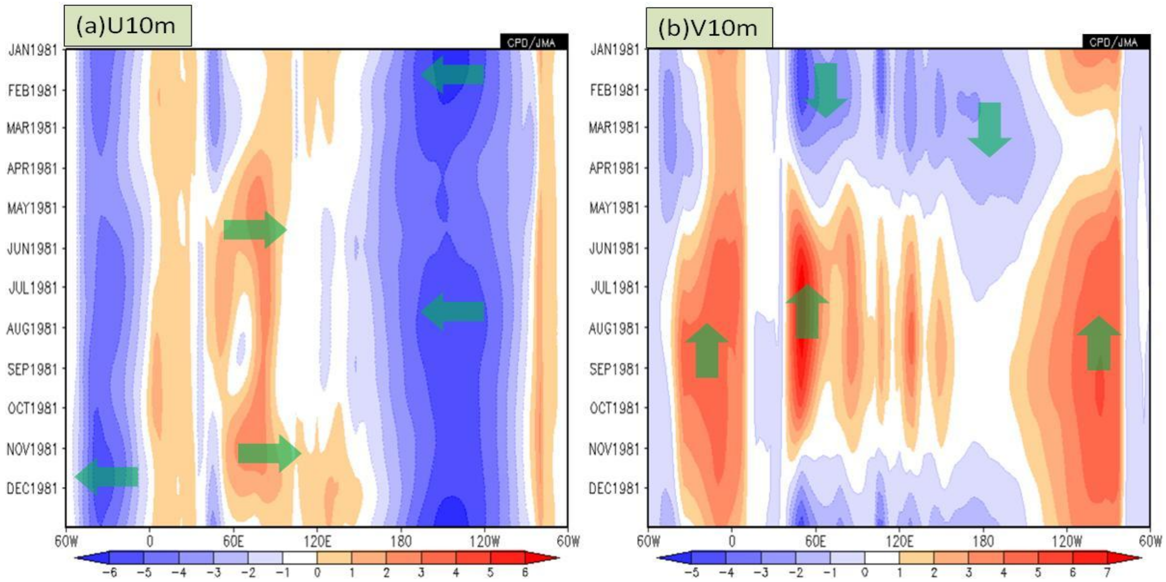

Figure 9 Annual cycle of daily-average normal surface winds along the equator (5˚S – 5˚N average)
The base period for the normal is 1981 – 2010. (a) The shading indicates zonal wind speeds at intervals of 1 m/s. Positive (warm color) and negative (cold color and white) values show westerly and easterly winds, respectively. (b) The shading indicates meridional wind speeds at intervals of 1 m/s. Positive (warm color and white) and negative (cold color) values denote southerly and northerly winds, respectively.

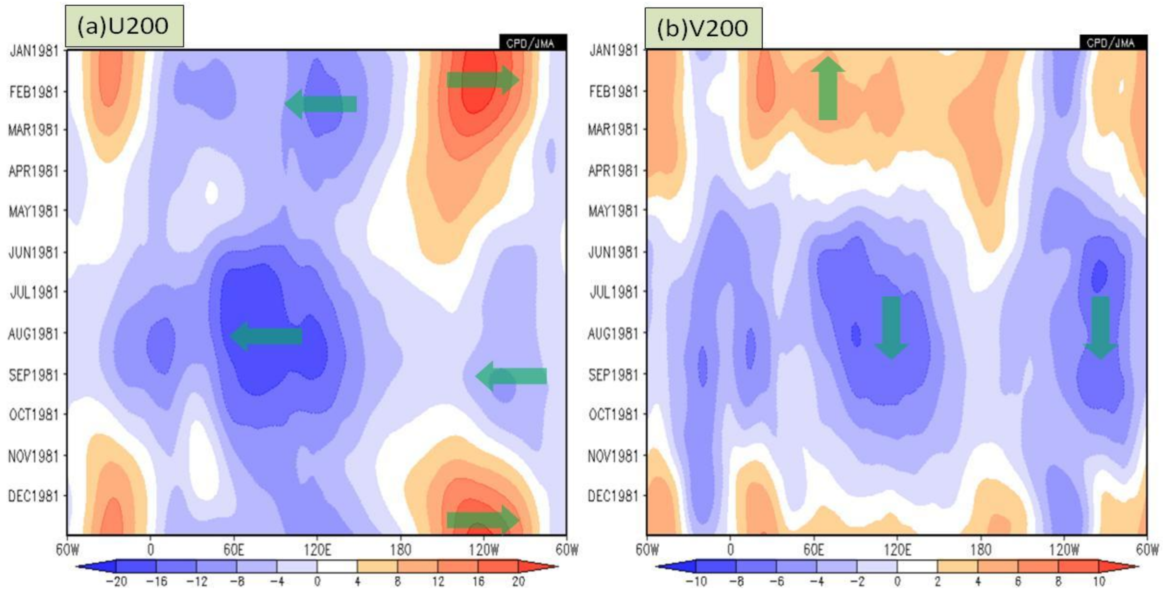

Figure 10 Annual cycle of daily-average normal 200-hPa winds along the equator (5˚S – 5˚N average)
The base period for the normal is 1981 – 2010. (a) The shading indicates zonal wind speeds at intervals of 4 m/s. Positive (warm color and white) and negative (cold color) values show westerly and easterly winds, respectively. (b) The shading indicates meridional wind speeds at intervals of 2 m/s. Positive (warm color and white) and negative (cold color) values denote southerly and northerly winds, respectively.

Annual cycle of Asian monsoon circulation

Annual cycle of Asian monsoon circulation

This report summarizes characteristics seen in the annual cycle of large-scale atmospheric circulation associated with the Asian monsoon using climatological normal data (i.e., the 1981 – 2010 average). JRA/JCDAS (Onogi et al. 2007) atmospheric circulation data and COBE-SST (JMA 2006) sea surface temperature (SST) data were used for this explanatory text. The outgoing longwave radiation (OLR) data referenced to infer tropical convective activity were originally provided by NOAA.

1. General characteristics of Asian monsoon circulation

The term *monsoon* primarily refers to seasonal winds (i.e., the annual cycle of a prevailing wind system), and is broadly defined as such winds accompanied by an annual cycle of rainfall (i.e., wet/dry seasons). Regions where seasonal winds prevail are called monsoonal climate zones, and Asia is the world's most prominent.

The Asian monsoon is a large-scale wind system driven by the thermal contrast between the Eurasian Continent and oceans caused by the heat capacity difference between the two (i.e., the continent heats and cools more readily).

In boreal summer, the Eurasian Continent is effectively heated due to high solar elevation, leading to increased near-surface temperatures over the continent (i.e., reduced surface pressure). Consequently, continental surface pressure is lower than that over oceans, and surface air flows from the latter to the former. Surface air flowing from the Indian Ocean to the continent curves to the right of its travel direction under the influence of the Coriolis force in the Northern Hemisphere (and vice-versa in the Southern Hemisphere). As the vast high mountains and highlands of southern Eurasia (e.g., the Himalayas and the Tibetan Plateau) prevent surface air from directly flowing inland to the continent, it flows anti-clockwise over the southern and eastern periphery of the Tibetan Plateau. As a result, southwesterly or westerly winds (i.e., monsoon westerlies) prevail over southern Asian areas including India and the Indochina Peninsula, and southerly winds are predominant over East Asia.

In boreal winter, radiation cooling outweighs solar-radiation heating due to low solar elevation, leading to reduced near-surface temperatures over Eurasia (i.e., increased surface pressure). Consequently, surface pressure is higher over the continent than over oceans, and surface air flows from the former to the latter. Northerly or northwesterly winds prevail over East Asia, and northeasterly or easterly winds are dominant over southern Asia due to the effect of the Coriolis force and the topographic features of the continent.

Figure 1 shows monthly mean atmospheric circulation in the upper and lower troposphere and convective activity for January and July in the climatological normal.

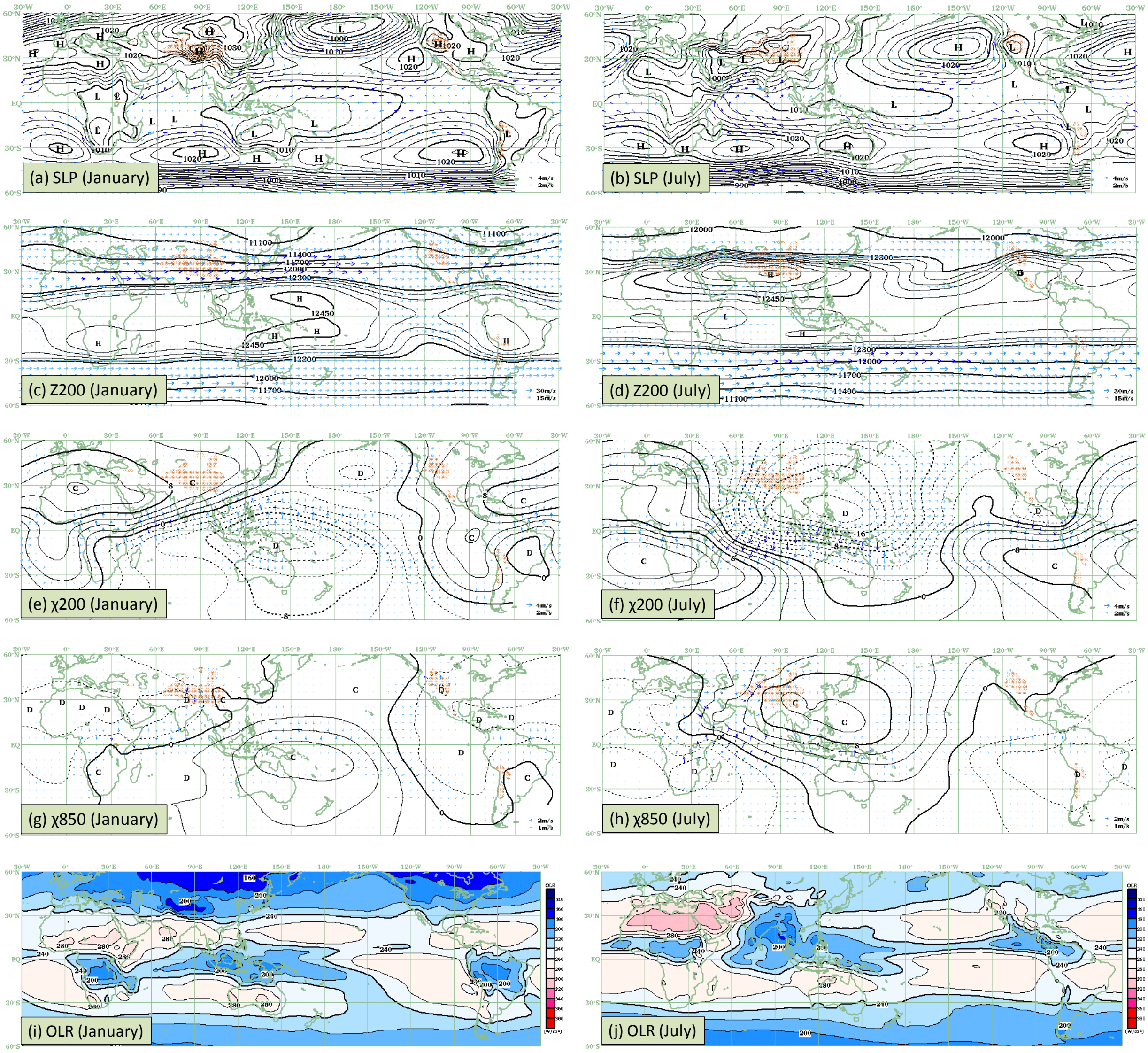

Figure 1 Monthly mean normal atmospheric circulation

The base period for the normal is 1981 – 2010. The panels on the left (a, c, e, g, i) and right (b, d, f, h, j) show monthly mean normal atmospheric circulation for January and July, respectively. (a) and (b): The contours indicate sea level pressure (SLP) at intervals of 10 hPa for values below 990 hPa and 2 hPa for values above 990 hPa. The arrows show wind vectors at 10 m above the surface. (c) and (d): The contours indicate 200-hPa geopotential height at intervals of 300 m for values below 12,300 m and 30 m for values above 12,300 m. The arrows show 200-hPa wind vectors. (e) and (f): The contours indicate 200-hPa velocity potential at intervals of 2×10^6 m^2/s. The arrows show 200-hPa divergent wind vectors. (g) and (h): The contours indicate 850-hPa velocity potential at intervals of 2×10^6 m^2/s. The arrows show 850-hPa divergent wind vectors. (i) and (j): The shading and contours indicate outgoing longwave radiation (OLR) at 20 W/m^2. Original data provided by NOAA.

In the sea level pressure (SLP) and near-surface field for July (Figure 1 (b)), a broad low-pressure system is seen over Eurasia centered in West Asia and the Tibetan Plateau, and monsoon westerly winds are predominant across the Arabian Sea and southern Asia on the southern side of the low-pressure system. The near-surface air diverging from the Mascarene High (a subtropical high over the South Indian Ocean) flows northwestward, converges east of Africa and flows northward across the equator. The flow moves to southern Asia with its direction changing from northward to westward over the Arabian Sea. The low-level strong winds blowing to the east of Africa are called the Somali jet, which transports large amounts of water vapor from the Arabian Sea and the South Indian Ocean to areas of southern Asia including India, contributing to monsoon rainfall. The Pacific High (a quasi-stationary large-scale subtropical anticyclone) is seen widely over the North Pacific centered to the west of North America. The ridge of the Pacific High extends northwestward to the south of Japan, and easterly winds (i.e., trade winds) are predominant on the equatorial side of the high. These winds meet with monsoon westerlies over parts of the northwestern tropical Pacific including the vicinity of the Philippines, converging and leading to active convection (Figure 1 (j)).

In the SLP and near-surface field for January (Figure 1 (a)), a wide high-pressure system (i.e., the Siberian High) is observed over Eurasia centered southwest of Lake Baikal, and a large low-pressure system (i.e., the Aleutian Low) is seen over the northern North Pacific. In association, strong zonal SLP gradients and prominent northerly winds are seen in and around Japan, which is located between the Siberian High and the Aleutian Low. The continental high-pressure system extends to southern China and West Asia, and northeasterly winds are seen over the South China Sea and the Arabian Sea.

Convective activity associated with the Asian summer monsoon is enhanced over India, the Bay of Bengal, the Indochina Peninsula and the Philippines (Figure 1 (j)). In association, large-scale divergence and convergence are seen over these areas in the upper and lower troposphere, respectively (Figures 1 (f) and (h)). The tropospheric atmosphere is warmed by condensation heating caused by convective activity. In boreal winter, active convection areas are seen over Indonesia, northern Australia and the western equatorial and southwestern tropical Pacific (Figure 1 (i)). In line with this, cores of upper-level divergence and lower-level convergence are observed northeast of Australia (Figures 1 (e) and (g)). The large-scale convection area associated with the Asian-Australian monsoon migrates from the northwest to the southeast in its annual cycle.

In the upper troposphere for the summer monsoon season (Figure 1 (d)), a zonally elongated large-scale anticyclone (i.e., the Tibetan High) is seen across southern Eurasia and northern Africa centered over the Tibetan Plateau. The development of the Tibetan High is associated with effectively warmed atmospheric conditions in the middle and upper troposphere due to the effects of the Tibetan Plateau and condensation heating due to large-scale monsoon convection. Tropospheric air temperatures between the equator and the Tibetan High increase in a northward direction, and easterly winds are predominant in the upper troposphere over parts of southern Asia (Figure 2 (b)) including India and the Indochina Peninsula. In line with the predominant westerly winds seen in the lower troposphere over southern Asia, the vertical structure of zonal winds over the area exhibits easterly shear with height (Figure 3 (b)). The subtropical jet stream over southern Eurasia (i.e., the Asian jet) flows over the northern periphery of the Tibetan High, which is clearly seen from June to September and is not developed in boreal winter. In association, the Asian jet flows over the northern Tibetan Plateau (40˚N – 45˚N) in boreal summer (Figure 2 (b)) and on the southern side of the plateau (25˚N – 30˚N) in boreal winter (Figure 2 (a)). In line with predominant easterly winds seen in the lower troposphere over southern Asia, the vertical structure of zonal winds over the area shows westerly shear with height in boreal winter (Figure 3 (a)).

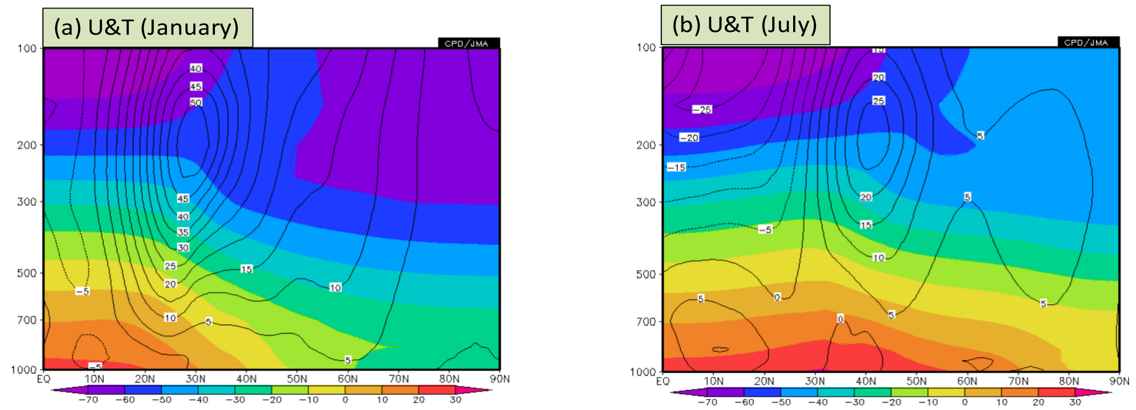

Figure 2 Vertical-latitude section of monthly mean normal zonal wind speeds and temperatures (60˚E – 120˚E averages)
(a) and (b) denote January and July, respectively. The contours show zonal wind speeds at intervals of 5 m/s. The shading indicates temperatures at intervals of 10˚C.

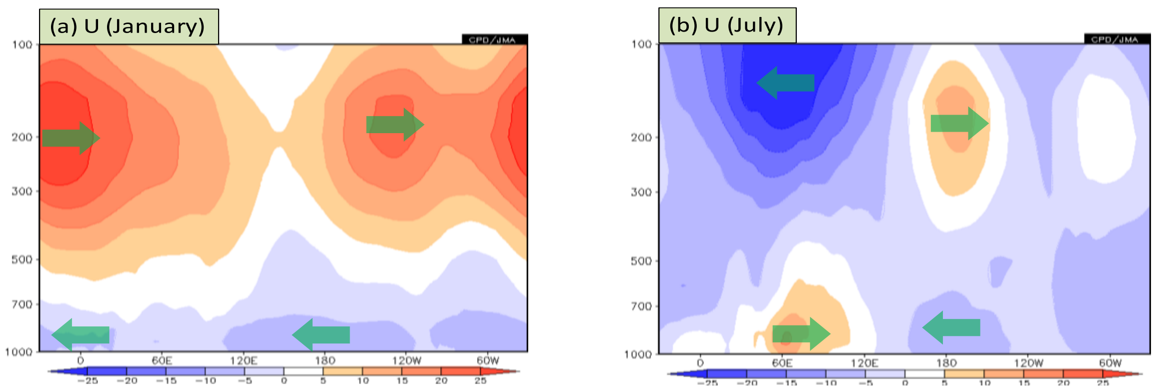

Figure 3 Vertical-longitude section of monthly mean normal zonal wind speeds (10˚N – 20˚N averages)
(a) and (b) denote January and July, respectively. The shading shows zonal wind speeds at intervals of 5 m/s; warm and white shading indicates westerly winds, and cold shading indicates easterly winds.

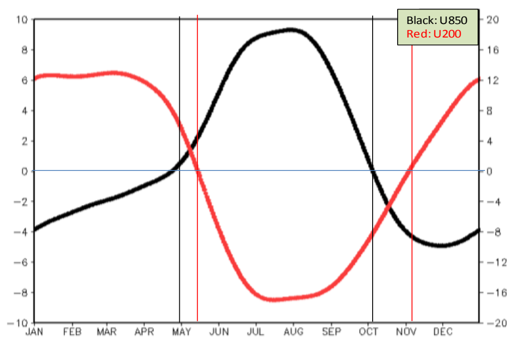

Figure 4 Annual cycle of 850-hPa (black line; left axis) and 200-hPa (red line; right axis) daily mean normal zonal-wind speeds averaged over southern Asia (10˚N – 20˚N, 60˚E – 120˚E)
Positive and negative values (unit: m/s) indicate westerly and easterly winds, respectively. The straight black and red lines denote the timing with which 850-hPa and 200-hPa zonal winds reverse, respectively.

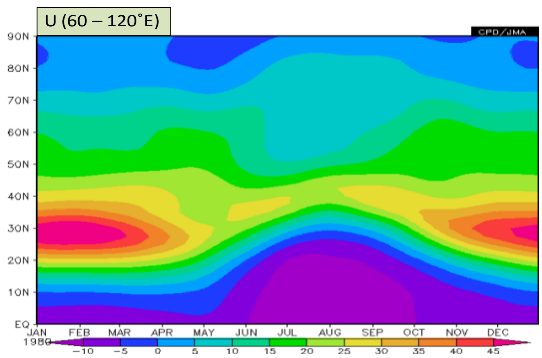

Figure 5 Annual cycle of 250-hPa daily mean normal zonal-wind speeds (60˚E – 120˚E averages)
The shading shows zonal wind speeds at intervals of 5 m/s. Positive and negative values indicate westerly and easterly winds, respectively.

In normal years, the zonal component of low-level wind averaged over southern Asia (10˚N – 20˚N, 60˚E – 120˚E) reverses from easterly to westerly in late April and vice versa in early October, exhibiting a change from winter to summer monsoon circulation and vice versa, respectively (black line shown in Figure 4). Upper-level zonal winds averaged over southern Asia reverse from westerly to easterly in mid-May and vice versa in early November (red line shown in Figure 4), and the upper-level reversal timing lags that of low-level circulation by up to a month. The Asian jet shows its annual maximum speed and its southernmost position in January and February, and exhibits its annual minimum speed and its northernmost position in the second half of July and the first half of August (Figure 5). The jet rapidly shifts northward in May, and then southward while strengthening in September and October.

2. March of the Asian summer monsoon

This section outlines the characteristics of atmospheric circulation associated with the Asian summer monsoon for each related month with focus on its time evolution (Figures 6 – 8).

April: A low-level ridge extends from the subtropical high over the North Pacific to the Indochina Peninsula. Convective activity is enhanced over the Maritime Continent (i.e., the Indonesian archipelago) and surrounding seas. Low-level monsoon westerly winds are not yet seen.

May: The low-level ridge extending from the subtropical North Pacific withdraws to the South China Sea. Cyclonic circulation appears over southern Asia, and the Somali jet and low-level monsoon westerly winds develop. Southwesterly moisture flow prevails over the Bay of Bengal and contributes to enhanced convective activity over the Indochina Peninsula, marking the onset of the summer monsoon over the peninsula.

June: The low-level monsoon westerly winds are enhanced and shift northward, and a monsoon trough develops from northern India to the northern Indochina Peninsula and in the vicinity of the Philippines. Convective activity is enhanced over India, the Indochina Peninsula and the Philippines. The Indian summer monsoon forms in June. In the upper troposphere, the Tibetan High develops and is seen from the Arabian Peninsula to north of the Indochina Peninsula.

July – August: Monsoon circulation and convective activity are further enhanced in July, and the strengthened conditions persist in August. The eastern part of the Tibetan High extends over Japan except its northern part from late July and late August. The trough from the South China Sea to east of the Philippines is enhanced, shifts northward and extends eastward from July to August.

September: Summer monsoon circulation and convective activity moderately weaken and shift slightly southward in comparison with those of July and August (i.e., their mature conditions). The northwestern Pacific trough to the east of the Philippines remains dominant, but also moderately weakens and shifts slightly southward.

October: Summer monsoon circulation is gradually replaced by winter monsoon circulation. Low-level winds over the South China Sea and the Indochina Peninsula change from westerly/southwesterly to easterly/northeasterly. Active convection areas move further southward, and convective activity over India and the Indochina Peninsula is suppressed, marking the end of the summer monsoon in these areas. The northwestern

Pacific trough east of the Philippines is obscured.

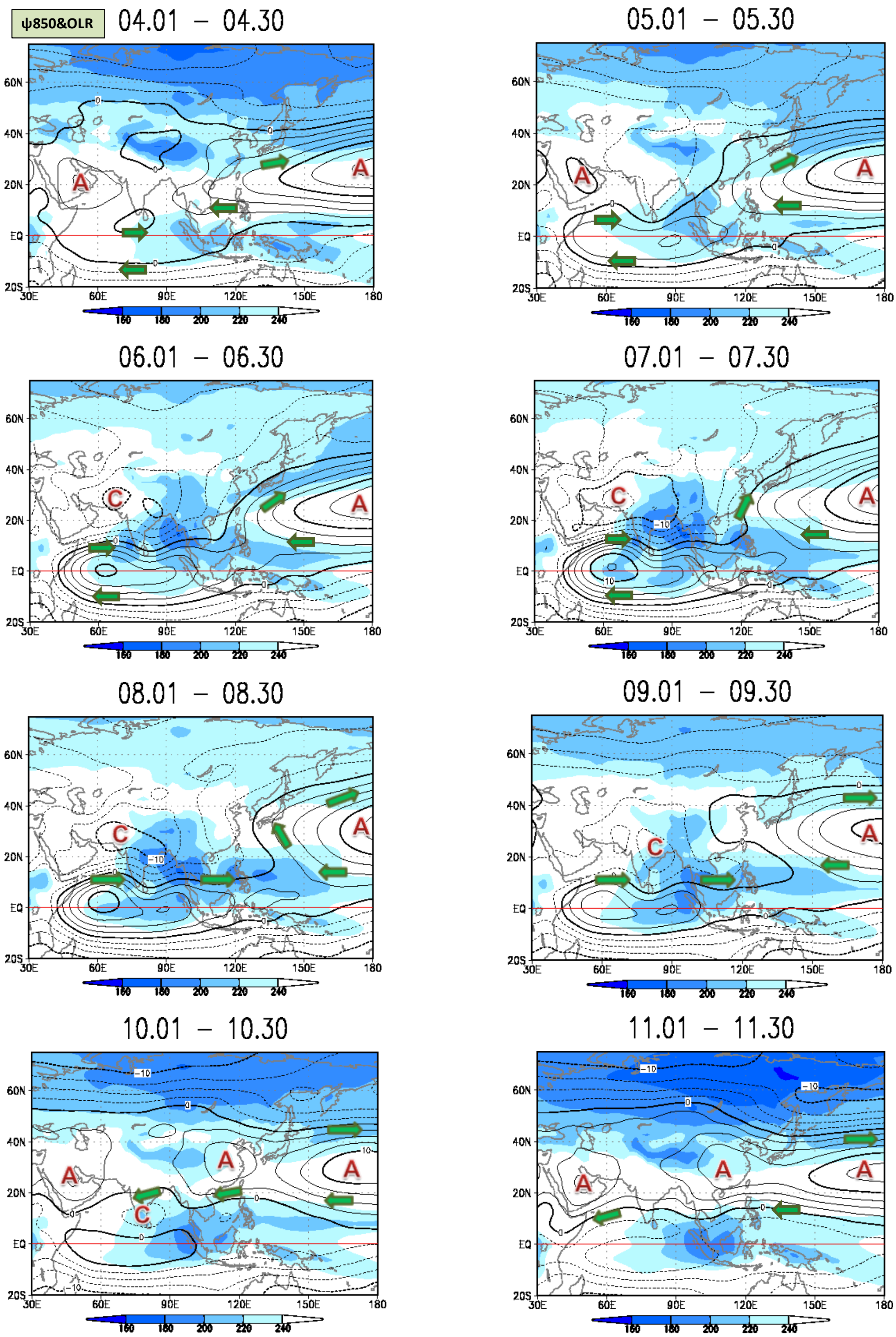

Figure 6 30-day mean 850-hPa stream function and OLR for normal months from April to November
The contours indicate the stream function at intervals of 2.5×10^6 m^2/s. The shading shows OLR at intervals of 20 W/m^2, and the green arrows denote the prevailing wind direction. “A” and “C” indicate the centers of anticyclonic and cyclonic circulation areas, respectively.

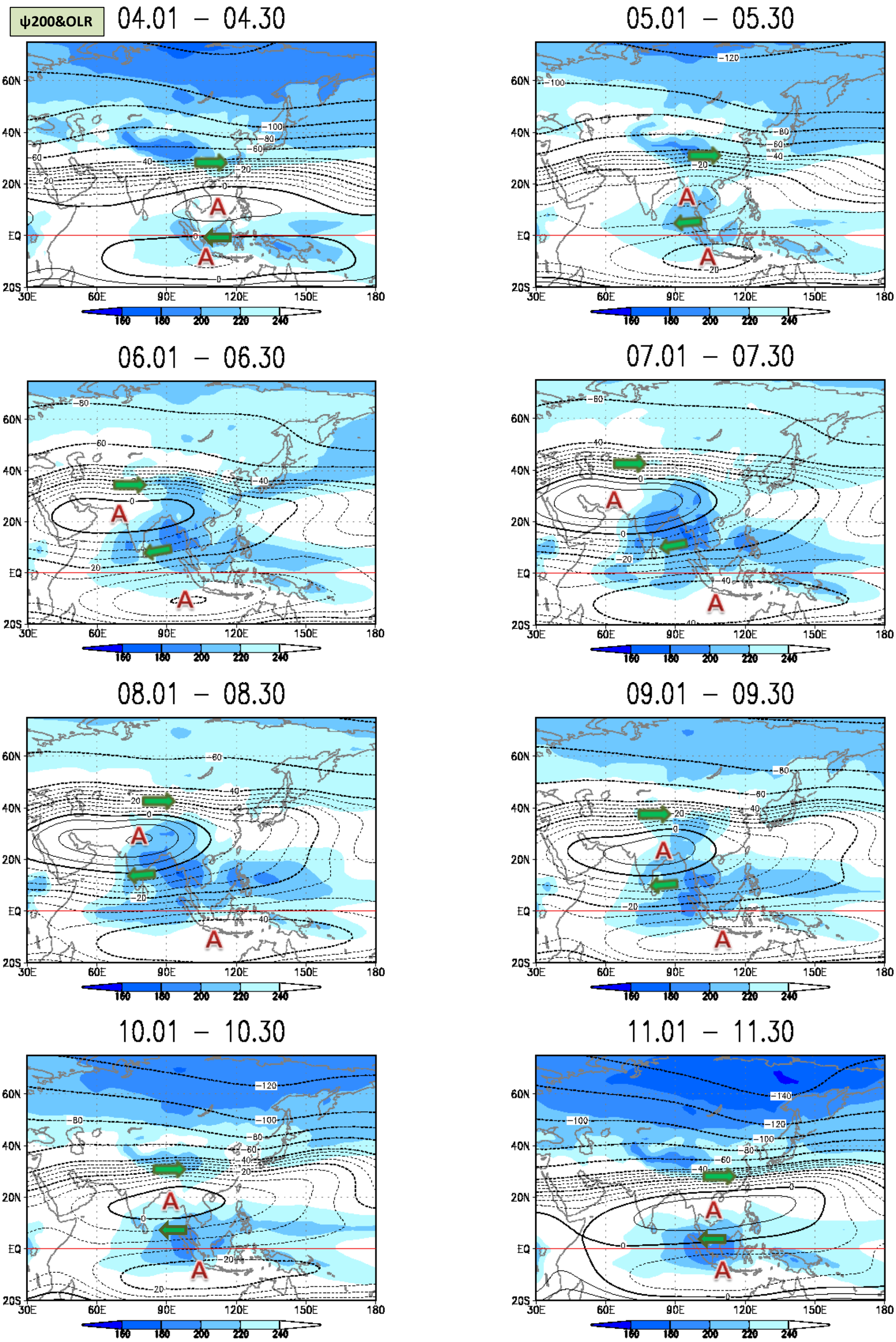

Figure 7 30-day mean 200-hPa stream function and OLR for normal months from April to November
The contours indicate the stream function at intervals of 5 × 10^6 m^2/s. The shading shows OLR at intervals of 20 W/m^2, and the green arrows denote the prevailing wind direction. “A” and “C” indicate the centers of anticyclonic and cyclonic circulation areas, respectively.

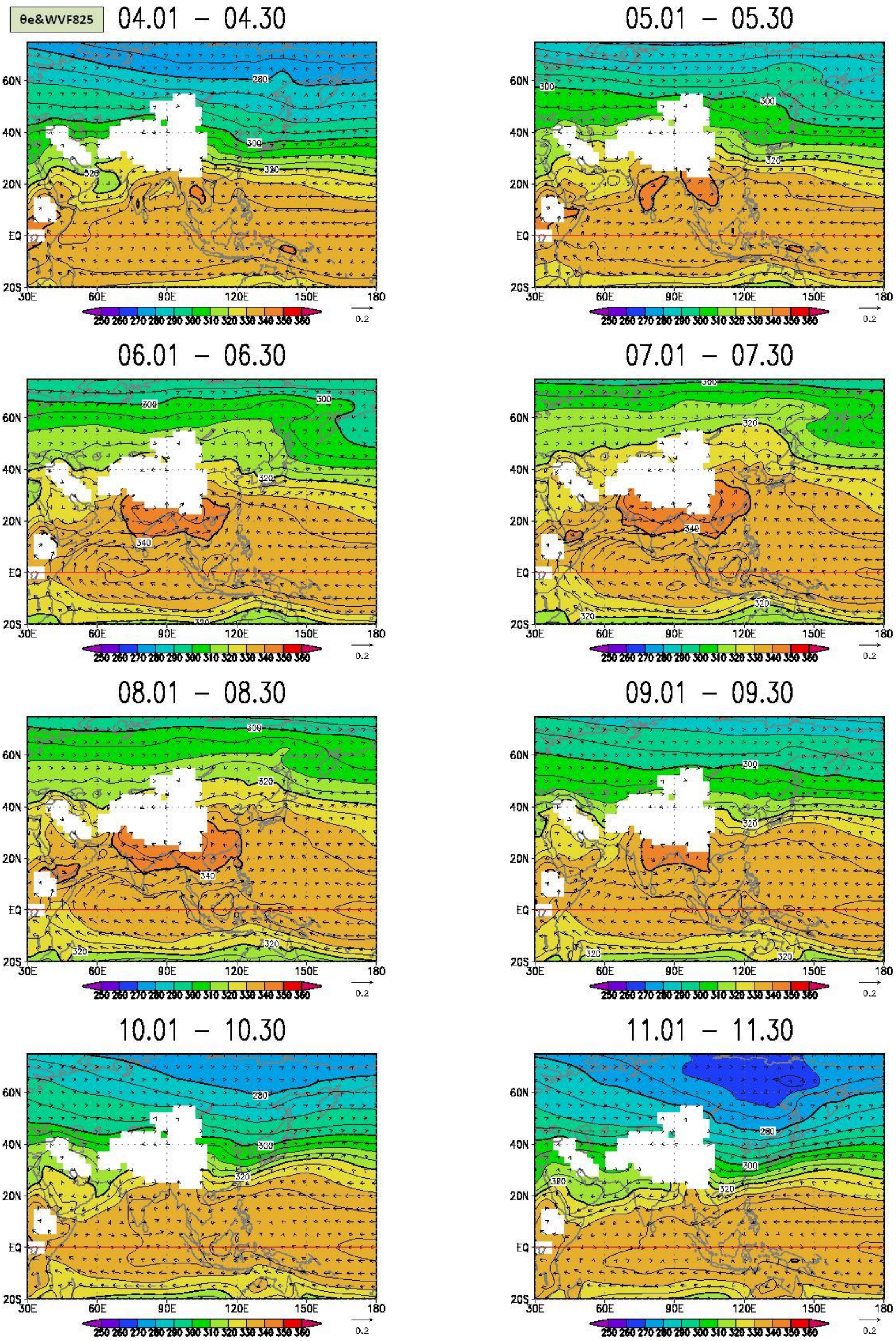

Figure 8 30-day mean 850-hPa equivalent potential temperature and water vapor flux for normal months from April to November

The contours and shading indicate equivalent potential temperatures at intervals of 10 K. The arrows show water vapor flux (unit: m/s × kg/kg), and areas with altitudes exceeding 1,500 m are masked out.

3. March of the Asian winter monsoon

This section outlines the characteristics of atmospheric circulation associated with the Asian winter monsoon for each related month with focus on its time evolution (Figure 9).

September: Low-level temperatures over parts of southern Eurasia including the Arabian Peninsula and the Tibetan Plateau are higher than those over the Indian Ocean. A low-pressure system in the SLP field is seen in southern Eurasia, and the Somali jet and low-level monsoon westerly winds are predominant. These characteristic circulation patterns echo those seen in the summer monsoon.

October: Low-level temperatures decrease over Eurasia, and a high-pressure system on the surface forms in the middle of the continent. Atmospheric circulation is gradually reversed from the pattern seen in boreal summer to that seen in boreal winter, marking the transition from the summer to the winter monsoon.

November: In the lower troposphere, a core of cold air develops over eastern Siberia, and the continental high-pressure system centered southwest of Lake Baikal is enhanced and expanded, marking the development of the Siberian High. A low-pressure system is clearly seen over the northern North Pacific, marking the enhancement of the Aleutian Low. Consequently, zonal SLP gradients between Eurasia and the North Pacific are strengthened. Northerly and easterly winds are seen in East Asia and southern Asia, respectively. Northeasterly winds prevail over the South China Sea and the eastern coast of the Indochina Peninsula. This circulation is characteristic of the winter monsoon type.

December: Low-level temperatures over Eurasia fall further, and the Siberian cold-air core is enhanced. The Siberian High and the Aleutian Low are enhanced, and the winter-monsoon SLP pattern strengthens in northeastern Asia. The near-surface northeasterly wind area over the South China Sea extends over the eastern coast of the Malay Peninsula.

January: Winter monsoon circulation shows its seasonal maximum strength, marking the mature phase of the Asian winter monsoon.

February: Signs of reduced winter monsoon circulation appear in Siberia and East Asia. Low-level temperatures over southern Asia start to rise, and northeasterly winds around the South China Sea weaken.

March: Low-level temperatures over Eurasia increase, while low Siberian temperatures increase and their areas shift northward. The Siberian High and the Aleutian Low weaken. Near-surface winds around the South China Sea change from northeasterly to easterly.

April: Increasing low-level temperatures over the Arabian Peninsula and southern Asia exceed those over the Indian Ocean, marking a reversal of meridional temperature gradients. The Siberian High and the Aleutian Low further weaken and are obscured, while a distinct subtropical high-pressure system is seen over the North Pacific.

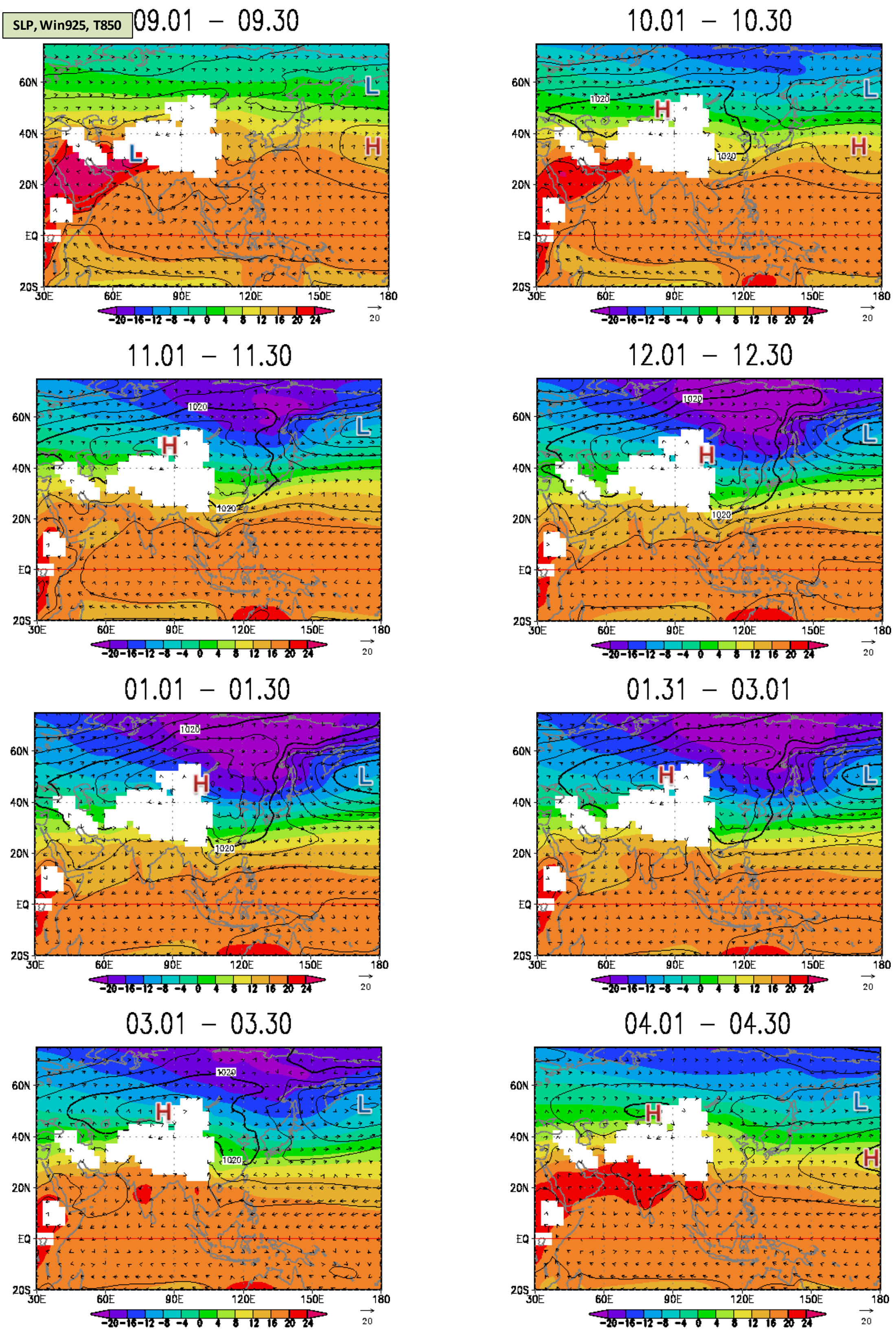

Figure 9 30-day mean sea level pressure (SLP), 850-hPa temperatures and 925-hPa winds for normal months from September to April

The contours indicate SLP at intervals of 4 hPa, and the shading shows temperature at intervals of 4˚C. The arrows show wind vectors (unit: m/s). "H" and "L" indicate the centers of high- and low-pressure systems, respectively. Areas with altitudes exceeding 1,500 m are masked out.

Introduction and Basic Operation of ITACS

JMA's web-based application for climate analysis

ITACS: Interactive Tool for Analysis of the Climate System

Climate Prediction Division, Japan Meteorological Agency

ITACS is the Interactive Tool for Analysis of Climate System since 2007. The aims are analyzing the causes of climate events and monitoring current climate status. And, the system consists of Web interface, programs, GrADS and data files on the web server.

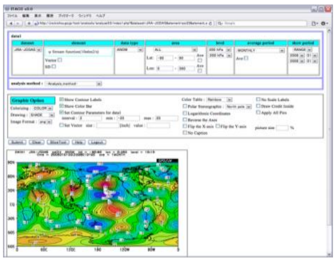

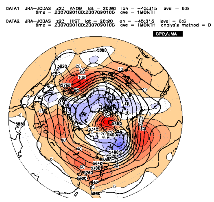

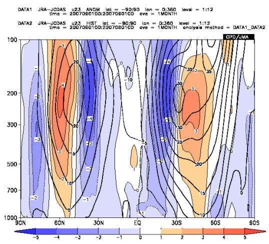

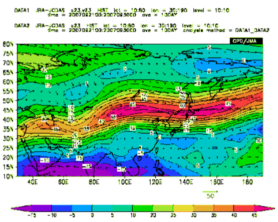

Data sets

Atmospheric analysis data / Outgoing Longwave Radiation (OLR) data / Sea surface temperature analysis data / ocean analysis data / CLIMAT reports …

Application and contact

There is application form and introduction about ITACS on the homepage of Tokyo Climate Center.

http://ds.data.jma.go.jp/tcc/tcc/index.html

tcc@met.kishou.go.jp

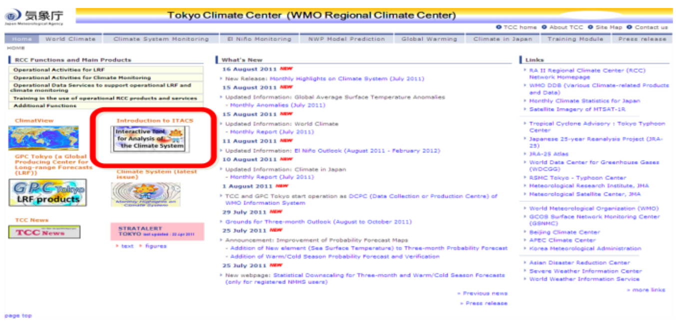

Tokyo Climate Center homepage

ITACS

Climate Prediction Division, JMA

menu

- What's ITACS
- Data
- Application to use
- Exercise and learning by using ITACS

What's ITACS

ITACS is the Interactive Tool for Analysis of Climate System since 2007.

Aim:
Analyzing the causes of climate events and monitoring current climate status.
System:
Web interface + programs(Ruby, Gphys…) + GrADS + data files on the web server

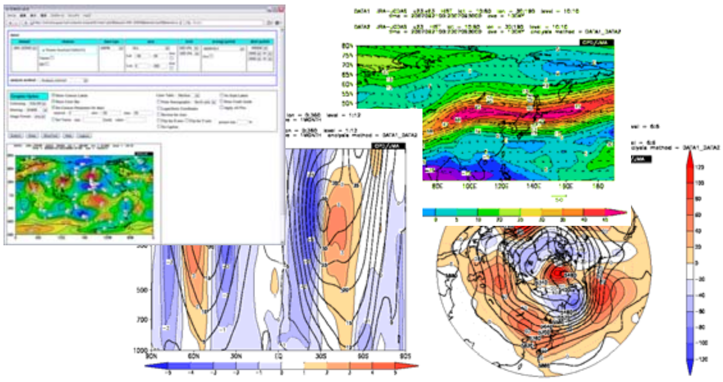

data

- CLIMAT
  - Monthly world climate data derived from CLIMAT messages via the GTS line from WMO Members around the world.
- INDEX
  - El Nino Monitoring Indices consisting of monthly mean Sea Surface Temperature produced by COBE-SST.
- JRA-JCDAS
  - Atmospheric circulation data produced by JMA's Climate Data Assimilation System (JCDAS), which is consistent quality with Japanese 25-year reanalysis (JRA-25).
- MOVE-G
  - Oceanic assimilation produced by the system operated by JMA.
- SAT
  - Outgoing Longwave Radiation (OLR), which is derived from observations by NOAA's polar orbital satellites, and provided by Climate Prediction Center (CPC) in the National Centers for Environmental Prediction (NCEP) of the National Oceanic and Atmospheric Administration (NOAA).
- SST
  - Sea Surface Temperature produced by the system operated by JMA (COBE-SST).

Application to use

There is banner link about application to use ITACS in the TCC homepage:
http://ds.data.jma.go.jp/tcc/tcc/index.html

Exercise

Now, let's access and use ITACS. Using it will help you to understand ITACS.

Sample image

Making image like sample image by yourself

⇩ If we have enough time after every exercises…

Let's try to change sample image as you like (self study)

Let's start exercise. Please access to following site:
http://extreme.kishou.go.jp/tool/itacs-tcc2011/

Appendix) Self study

Let's try to draw maps as you like if you know basic use of ITACS.
For example, you can make a map around your country…

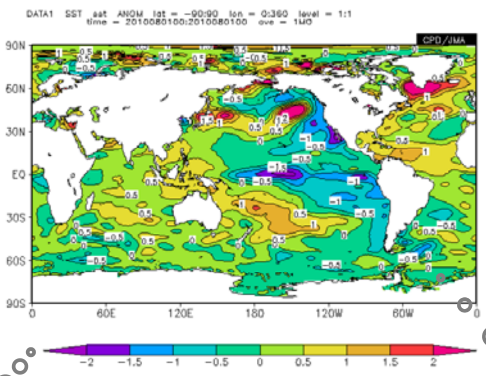

Season
Summer or winter

area

Index of today's Exercise

- Sea surface temperature(SST)
- Average of SST anomaly
- Stream function of historical data
- Subtraction of monthly SST
- 500-hPa height and anomaly (polar stereographic plot)
- Time-longitude cross section of 200-hPa velocity potential
- Water vapor flux(vector) anomaly and specific humidity anomaly
- Interannual variation of monthly mean 850-hPa air temperature
- SST composite of La Nina years
- Regression Analysis and Correlation Analysis

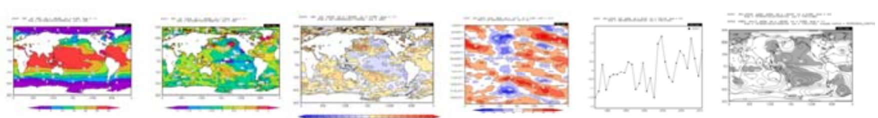

Sea surface temperature(SST)

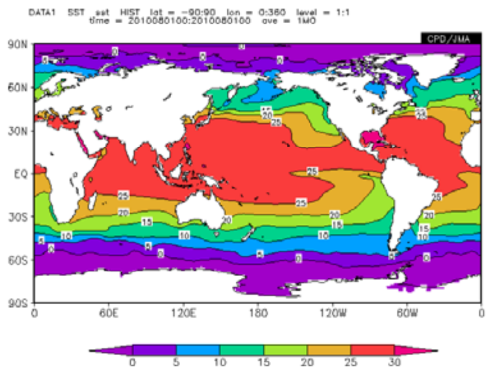

Sea Surface Temperature in August 2010

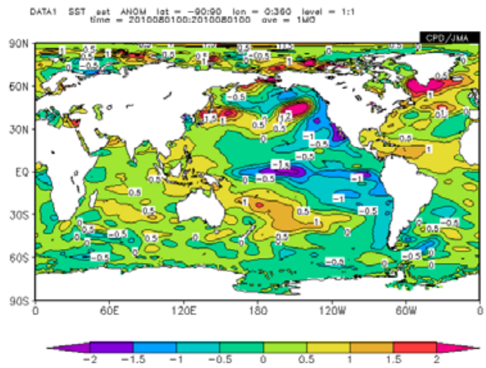

Sea Surface Temperature anomaly in August 2010

This is tutorial for making a map of Sea Surface Temperature(SST) and its anomaly. Let's know basic use of ITACS.

Sea surface temperature(SST)

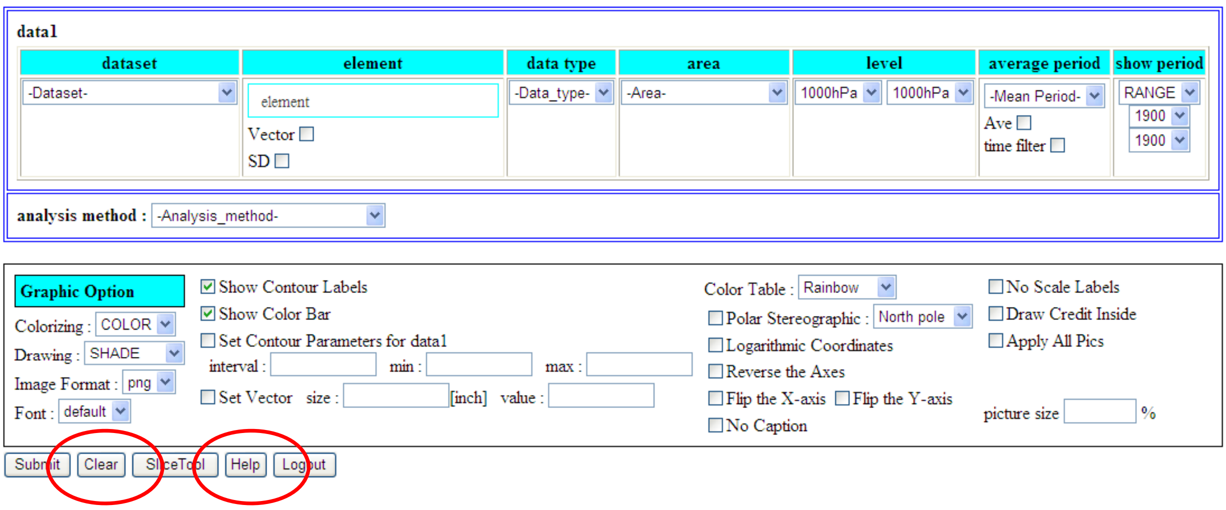

This is default screen of ITACS. Click "Clear" button if you need default screen. "Help" button gives you help page.

Sea surface temperature(SST)

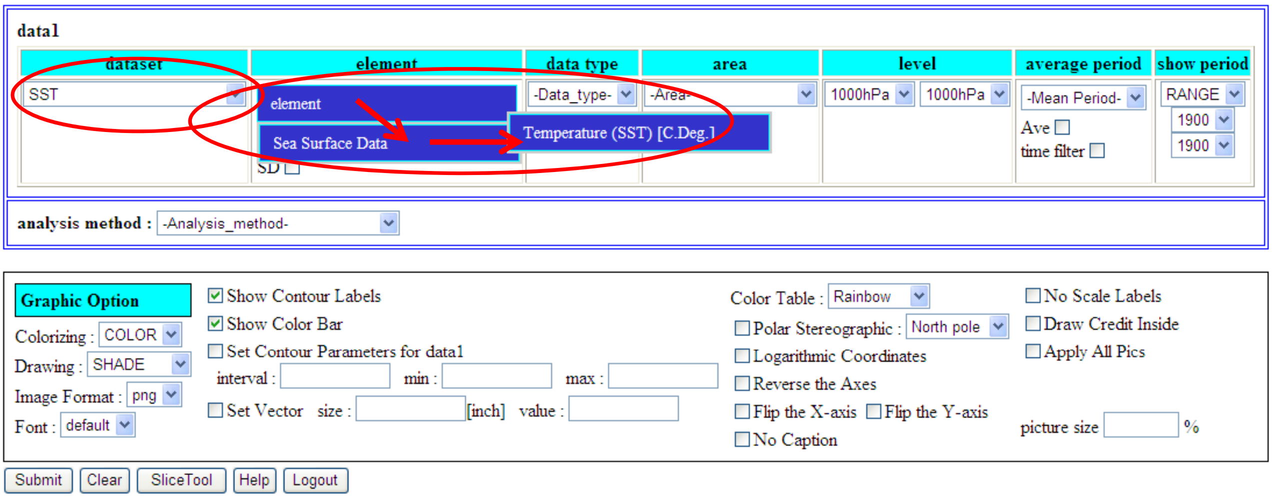

First, select “dataset” - “SST” and its “element” - “Temperature”.

Sea surface temperature(SST)

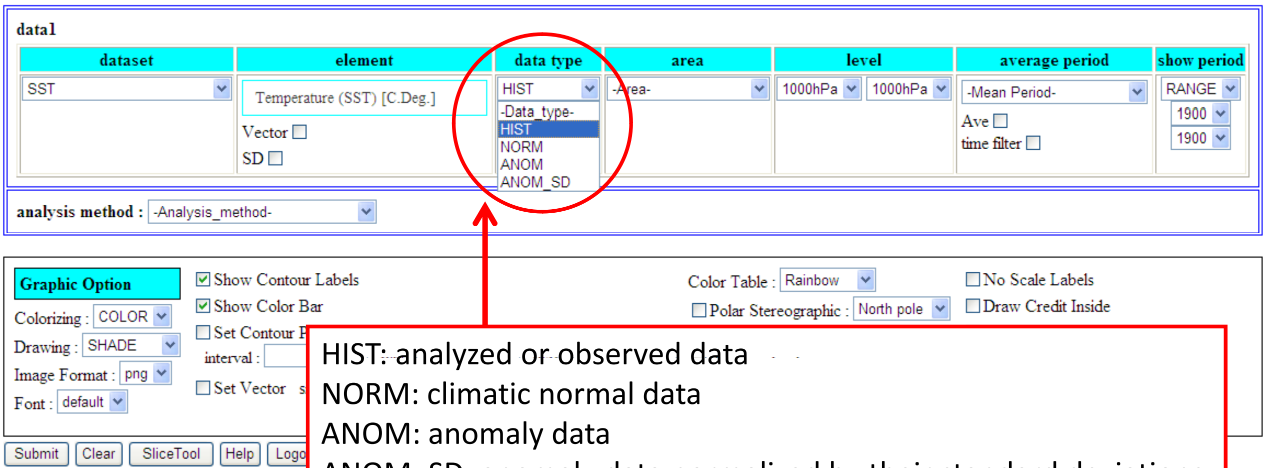

HIST: analyzed or observed data
NORM: climatic normal data
ANOM: anomaly data
ANOM_SD: anomaly data normalized by their standard deviations

Note:
"HIST" minus "NORM" is "ANOM"
"ANOM" divided by σ is "ANOM_SD"

Secondly, select “data type” - “HIST”(historical data).
Please note there are some data type.

Sea surface temperature(SST)

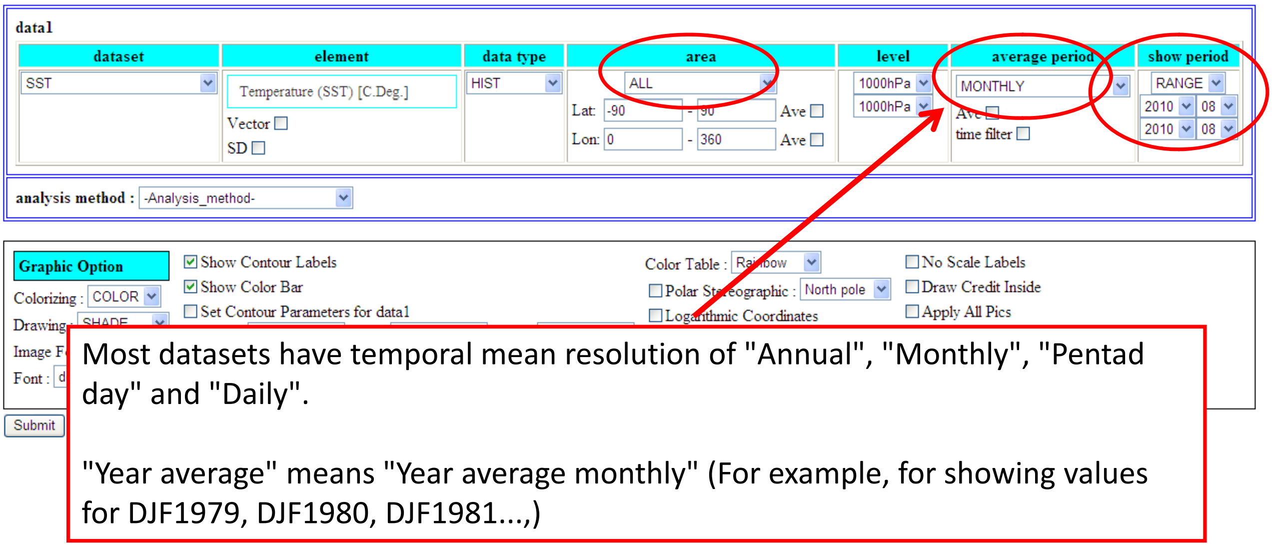

Next, select “area”, “average period” and “show period”.

Sea surface temperature(SST)

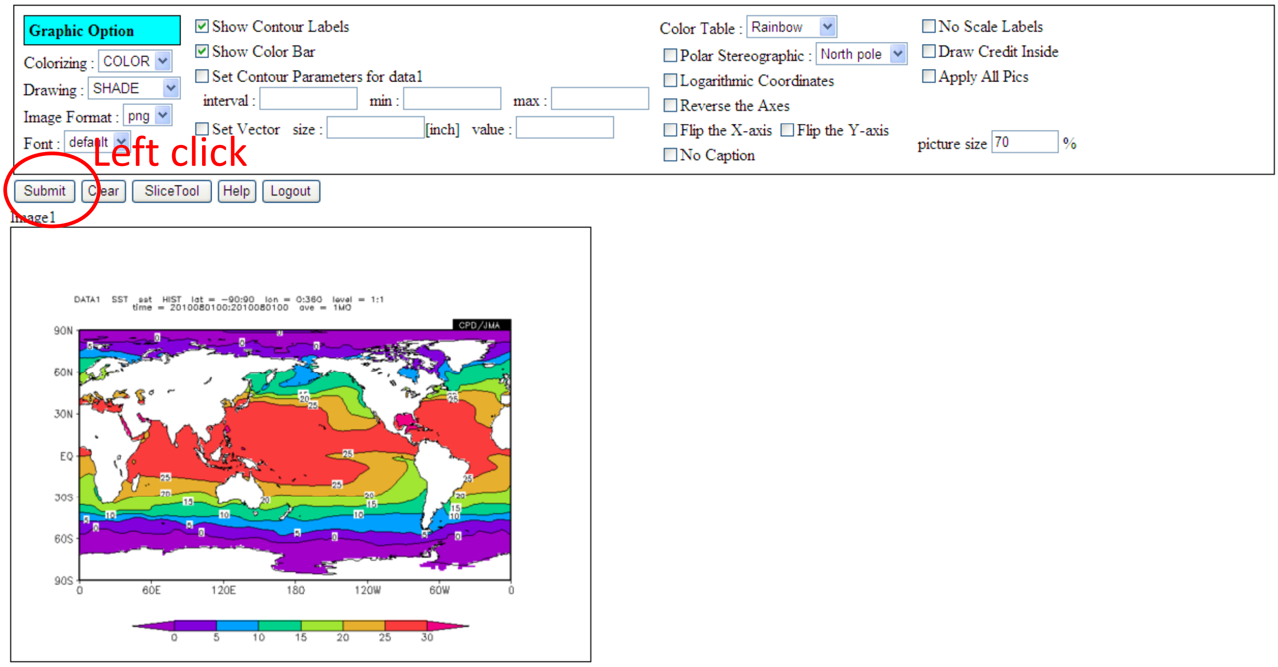

Finally, click “Submit” button. A map of Sea Surface Temperature(SST) will be made.

Sea surface temperature(SST) anomaly

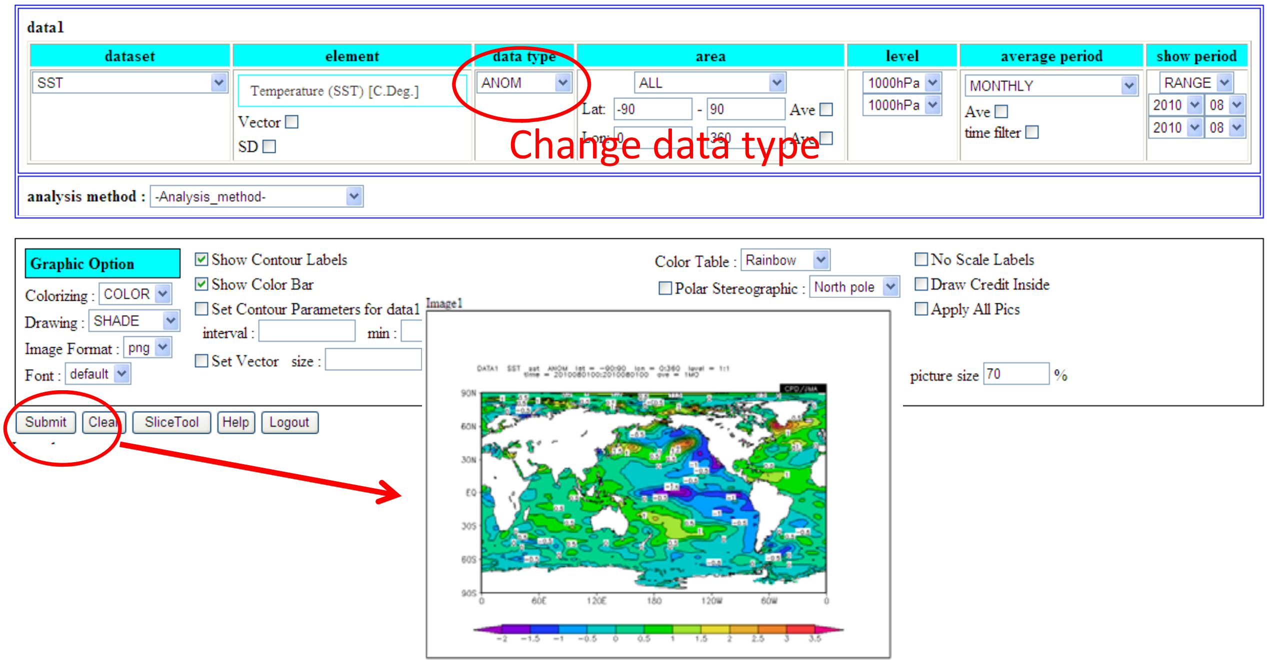

Let's change "data type" – "ANOM" to make map of SST anomaly and click "Submit".

Sea surface temperature(SST) anomaly

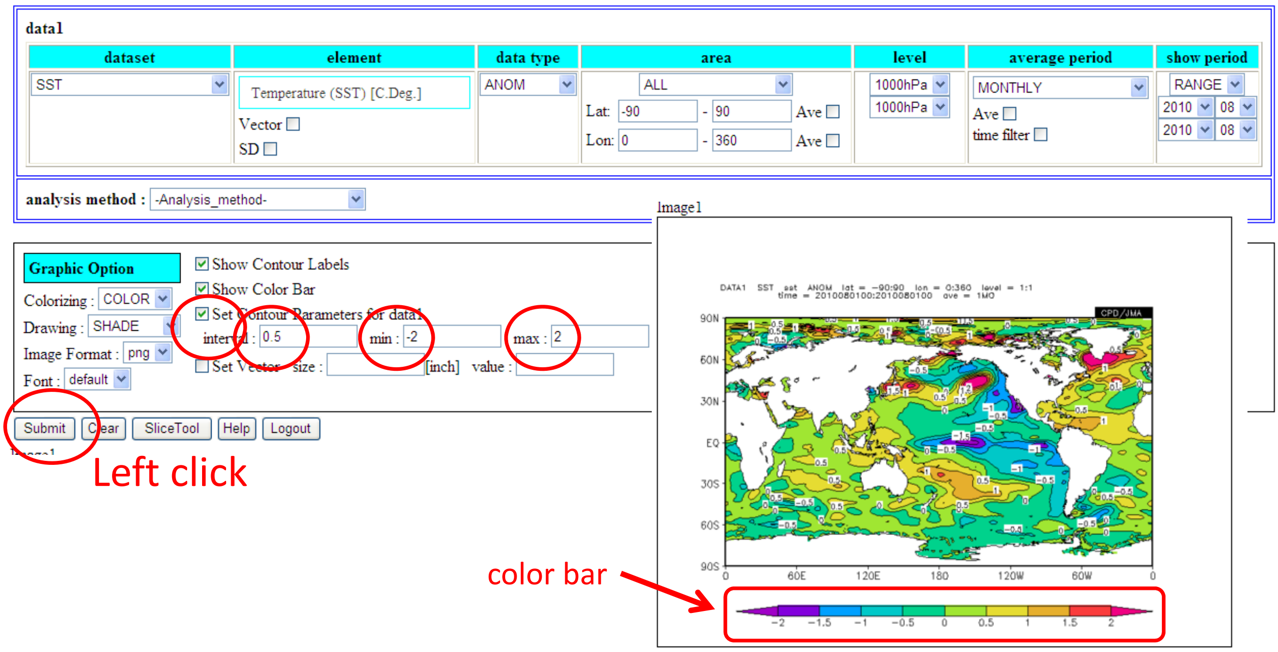

If you want to change the range of colors in the color bar, please use "Graphic Options". Check "Set Contour Parameters for data1" and input parameters for interval, min and max of values.

Average of SST anomaly

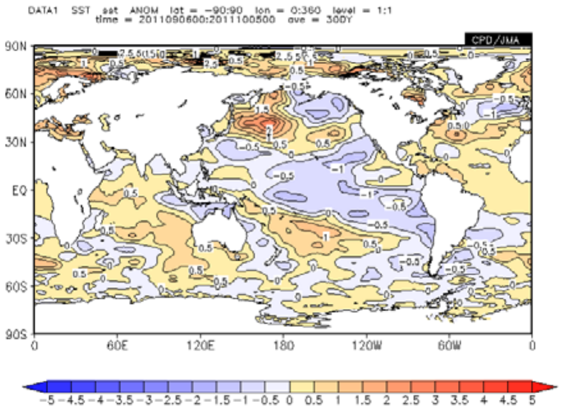

Average of SST anomaly between 6 September and 5 October

Let's know how to figure out the average of daily data.

Average of SST anomaly

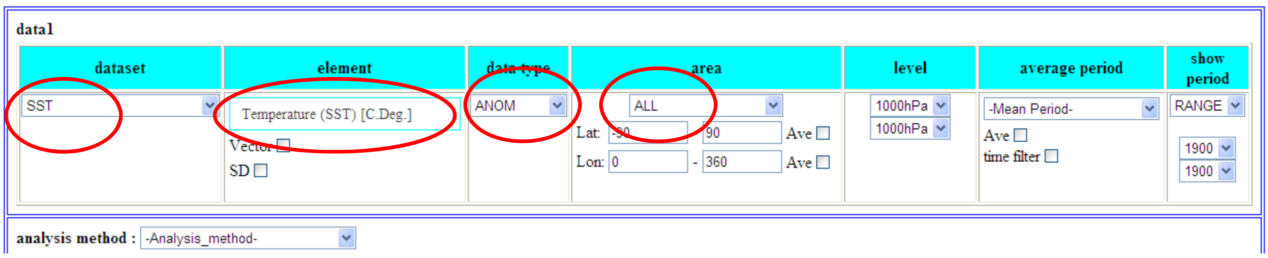

First, select "dataset" - "SST" and its "element" - "Temperature".
And, select "data type" - "ANOM"(anomaly data) and "area" – "ALL".

Average of SST anomaly

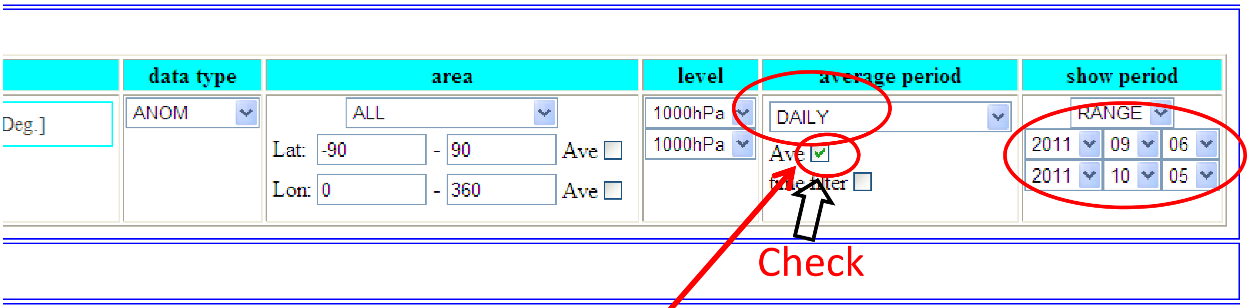

Check

"Ave" gives average of data.

Note:
ITACS figures out the monthly data if you select "MONTHLY" in the "average period".

Next, please select "average period" – "DAILY" and check "Ave" – "ON(checked)". And, select "show period"(2011.09.06 – 2011.10.05).

Average of SST anomaly

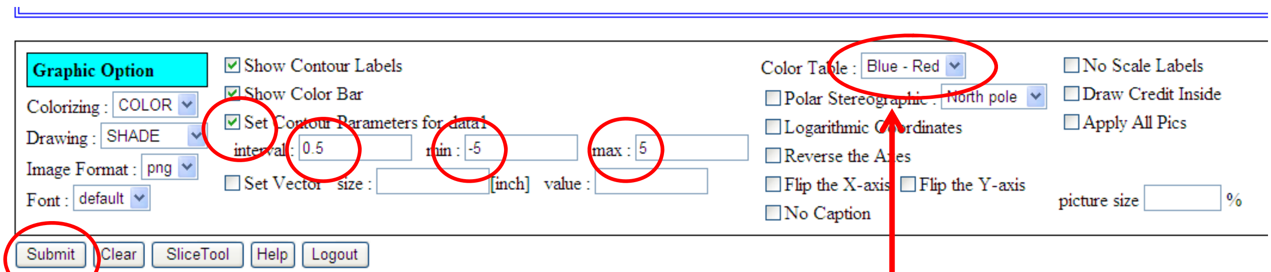

Left click

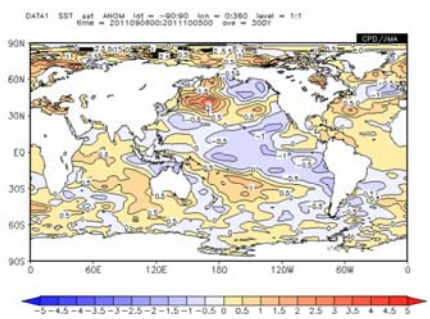

Note:
"Color Table" option set the color of the plotted contours. Rainbow is selected by default.

Finally, please select "Set Contour Parameters" of Graphic Option. Let's change "Color Table" if you want to set the color of the plotted contours. And, click "Submit".

Stream function of historical data on 850hPa

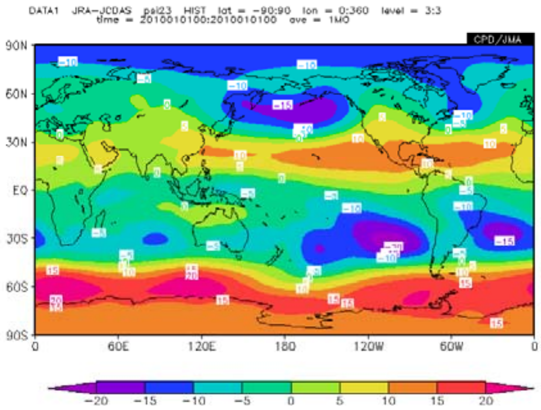

Ψ(Stream function) of historical data on 850hPa

Let's know how to change vertical level of the data.

Stream function of historical data on 850hPa

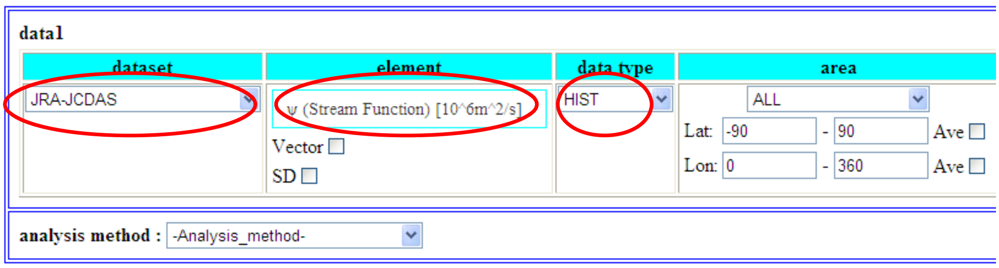

First, please select "dataset" – "JRA-JCDAS", "element" – "Ψ(Stream function)" and "data type" – "HIST".

Stream function of historical data on 850hPa

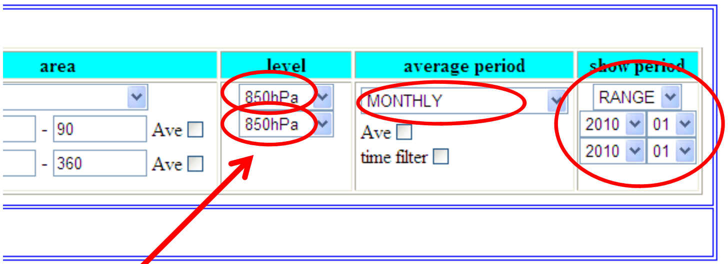

Two pull-down menus are prepared in this field and available vertical levels are listed on them. If different levels are chosen from each menu by users, the drawing will be a vertical cross section chart.

Secondly, please select “level” – “850hPa”, “average period” - “MONTHLY” and “show period”.

Stream function of historical data on 850hPa

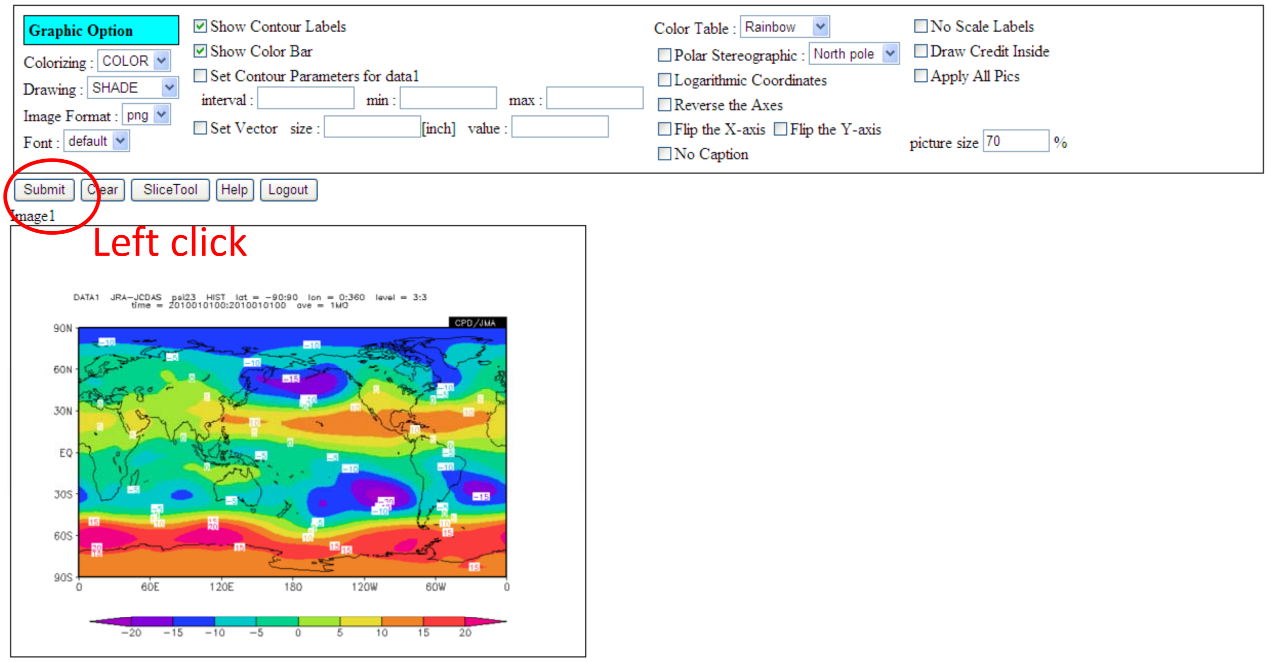

Finally, click “Submit” button. A map on 850hPa will be made.

Stream function of historical data and anomaly data on 850hPa

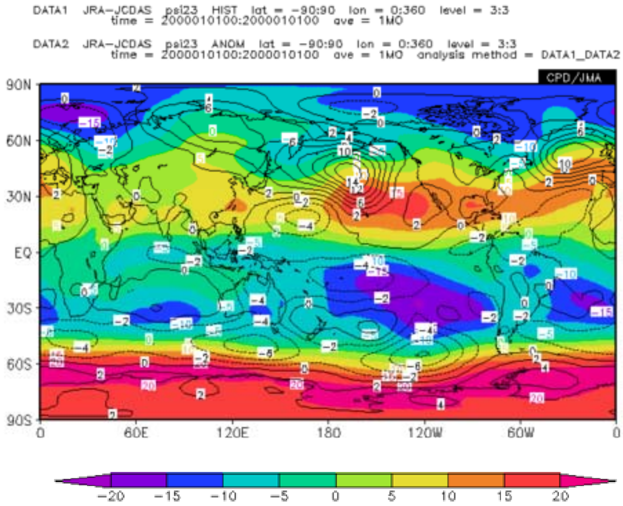

Stream function of historical data and anomaly data on 850hPa

Let's know how to superimpose a map on other map.

Stream function of historical data and anomaly data on 850hPa

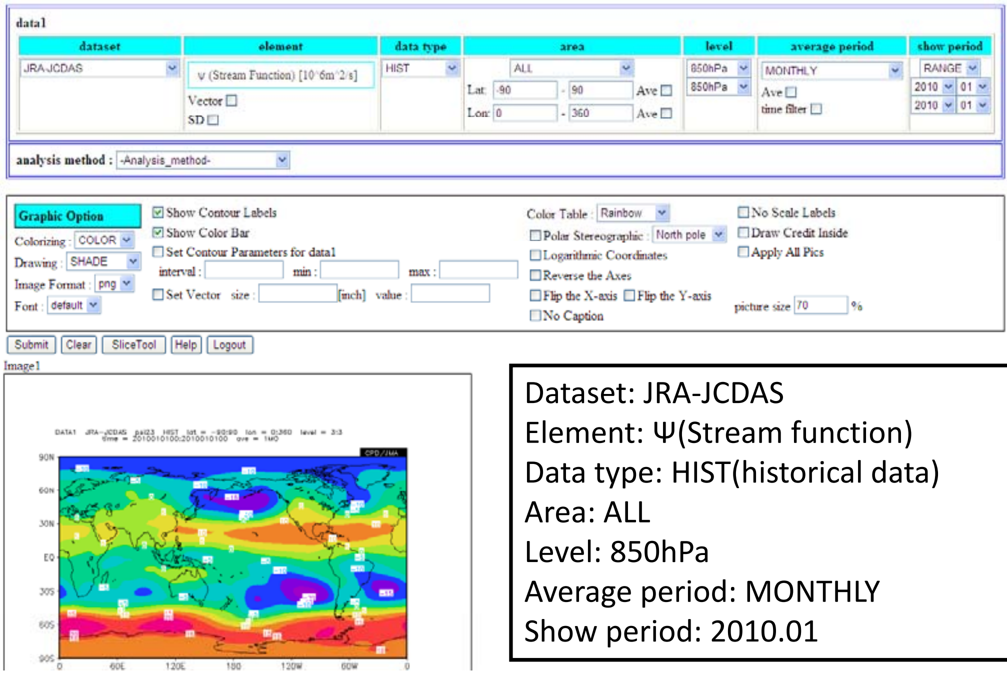

Dataset: JRA-JCDAS
Element: Ψ(Stream function)
Data type: HIST(historical data)
Area: ALL
Level: 850hPa
Average period: MONTHLY
Show period: 2010.01

First, please draw Stream function of historical data on 850hPa.

Stream function of historical data and anomaly data on 850hPa

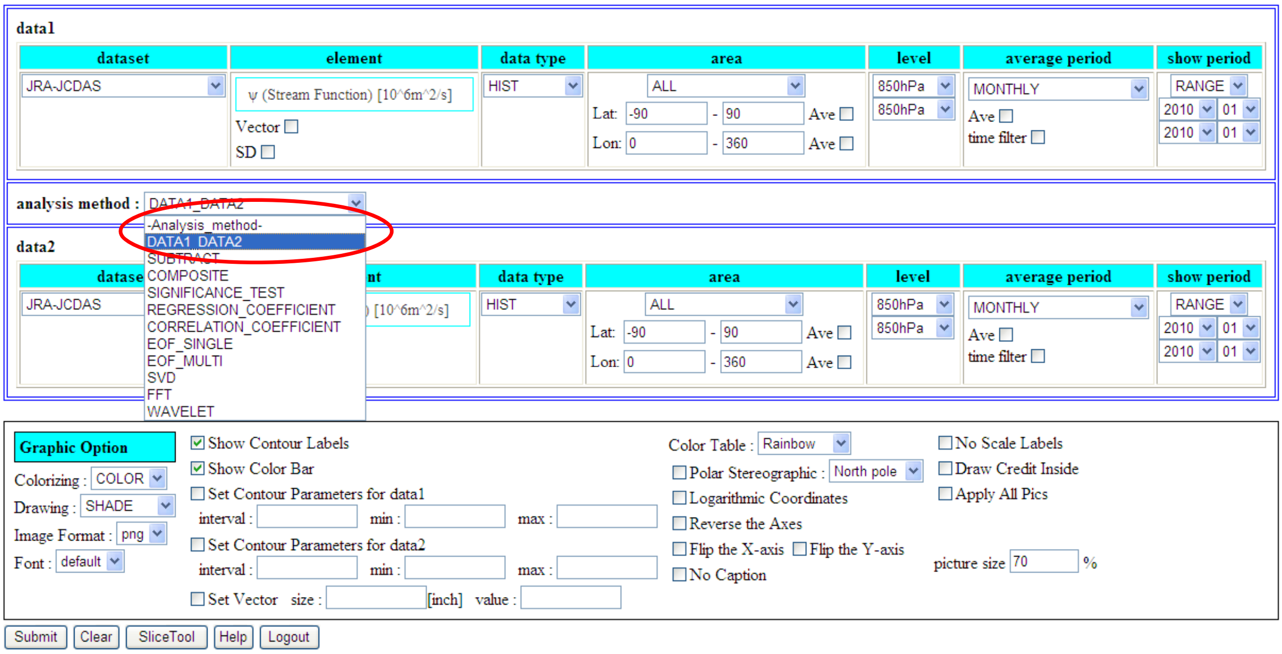

Secondly, please select “analysis method” – “DATA1_DATA2”.
Box “data2” will appear.

Stream function of historical data and anomaly data on 850hPa

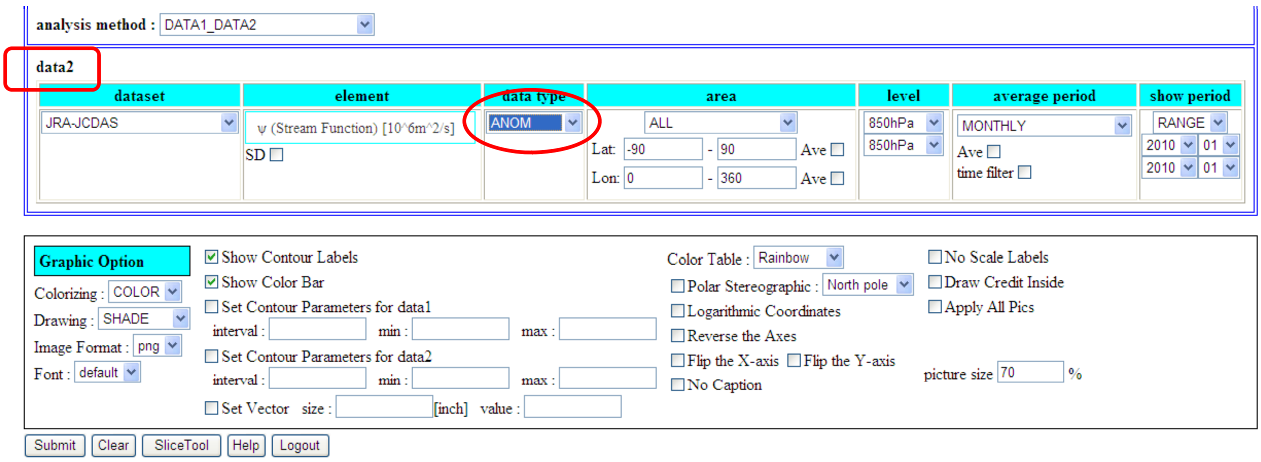

And, please change “data type” – “ANOM” of box “data2”.
Don’t change other options.

Stream function of historical data and anomaly data on 850hPa

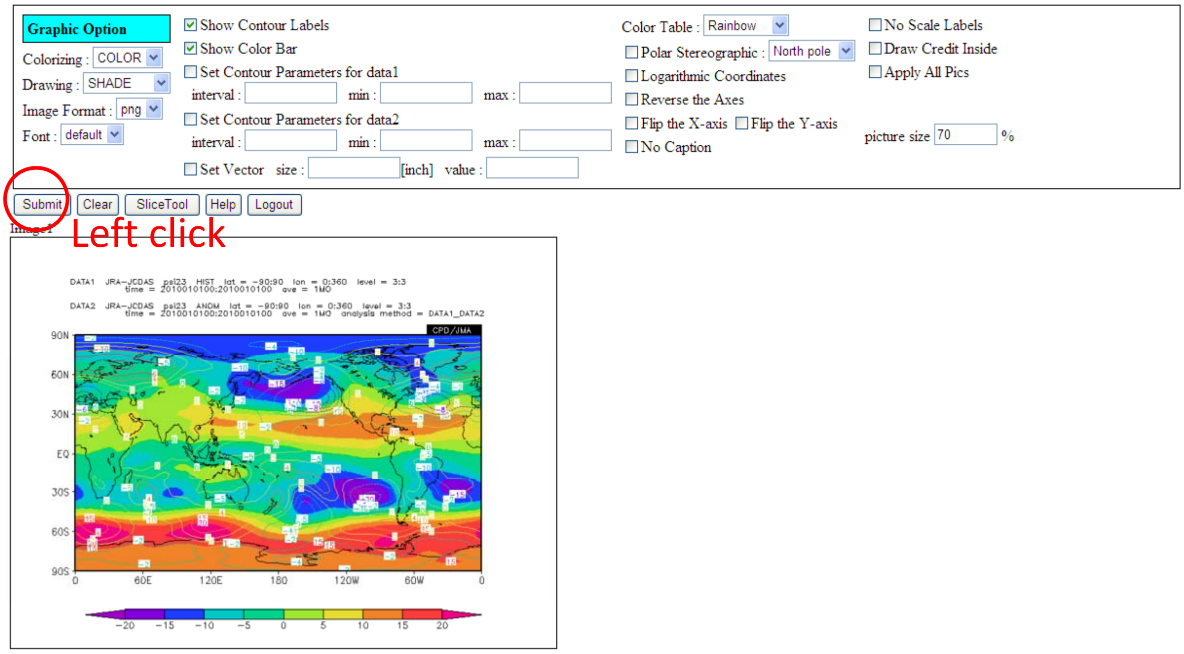

Finally, click “Submit” button and draw a map.
In addition, the color of contour can be changed… => go next page

Stream function of historical data and anomaly data on 850hPa

Before:

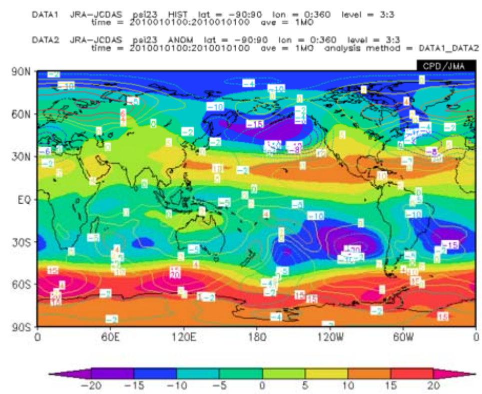

After:

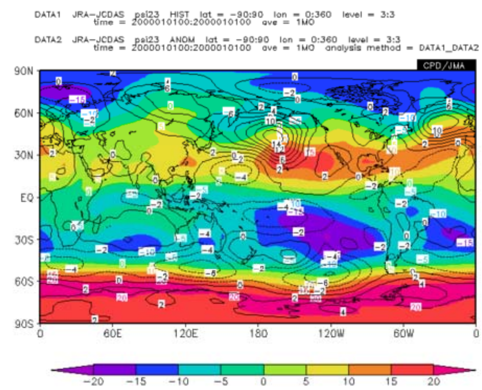

Let’s change the color of contour of upper layer.

Stream function of historical data and anomaly data on 850hPa

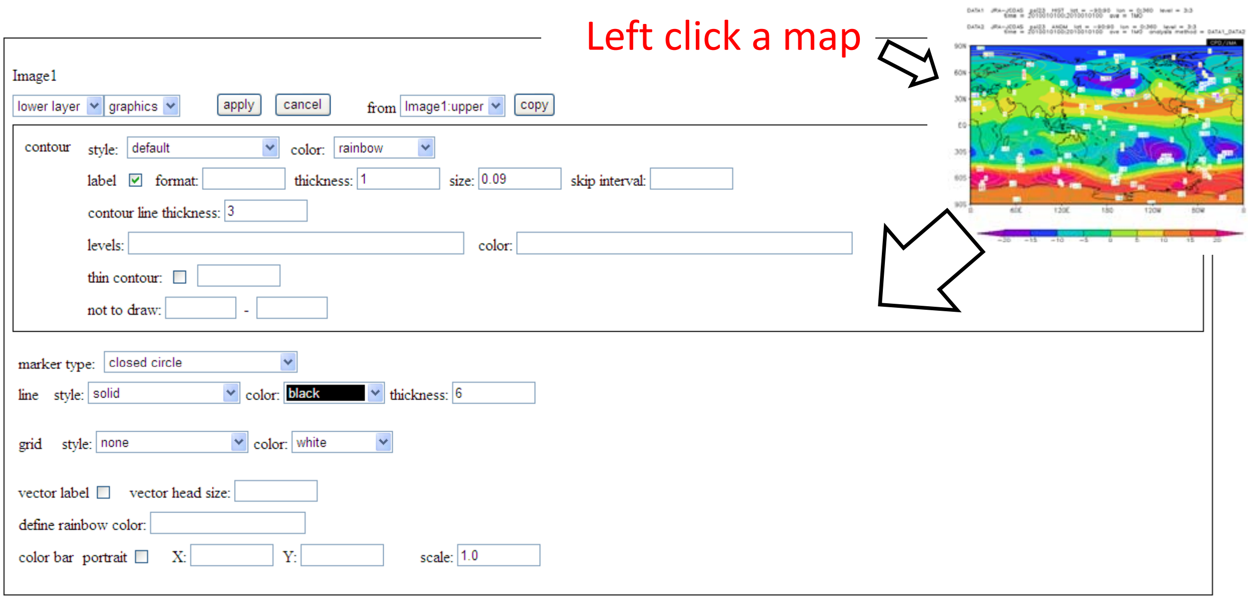

Please click a map. New option box “Image” will appear.

Stream function of historical data and anomaly data on 850hPa

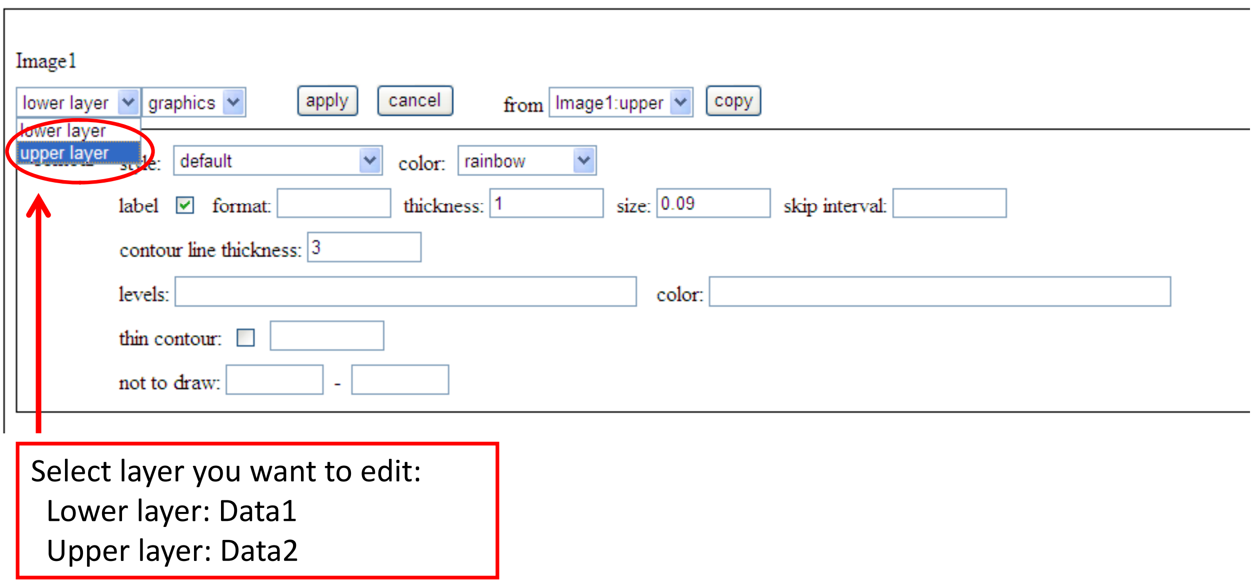

Secondly, please select layer you want to edit. In this example, select “upper layer”.

Stream function of historical data and anomaly data on 850hPa

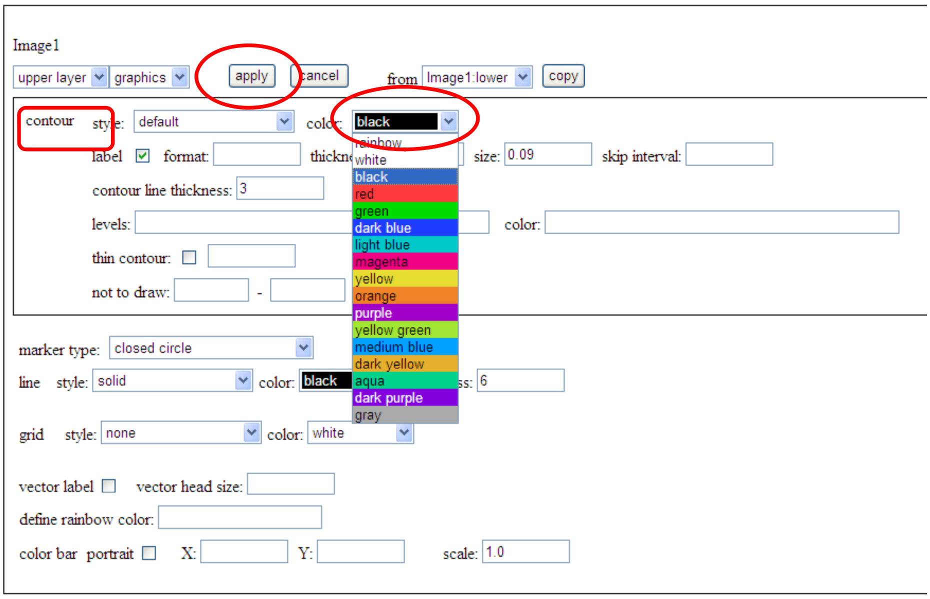

Next, please select “color” – “black” and click “apply” button.
Don’t forget to click “apply” button.

Stream function of historical data and anomaly data on 850hPa

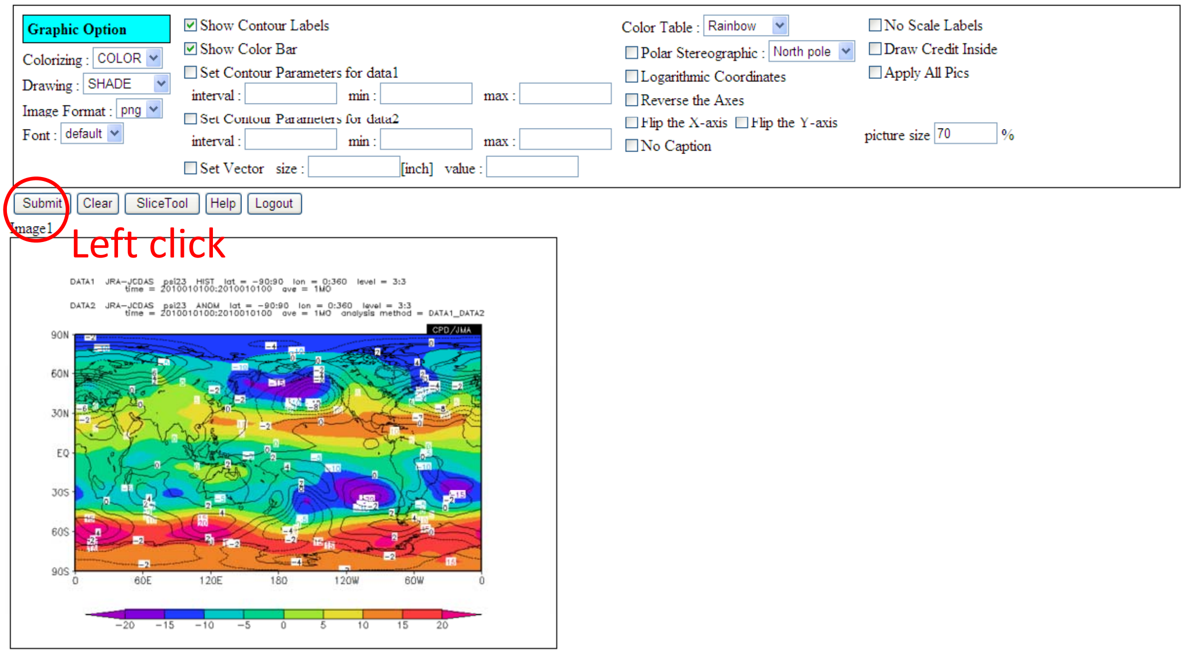

Finally, click “Submit” button. The contour will be black.

Subtraction of monthly SST

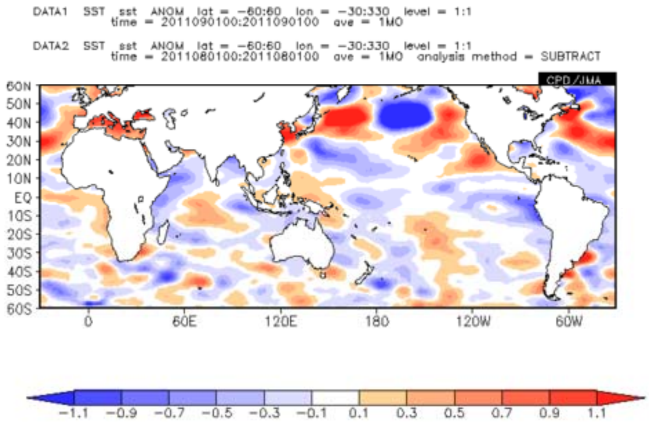

Subtraction of monthly SST between September and August

Let's know how to subtract data from data of other period.

Subtraction of monthly SST

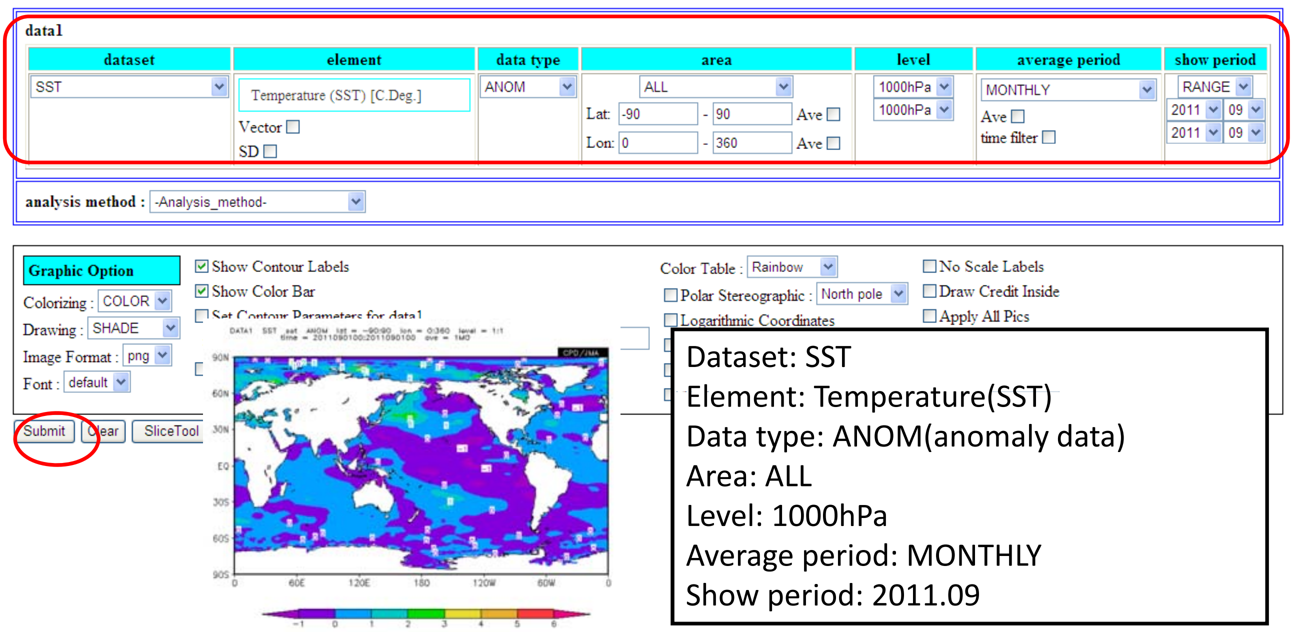

Dataset: SST
Element: Temperature(SST)
Data type: ANOM(anomaly data)
Area: ALL
Level: 1000hPa
Average period: MONTHLY
Show period: 2011.09

First, please make a map of monthly SST in September 2011 as mentioned above.

Subtraction of monthly SST

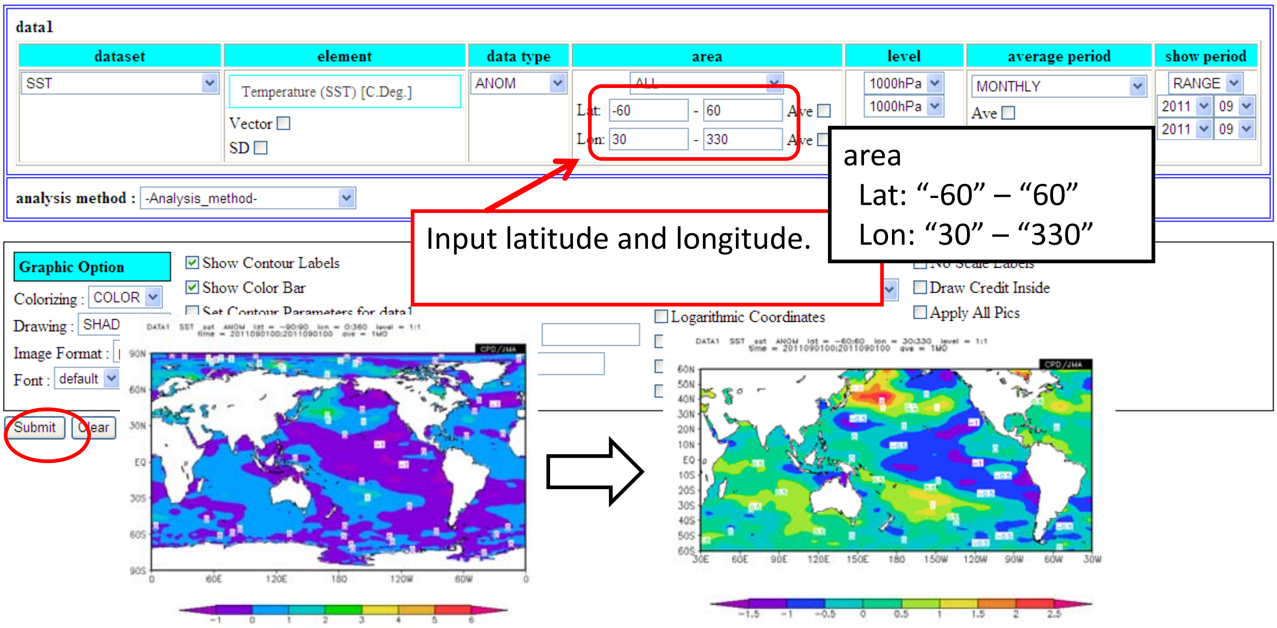

Now, let's try to change area. Please input latitude and longitude and click submit.

Subtraction of monthly SST

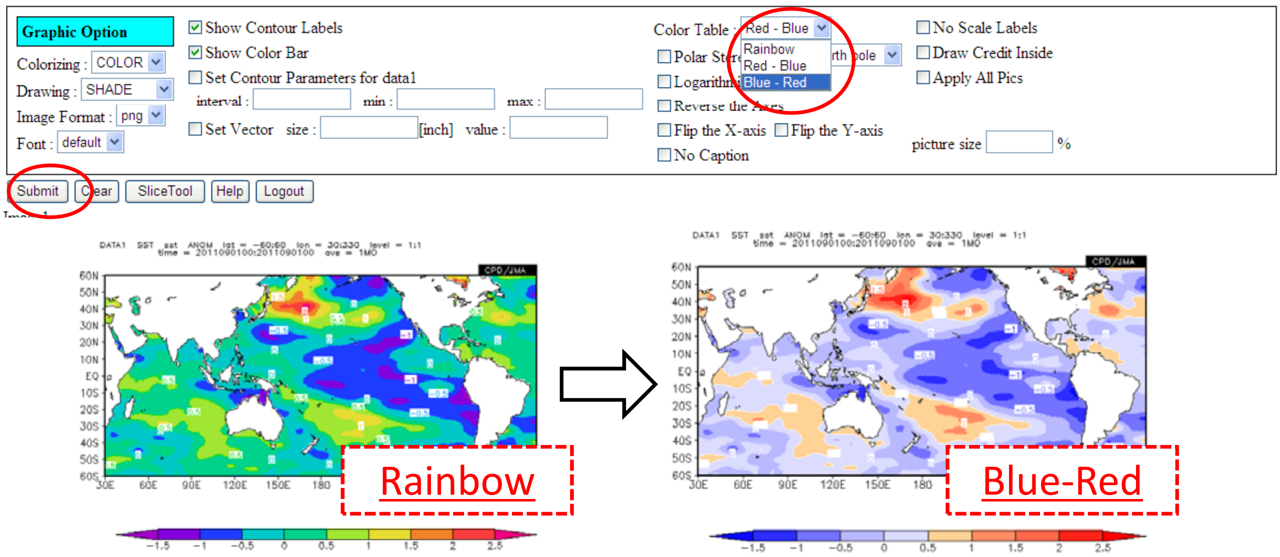

Next, let's change color table.
Please change "Color Table" – "Blue - Red" and click "Submit" button.

Subtraction of monthly SST

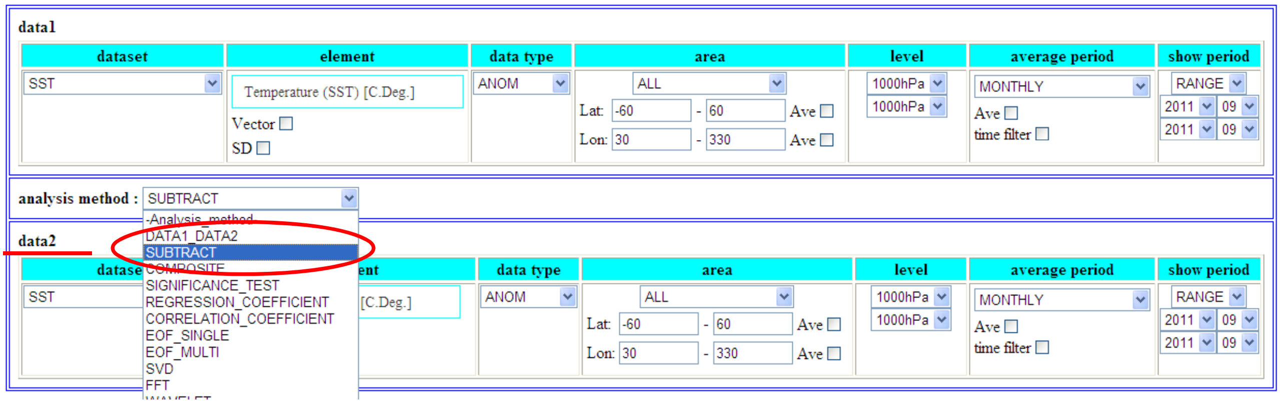

Please select "analysis method" – "SUBTRACT".
Box "data2" will appear.

Subtraction of monthly SST

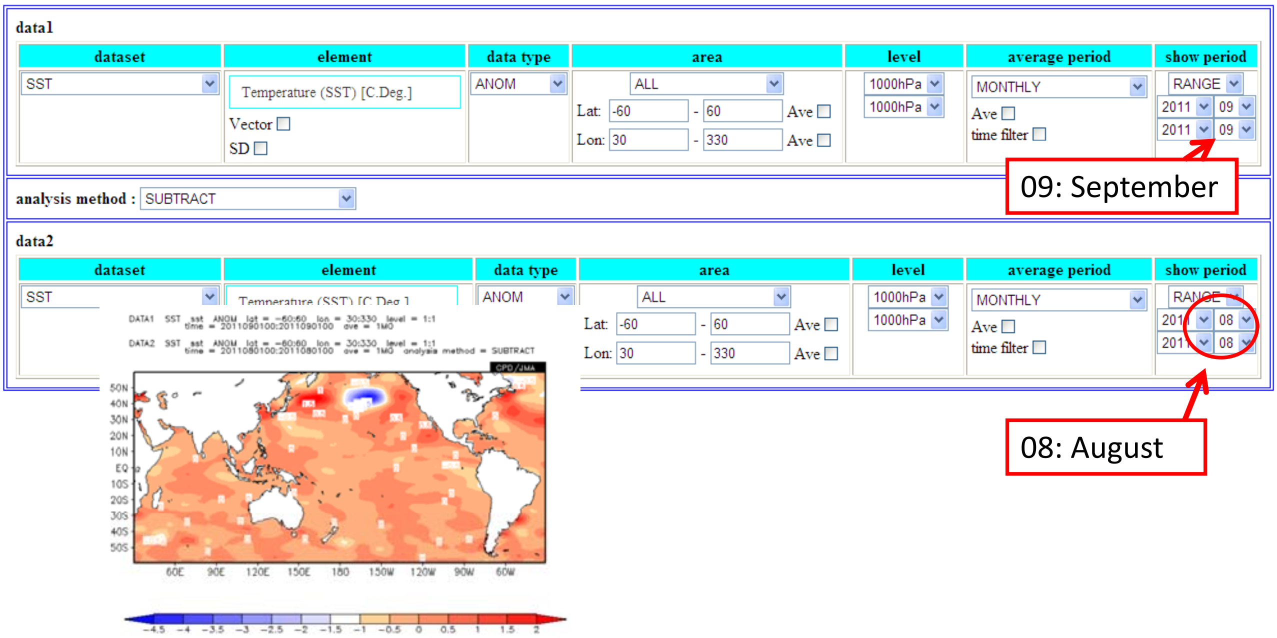

Next, please change month, in "data2" box and click "Submit" button.
Almost area of sea will be painted red. Let's change contour parameter in next step…

Subtraction of monthly SST

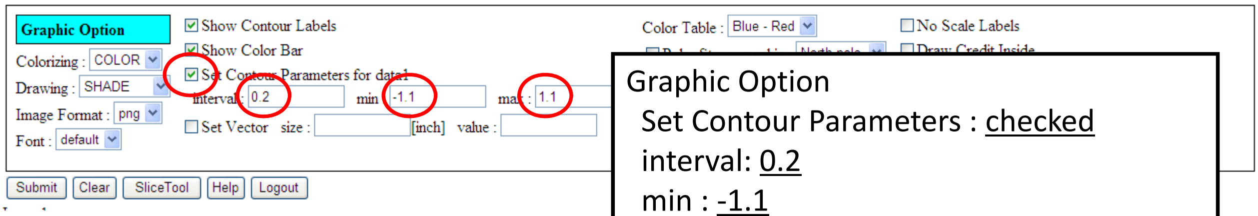

Graphic Option
Set Contour Parameters : <u>checked</u>
interval: <u>0.2</u>
min : <u>-1.1</u>
max : <u>1.1</u>

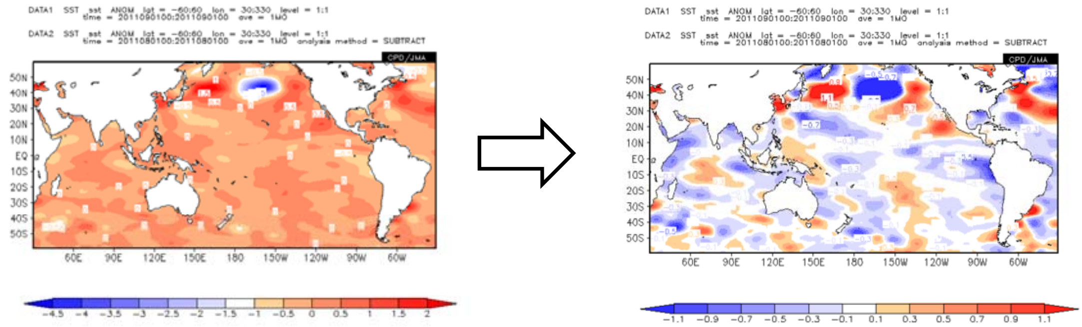

Finally, let's change the range of color bar to see change of SST in detail.

500-hPa height and anomaly

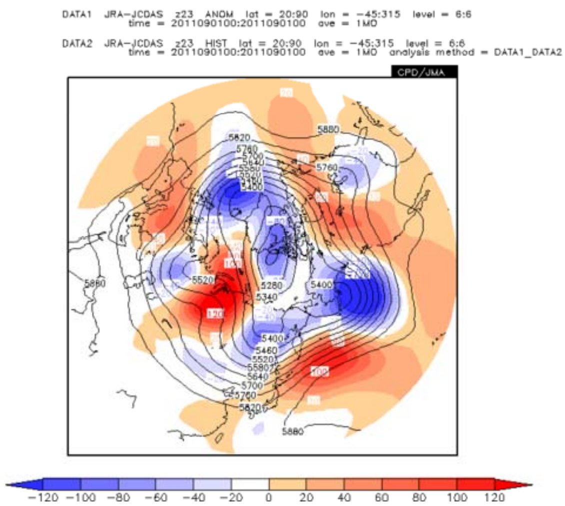

500-hPa height and anomaly

Let's know how to make a map as polar stereographic plot.

500-hPa height and anomaly

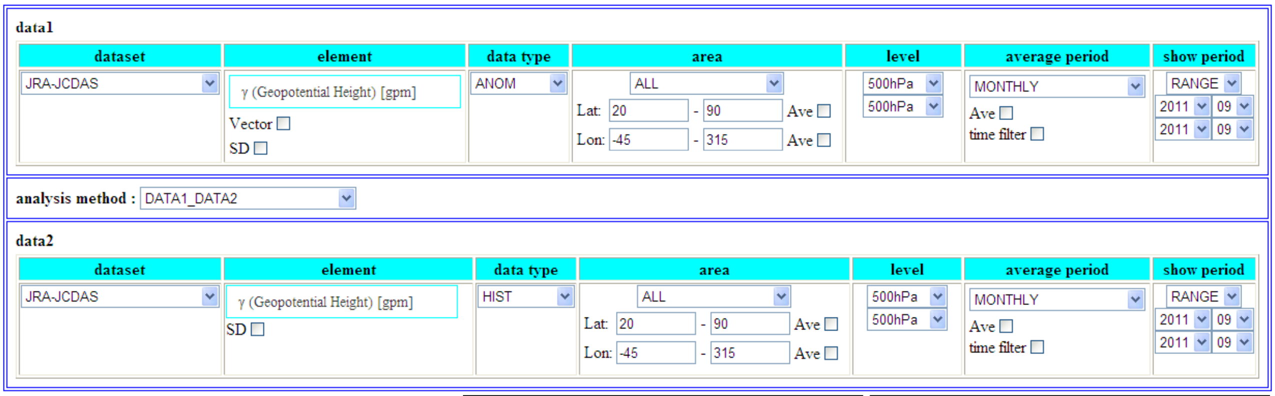

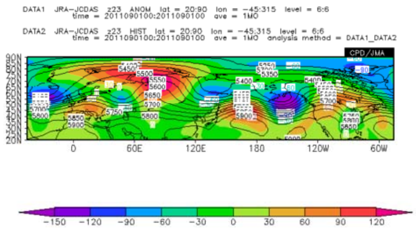

(data1)
Dataset: JRA-JCDAS
Element: γ (Geopotential Height)
Data type: ANOM
Area:
Lat: "20" - "90"
Lon: "-45" - "315"
Level: 500hPa
Average period: MONTHLY
Show period: 2011.09

(data2)
Dataset: JRA-JCDAS
Element: γ (Geopotential Height)
Data type: HIST
Area:
Lat: "20" - "90"
Lon: "-45" - "315"
Level: 500hPa
Average period: MONTHLY
Show period: 2011.09

First, please make a map of 500-hPa height and anomaly in September 2011 as mentioned above.

500-hPa height and anomaly

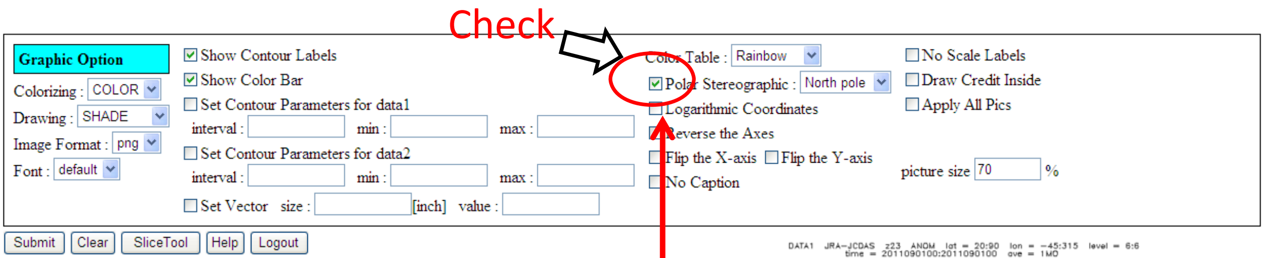

Polar Stereographic
Show polar stereographic plot, Check here and choose north polar stereographic or south polar stereographic.

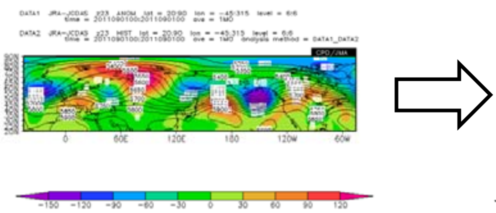

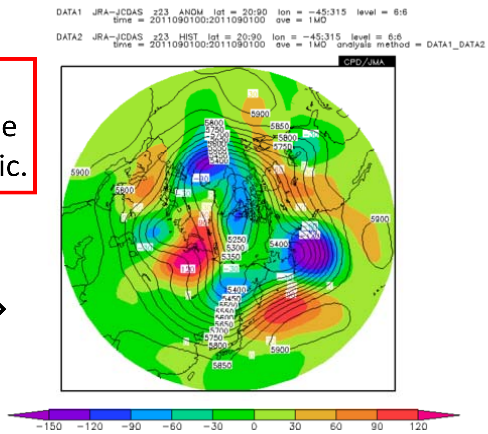

Secondly, let's make a polar stereographic plot. Check "Polar stereographic" option as mentioned above and click "Submit" button.

500-hPa height and anomaly

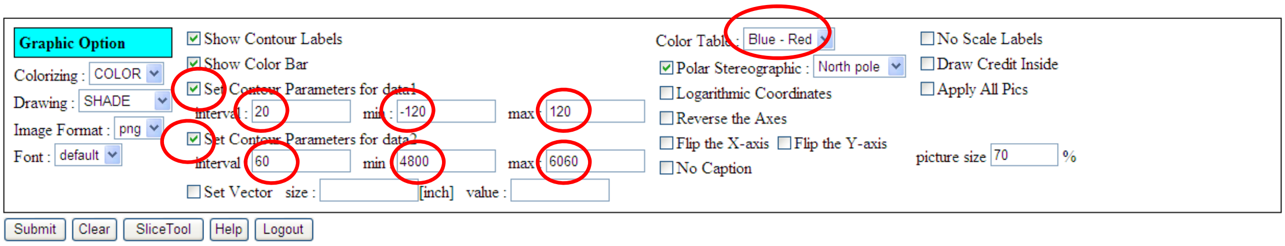

(Graphic Options)
Set contour Parameters for data1
Intervel: “20” Min: “-120” Max: “120”

Set contour Parameters for data2
Intervel: “60” Min: “4800” Max: “6060”

Color Table: “Blue-Red”

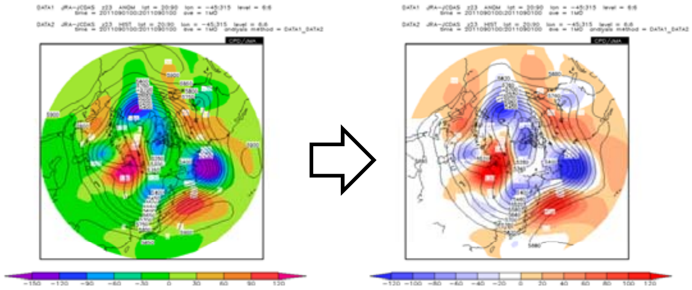

Finally, let’s change graphic options as mentioned above.

Time-longitude cross section of 200-hPa velocity potential

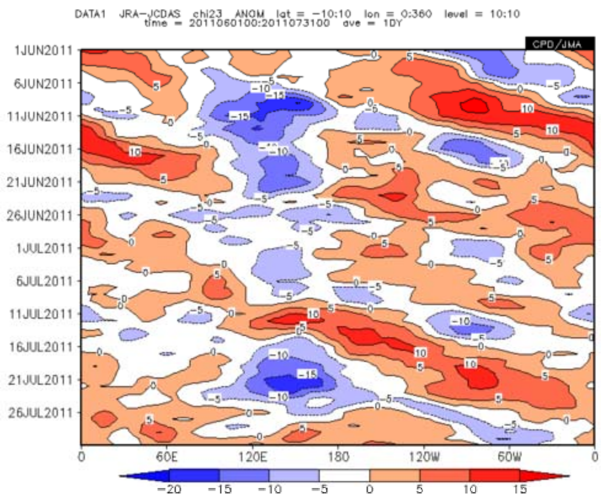

Time-longitude cross section of 200-hPa velocity potential

Let’s know how to draw time-longitude cross section of data.

Time-longitude cross section of 200-hPa velocity potential

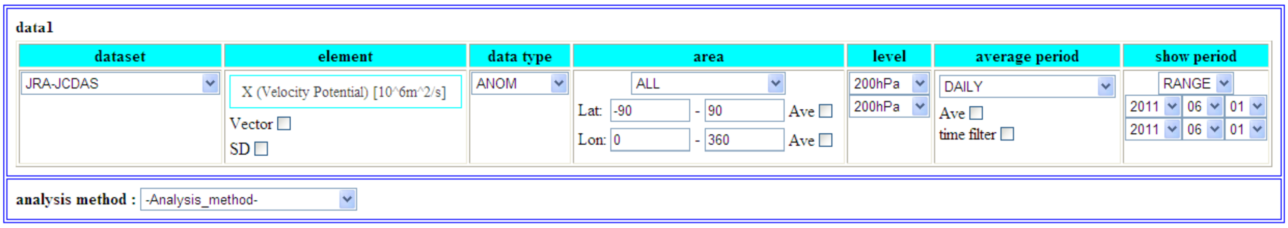

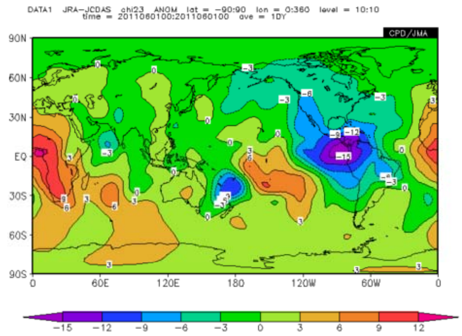

(data1)
Dataset: JRA-JCDAS
Element: X (Velocity Potential)
Data type: ANOM
Area: ALL
Level:
200hPa
200hPa
Average period: DAILY
Show period: 2011.06.01

First, please make a map of 200-hPa velocity potential anomaly on 1st June 2011 as mentioned above.

Time-longitude cross section of 200-hPa velocity potential

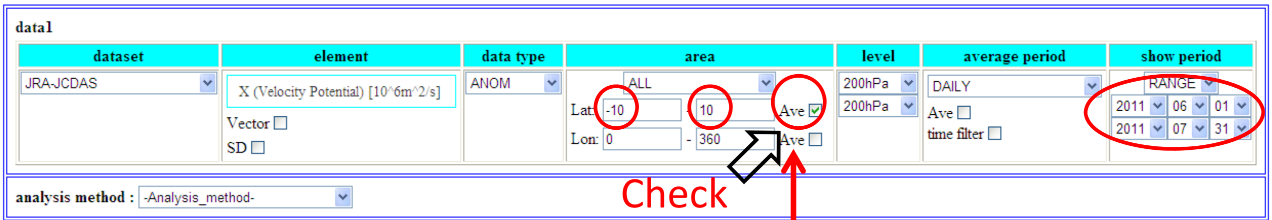

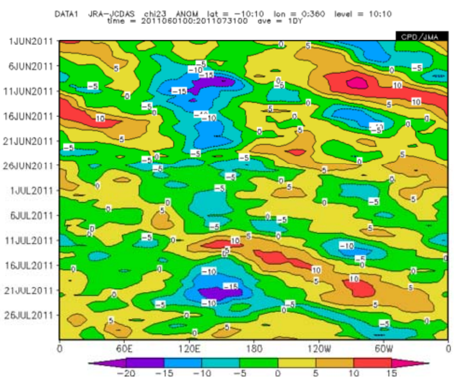

In the case of drawing a time-longitude cross section diagram, check "Ave" box of latitude(Lat) off.

(data1)
Lat: “-10” – “10”
Show period: 2011.06.01 – 2011.07.31

Secondly, input latitude and check “Ave” box off. And select “show period”.
Could you draw a map like sample?

Time-longitude cross section of 200-hPa velocity potential

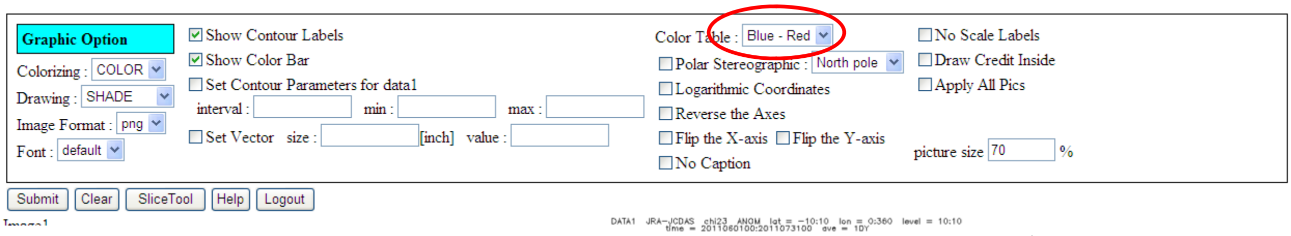

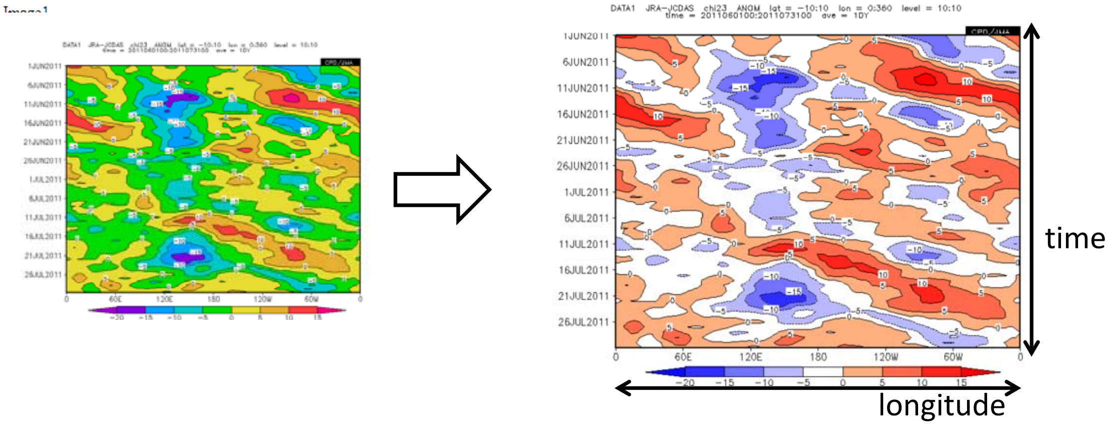

Finally, let's select "Color Table" – "Blue - Red" and click "submit" button.

Water vapor flux(vector) anomaly and specific humidity anomaly

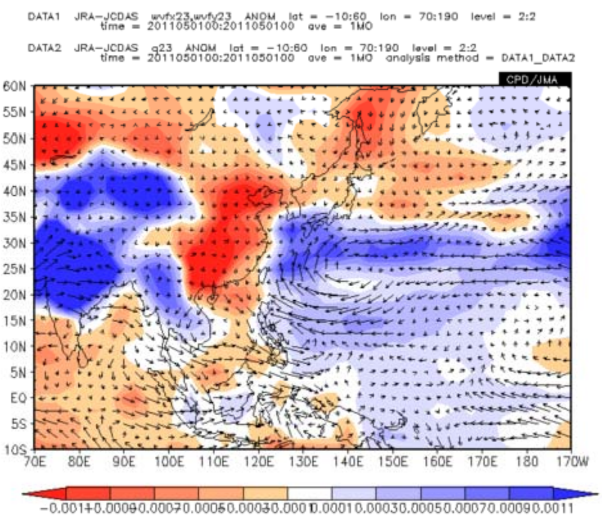

Water vapor flux(vector) anomaly and specific humidity anomaly in May 2011

Let's try to draw vector.

Water vapor flux(vector) anomaly and specific humidity anomaly

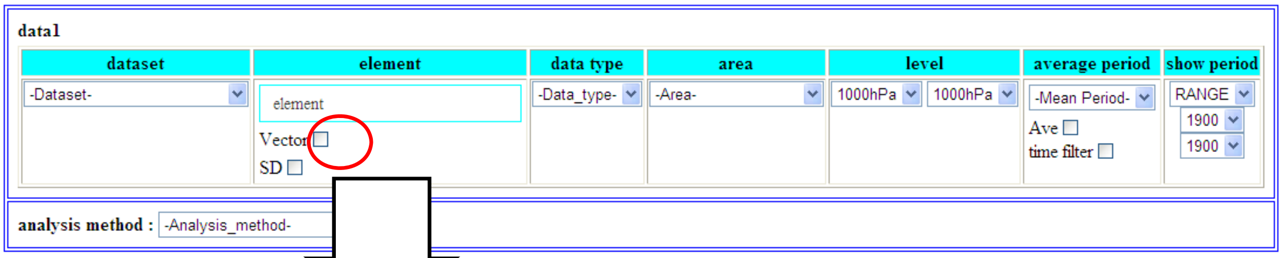

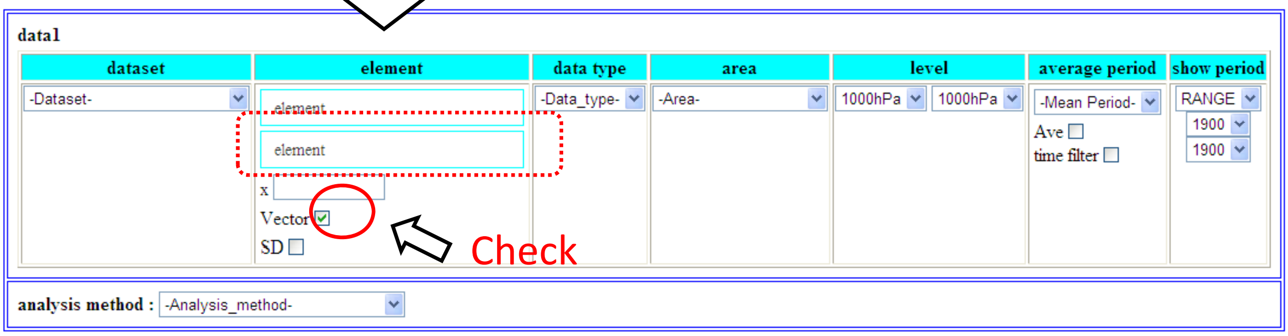

First, check "Vector" box off to add new element box.

Water vapor flux(vector) anomaly and specific humidity anomaly

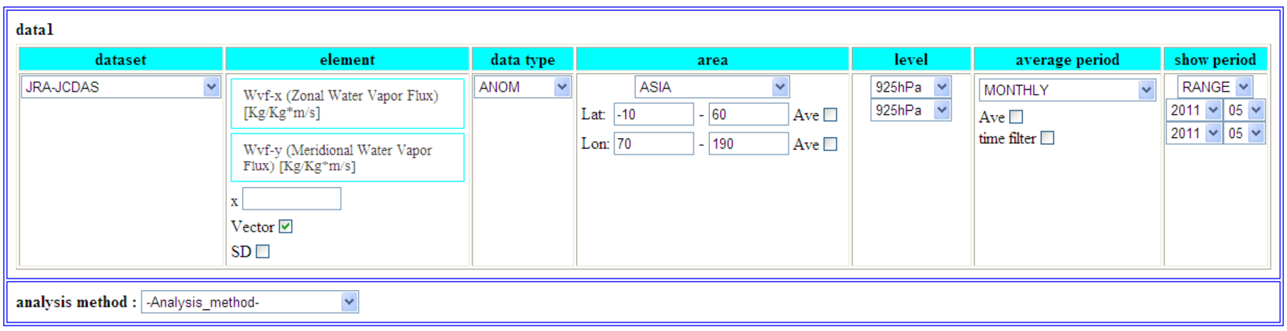

(data1)

Dataset: JRA-JCDAS
Element:
Wvf-x (Zonal Water Vapor Flux)
Wvf-y (Meridional Water Vapor Flux)
Data type: ANOM

Area: ASIA
Lat: "-10" - "60"
Lon: "70" - "190"
Level: 925hPa / 925hPa
Average period: MONTHLY
Show period: 2011.05 / 2011.05

Secondly, let's try to make a map of water vapor flux anomaly.

Water vapor flux(vector) anomaly and specific humidity anomaly

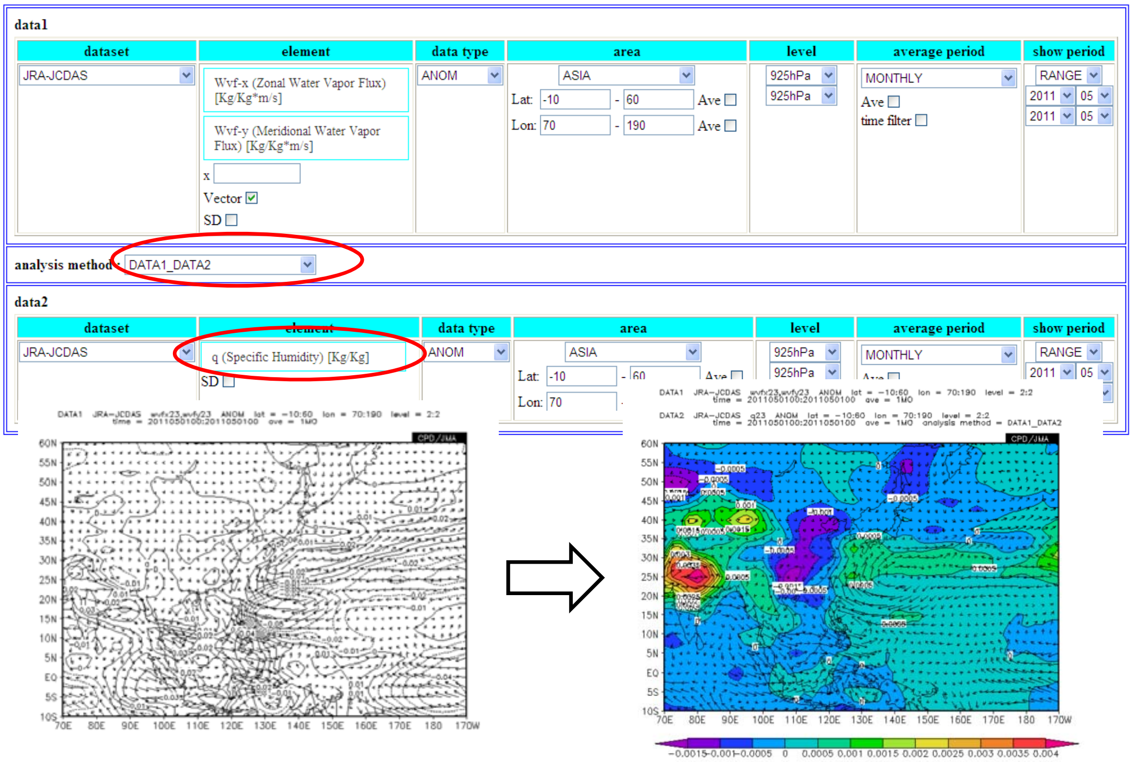

Next, please select “analysis method” – “DATA1_DATA2” and add “data2” - “q (Specific Humidity) anomaly”.

Water vapor flux(vector) anomaly and specific humidity anomaly

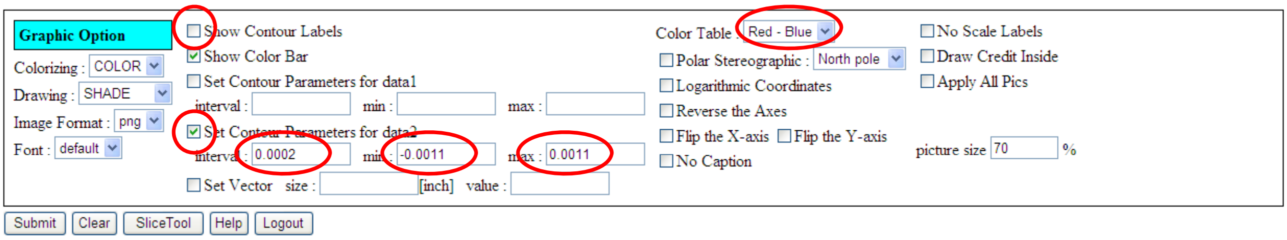

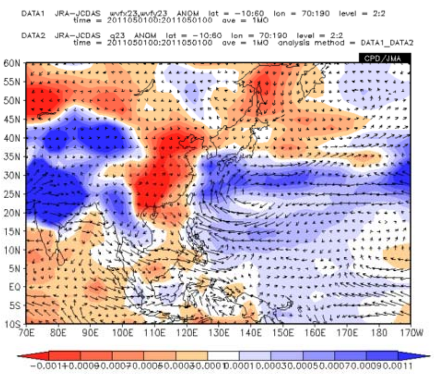

(Graphic Options)
Show contour labels: unchecked
Set contour Parameters for data2
Intervel: “0.0002” Min: “-0.0011” Max: “0.0011”
Color Table: “Red-Blue”

Finally, let’s change graphic options as mentioned above and click “Submit” button.

Interannual variation of monthly mean 850-hPa air temperature

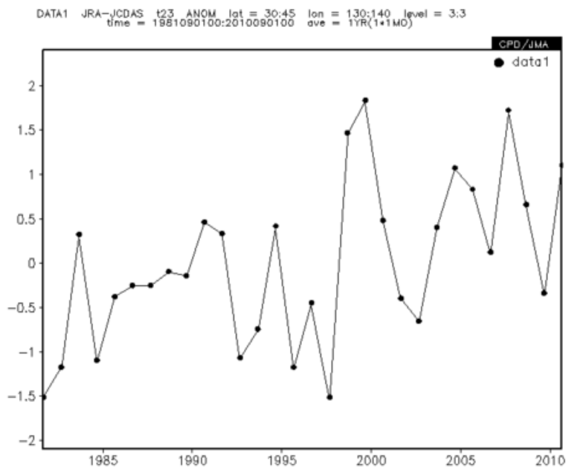

Interannual variation of monthly mean 850-hPa air temperature around Japan

Let's try to draw line graph.

Interannual variation of monthly mean 850-hPa air temperature

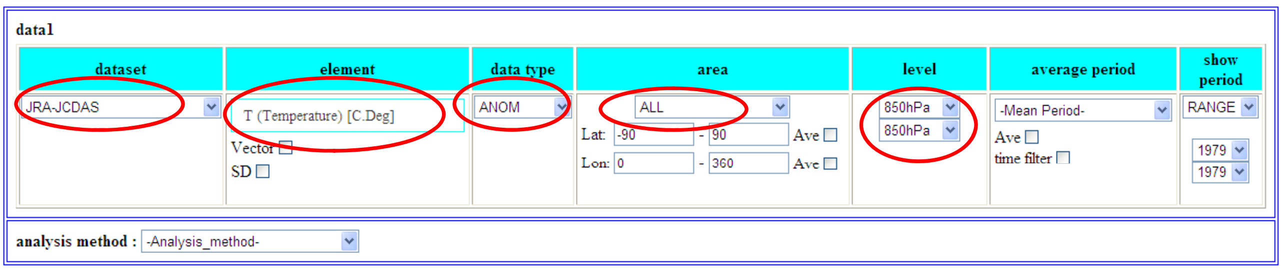

Dataset: JRA-JCDAS
Element: T(Temperature)
Data type: ANOM(anomaly data)
Area: ALL
Level: 850hPa / 850hPa

First, please set parameters as mentioned above.

Interannual variation of monthly mean 850-hPa air temperature

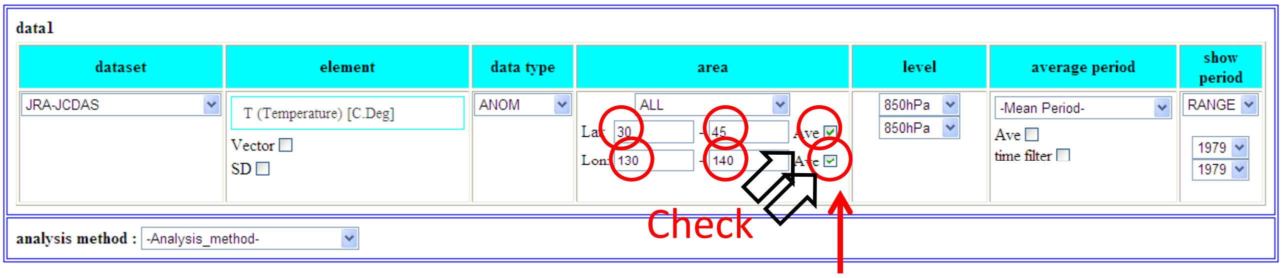

Lat: “30”-”45” Ave: checked
Lon: “130”-”140” Ave: checked

Checking both “AVE” box off gives average data of area.

Secondly, input latitude and longitude. And check both “Ave” box off.

Interannual variation of monthly mean 850-hPa air temperature

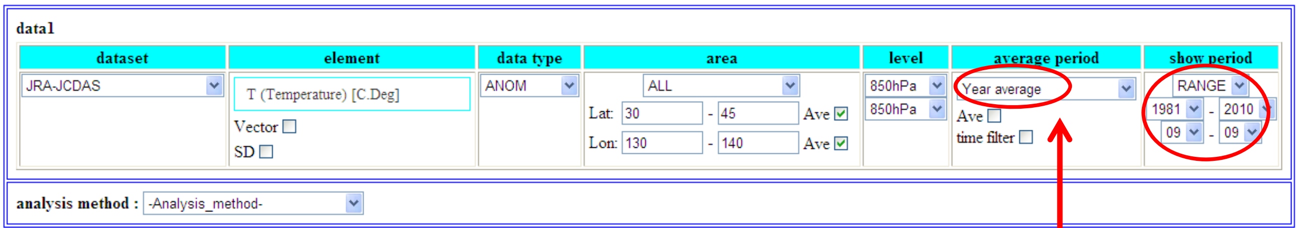

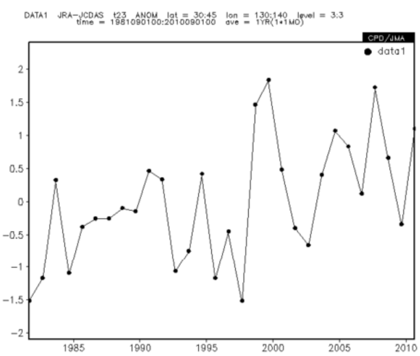

"Year average" means "Year average monthly“. This example gives us temperature in September between 1981 and 2010.

Average period: “Year average”
Show period:
“1981” – “2010”
“09” – “09”

Finally, select “average period” – “Year average” and “show period” as mentioned above. And let’s click “Submit” button.

SST composite of La Nina years

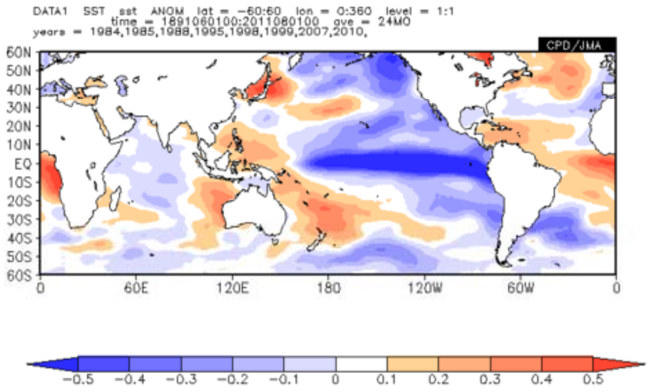

SST composite of La Nina years

Let's know how to draw composite map.

SST composite of La Nina years

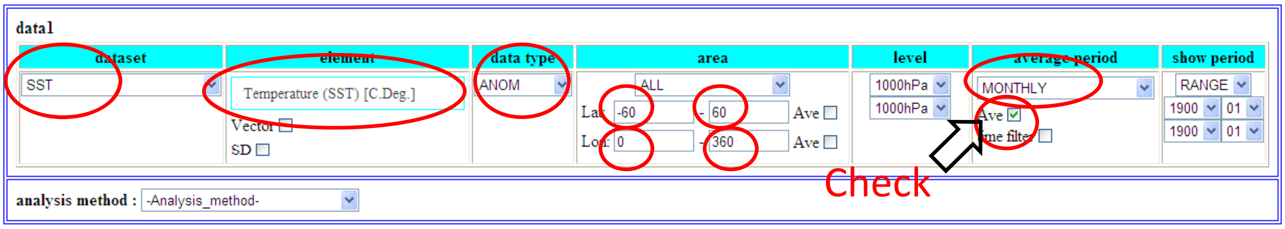

(data1)
Dataset: SST
Element: Temperature(SST)
Data type: ANOM
Area:
 Lat: "-60" - "60"
 Lon: "0" - "360"
Level: 1000hPa / 1000hPa
Average period:
 MONTHLY
 Ave: checked

First, please select parameters as mentioned above.

SST composite of La Nina years

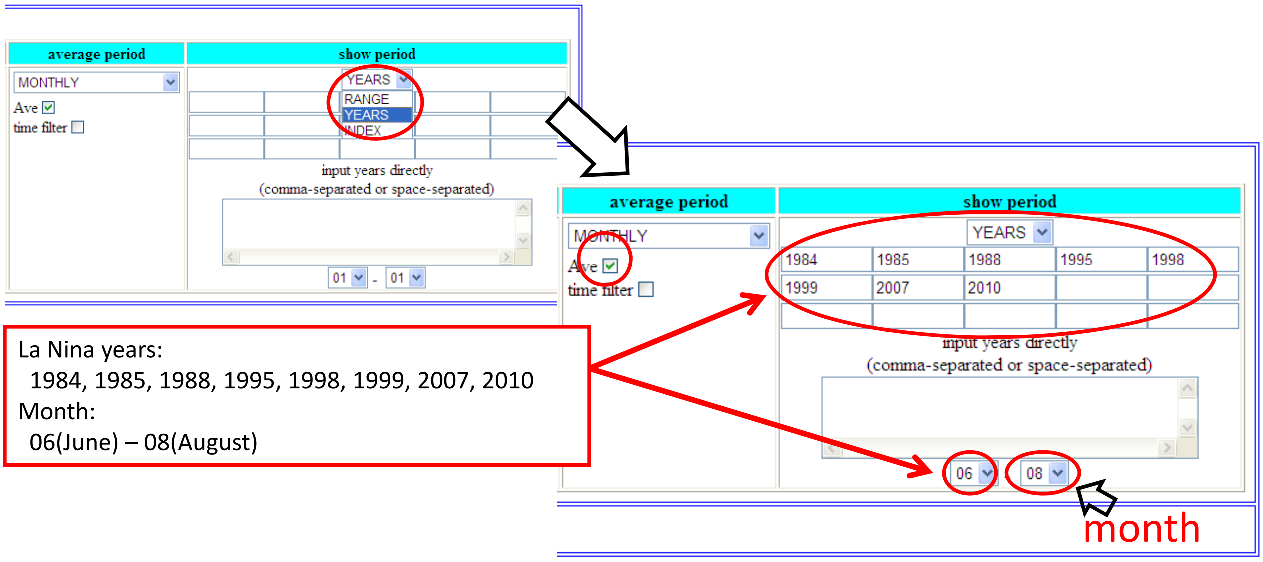

Secondly, select “show period” – “YEARS” and input La Nina years. And select month, June and August. These settings means average of data(SST) of La Nina years in summer.

SST composite of La Nina years

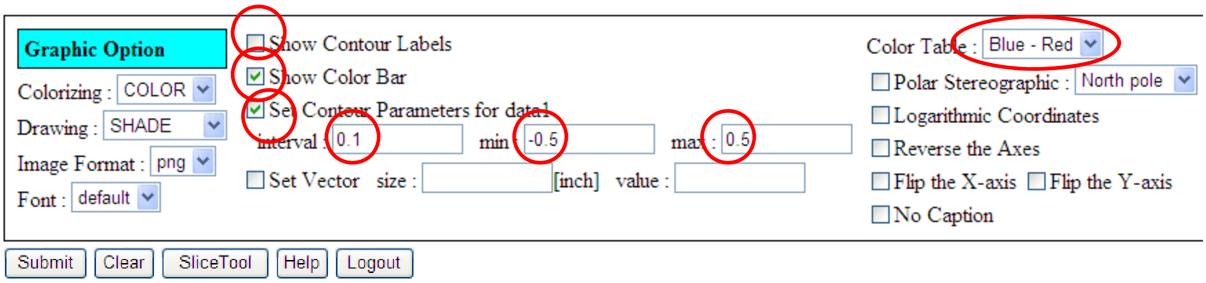

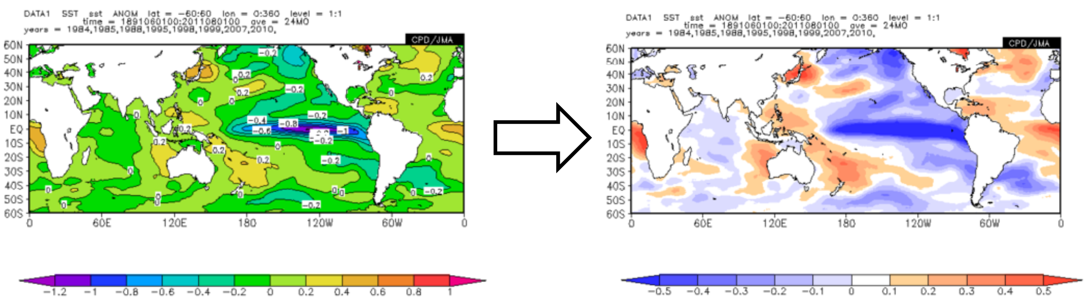

Finally, let’s use graphic options as mentioned above and draw a map.

Regression Analysis : NINO.3 SST and 850hPa Stream Function

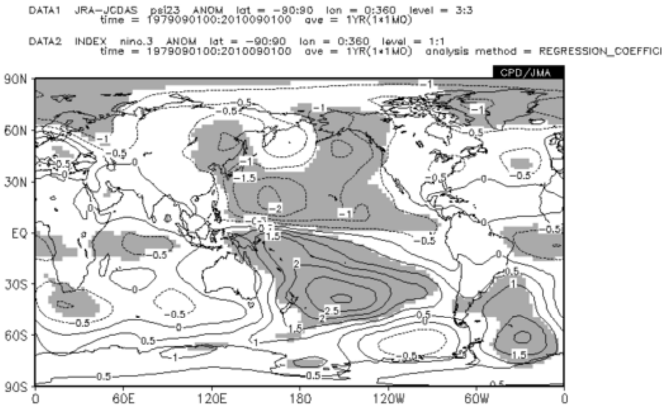

Regression Analysis : NINO.3 SST and 850hPa Stream Function

Let's know regression analysis. In shaded area of a map, stream function has a close connection with SST of NINO.3.

*NINO.3: 5S-5N, 150-90W

Regression Analysis : NINO.3 SST and 850hPa Stream Function

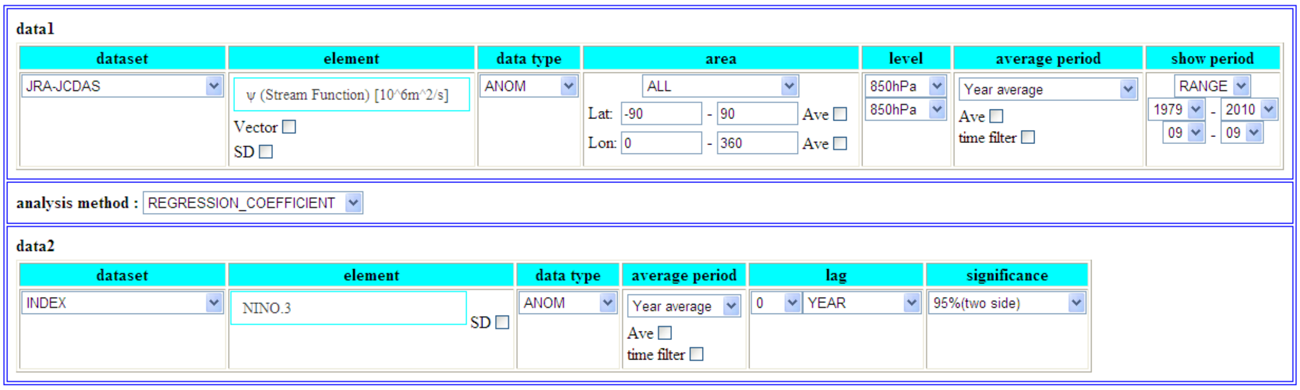

(data1)
Dataset: JRA-JCDAS
Element: Ψ(Stream function)
Data type: ANOM(anomaly data)
Area: ALL
Level: 850hPa / 850hPa
average period: Year average
show period: 1979-2010 / 09-09

(analysis method)
REGRESSION_COEFFICIENT

(data2)
Dataset: INDEX
Element: NINO.3
Data type: ANOM(anomaly data)
Significance: 95%

Let's try to set parameters as mentioned above and click submit button. A map like sample will be made.

Hint: (Graphic option) Drawing: CONTOUR

Correlation Analysis

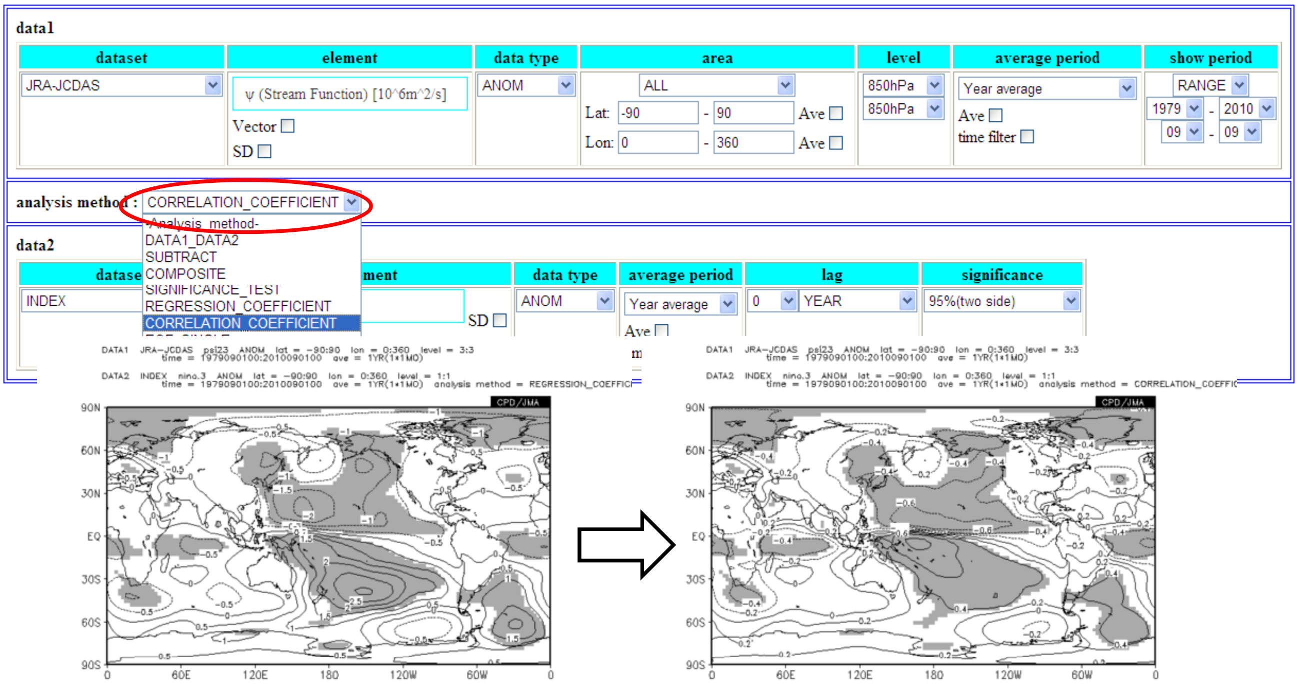

Regression Analysis   Correlation Analysis

Next, let's try correlation analysis.
Please change "analysis method" – "CORRELATION..." and click "submit" button.

Appendix

Correlation and Regression

Correlation

- The strength of the linear relationship between two variables
- Correlation coefficient must be between -1 and 1

> r < 0 : Negative correlation
> r = 0 : No correlation
> r > 0 : Positive correlation

Regression

- The slope of the linear relationship between two variables

Regression Coef.

y = a x + b + e

Residual

Intercept

y: Fields to be regressed e.g. Stream function
x: Explanatory variable e.g. Nino3-SST

Relationship between Nino-3 SST and Stream function (850hPa)

Composite **Correlation** **Regression**